TOPICS IN EXTENSIONS OF THE STANDARD MODEL OF ELEMENTARY PARTICLES AND THEIR SIGNATURES AT THE LARGE HADRON COLLIDER

A Dissertation

Presented to the Faculty of the Graduate School

of Cornell University

in Partial Fulfillment of the Requirements for the Degree of

Doctor of Philosophy

by

Christian Spethmann

August 2009

TOPICS IN EXTENSIONS OF THE STANDARD MODEL OF ELEMENTARY PARTICLES AND THEIR SIGNATURES AT THE LARGE HADRON COLLIDER

Christian Spethmann, Ph.D.

Cornell University 2009

The mechanism for electroweak symmetry breaking (EWSB) is yet unknown and the hierarchy between the EWSB scale and the Planck scale is not understood. Several alternative mechanisms for EWSB were postulated by theorists. In the near future, experiments at the Large Hadron Collider (LHC) at CERN will begin testing these theories. In this thesis, we explore two of the postulated mechanisms, supersymmetry and little Higgs models, and some of their consequences for the experiments at the LHC.

The "golden region" in the parameter space of the Minimal Supersymmetric Standard Model is the region where the experimental constraints are satisfied and the amount of fine-tuning is minimized. In this region, the stop trilinear soft term A_t is large, leading to a significant mass splitting between the two stop mass eigenstates. As a result, the decay $\tilde{t}_2 \to \tilde{t}_1 Z$ is kinematically allowed. The experiments at the LHC can search for this decay through an inclusive signature, $Z + 2j_b + \not{E}_T + X$. We evaluate the Standard Model backgrounds and identify cuts to isolate this signal. We also discuss other possible interpretations of such a signal.

We then construct an anomaly–free, weakly–coupled, renormalizable ultraviolet completion of the Littlest Higgs model with T-parity (LHT), based on an $SU(5) \times SU(2) \times U(1)$ gauge theory with a discrete Z_2 symmetry. The model re-

produces the complete structure of the LHT below the 10 TeV scale and contains additional states at the 1 TeV scale. We estimate the impact of these states on precision electroweak observables and discuss how the model can be embedded into a supersymmetric theory or a five-dimensional setup with a warped extra dimension.

Finally, we investigate the potential of the Compact Muon Solenoid (CMS) detector at the LHC to discriminate between supersymmetric and Little Higgs models. We find that the angular and momentum distributions of the observed jets are sufficient to discriminate between the two models in a simple test case scenario with a few inverse femtobarns of LHC data, provided that these distributions for both models and the dominant Standard Model backgrounds can be reliably predicted by Monte Carlo simulations.

BIOGRAPHICAL SKETCH

Christian Spethmann was born in the town of Haltern, West Germany on August 4, 1977 as the first child of his father Ewald, a schoolteacher, and his mother Elisabeth, an administrative assistant and homemaker.

Together with his younger brother Stephan, he spent his childhood and adolescense in his hometown. He graduated on top of his class, receiving the "Abitur" degree in 1997. After completing one year of obligatory civilian substitute service, he enrolled at the University of Münster and began his training as a physicist.

In the course of his studies he specialized in theoretical particle physics, investigating aspects of lattice gauge theory for his "Diplom" thesis under the guidance of his supervisor Gernot Münster. From 2002 until the completion of his degree in 2004 he was supported by the Germany National Merit Foundation ("Studienstiftung").

In 2004, he moved to the United States to pursue a Ph.D. from Cornell University. After receiving his degree, he will join the high energy theory group at Boston University as a postdoctoral research associate.

This document is dedicated to my daughter Livia Natalie.

ACKNOWLEDGEMENTS

I would like to thank my parents Ewald and Elisabeth for raising me and for the assistance they have given me over the years, as well as my brother Stephan for always being there when needed.

I am grateful to my collaborators — my advisor Maxim Perelstein, the other members of my committee Csaba Csáki and Julia Thom, as well as my fellow graduate student Johannes Heinonen — for being accessible and helpful, and for many stimulating discussions.

I would also like to thank Professor Georg Hoffstaetter for providing one year of funding in the context of an interesting accellerator physics research project.

I am grateful to my daughter Livia for being herself, and to her mother Catharina for giving her a loving home.

Finally, I want to thank my friends who were always there to help me through all difficulties.

TABLE OF CONTENTS

LIST OF TABLES

LIST OF FIGURES

CHAPTER 1

INTRODUCTION

1.1 Historical context

Since ancient times, humans have been wondering about the nature of matter and about the forces acting on it. Leucippus and Democritus were the first to hypothesize that everything is made out of discrete building blocks ("atoms") to account for both the stability of matter and the potential for change. They imagined that the atoms have different kinds of shapes that let them connect to each other, and that all the phenomena of the world could be explained from this.

In the year 2009, we are still following the same paradigm, although in the context of relativistic quantum field theories. Elementary matter fields and their excitations have replaced Democrit's "atoms", and are connected to each other by gauge fields and their quantum excitations, representing the fundamental forces of nature. This thesis is intended as a contribution to this ongoing effort to identify the fundamental constituents of the universe.

For most of human history, it was believed that the world is divided into the two fundamentally different regions of the earth and the heavens. It was asumed that the seemingly eternal motions of the planets and stars are different than the ordinary behavior of matter on earth. Only after the invention of calculus and classical mechanics was it possible to prove that the same universal force of gravity that lets apples fall to the ground is also responsible for the orbit of the moon around the earth.

Since Isaac Newtons times, it has been one of the goals of science to further unify our understanding of nature. The work of Faraday, Maxwell, Einstein and others established that electricity, magnetism and light can all be understood from a single entity, the electomagnetic field, and from the rules of relativity.

With the developement of quantum mechanics in the 1920s, it was possible to derive the multitude of shapes and colors that we observe in the world from the same electromagnetic field. At low energies, only two force carriers are therefore necessary to explain most of the world, the graviton and the photon.

There are, however, aspects of nature that do not fit into one of these two descriptions. The nuclei of atoms contain large amounts of positive charge and should therefore be unstable because of electrostatic repulsion. They are held together by the strong nuclear force, with an energy scale that is tens of thousand times larger than the typical electromagnetic binding energy of the electrons in the atom.

Also, the existence of radiactive β-decay proves the existence of a force that can transform different kinds of matter fields into each other. This is the weak nuclear force, which like the strong nuclear force can only act on very short distance scales, and is therefore not directly observable in our daily lives.

The observed matter fields are classified according to the forces they are subject to: The fundamental building blocks of nuclei are the quarks, which are affected by the strong force. The particles that do not feel this force are the charged leptons (electrons, muons, and taus) and the corresponding neutrinos, which only interact through the weak force (and gravity) with the rest of the world.

The main focus of elementary particle theory during the last sixty year has been to reconcile the existence of those short range forces with the long range forces of gravity and electromagnetism, and to find a unifying description of nature.

1.2 Electroweak symmetry breaking and the hierachy problem

The modern description of electromagnetism is in terms of Quantum Electrodynamics (QED), which describes the photon as the massless gauge boson of an unbroken local $U(1)$ symmetry. The electromagnetic field couples to fermionic matter fields with quantized charges, where the fundamental coupling strengh is energy dependent and has the approximate value

$$\alpha_{QED} \approx 1/137$$

at low energies. Since the symmetry is Abelian, the gauge fields themselves do not transform under the action of the symmetry, and the photons do not carry electric charge. Because of this unbroken Abelian symmetry, the range of the electromagnetic force is infinite.

The success of QED has been an inspiration to search for gauge theories that can be applied to the other fundamental forces of nature. The strong force is then described by Quantum Chromodynamics (QCD), with the quark fields transforming under an $SU(3)$ gauge symmetry. The short range of the strong force is explained by the confinement of color charges, caused by the self-interactions of the gauge bosons, the gluons. The characteristic energy scale Λ_{QCD} determines the masses of the nucleons, which are of order 1 GeV. Most of the mass of ordinary matter can therefore be explained as the binding energy of the quarks and

gluons inside nucleons.

At low energies, the weak force appears to be a pointlike interaction between four matter fields. In the fundamental process of β-decay for example, an up quark decays to a down quark, an electron, and an electron anti-neutrino. In quantum field theory, such a four fermion interaction requires a nonrenormalizable operator in the Lagrangian. Such an operator can only consistently be used in an effective theory, i.e. an approximation in terms of low energy degrees of freedom, indicating that at higher energies a different theoretical framework is needed.

Assuming that the coupling constant of weak interactions is dimensionless, it follows that a four fermion operator has to be suppressed by two powers of the fundamental energy scale. This suppression can be generated if the weak gauge boson (the "W") is massive, because the interaction requires a propagator of this gauge boson from the first to the second interaction vertex. However, such a gauge boson mass term is not invariant under the gauge symmetry, so the symmetry must be broken.

The W boson has an electric charge of $\pm e$, so that the weak and electromagnetic forces are not independent of each other. This observation has lead Weinberg, Glashow and Salam to the theory of electroweak symmetry breaking, and the Standard Model (SM) of elementary particles. The $U(1)$ gauge group of QED is now understood as the unbroken subgroup of a larger $SU(2)_L \times U(1)_Y$ electroweak gauge group. The electric charge is given by $Q = T_3 + Y$, where T_3 and Y are the charges under the weak isospin $SU(2)_L$ and the hypercharge group $U(1)_Y$. The photon is a linear combination of the hypercharge gauge boson and the uncharged $SU(2)$ gauge boson W_3, while the weak gauge bosons are lin-

ear combinations of the other two $SU(2)$ gauge bosons W_1 and W_2. The theory also contains a third weak gauge boson, the Z, which is the orthogonal linear combination to the photon.

Both the electroweak symmetry breaking scale and the mixing angle between the weak isospin and the hypercharge in the photon are known, and all measurements so far agree with the predictions of this theory. At this moment, however, it is still unclear what causes electroweak symmetry breaking. In the Standard Model, it is assumed that a fundamental complex scalar field (the "Higgs"), transforming as a doublet under $SU(2)$ and with a hypercharge of -1/2, accquires a vacuum expectation value (VEV) at an energy scale of 246 GeV. The gauge couplings of this field would then give masses to the weak gauge bosons. The existence, although not the magnitude, of matter field masses can also be explained by the Higgs mechanism, if Yukawa couplings between the Higgs and the fermions are introduced. Since three of the four degrees of freedom of the Higgs field are absorbed into the longitudinal components of the Gauge fields, only a single real scalar field remains observable. Its excitation is the physical Higgs particle.

There is, however, a potentially fatal flaw in the Standard Model. So far, gravity has not been considered. The coupling constant of gravity is Newton's constant, which has a mass dimension of negative two. The natural scale of gravitational interactions is therefore given by the Plank scale,

$$M_P = \sqrt{\frac{\hbar c}{G}},$$

which is of order 10^{19} GeV. Any fundamental scalar field in a quantum field theory will acquire quantum corrections to its propagator, which will increase its mass parameter to the largest scale in the theory. In the Standard Model, it

can therefore not be explained why the electroweak symmetry breaking scale is many orders of magnitude smaller than the Planck scale. This is known as the hierarchy problem.

1.3 The Minimally Supersymmetric Standard Model

A possible solution to the hierarchy problem is to postulate that nature is fundamentally supersymmetric. This new symmetry was first discovered by Golfand and Likhtman and independently by Wess and Zumino. Supersymmetry constitutes the only possible non-trivial extension of the Poincaré group. In a world with unbroken supersymmetry, every particle has a mirror particle that carries the opposite spin, but the same mass and gauge charges. Because of chiral symmetry, fermion masses can at most be logarithmically divergent, and this carries over to their scalar superpartners, solving the hierarchy problem. Obviously, in our world supersymmetry is broken. However, if the effective masses of the new particles are close to the electroweak scale, the hierarchy problem can still be solved.

In the Minimally Supersymmetric Standard Model (MSSM), each quark and lepton has a corresponding scalar-quark (or squark) and scalar-lepton (slepton), while each boson has a fermionic partner. The strong and electroweak gauge groups of the Standard Model therefore imply the existence of those partners, the so-called gluinos, winos and binos.

Instead of a single Higgs field as in the Standard Model, two seperate electroweak doublet scalars are required in the MSSM, out of which one couples to the up-type and one to the down-type quarks. This is necessary both to can-

cel all gauge anomalies as well as to construct a consistent superpotential. The MSSM therefore includes eight scalar degrees of freedom in the Higgs sector. Three of those are absorbed as the longitudinal components of gauge bosons after electroweak symmetry breaking, leaving five physical Higgs scalars. In addition, the Higgs sector contains an up-type and a down-type Higgsino as the superpartners of the Higgs scalar fields.

The uncharged and charged gauginos and Higgsinos are not mass eigenstates of the theory. By diagonalizing the mass matrices, once finds the observable four neutralino and two chargino states. If an additional discrete Z_2-Symmetry (R-Parity) is included, under which the SM states are even and their superpartners are odd, the lightest supersymmetric particle (LSP) can no longer decay. The lightest neutralino state is therefore an attractive candidate for dark matter.

In addition to solving the Hierarchy problem, the MSSM also predicts a unification of gauge couplings near the Planck scale, which does not occur in the non-supersymmetric Standard Model. This is widely regarded as another strong argument for supersymmetry.

Unfortunatly, there are also problems with the MSSM, one of which is the mass of the lightest Higgs scalar in the theory. Tree-level calculations predict that its mass should be lighter than that of the Z-boson, so that it should already have been detected at the Large Electron-Positron Collider (LEP). The only way the mass of the lightest Higgs can be increased over the LEP bound is to assume that large quantum corrections are present.

Another problem with the MSSM is that a remnant of the hierarchy problem

still remains. Cancellations between different terms at the percent level are necessary to produce the observed EWSB scale. In chapter two we discuss these issues more thoroughly and derive possible consequences for observations at the LHC.

1.4 Little Higgs Theories

An alternative solution to the hierarchy problem is to regard the Higgs field not as a fundamental scalar but as a composite field, such as in technicolor models. However, if the Standard Model is regarded as an effective theory, precision electroweak constraints indicate that the scale of new operators has to be of order 10 TeV or larger, and it would be natural to expect the EWSB scale to be of the same size. This problem can be solved by the mechanism of collective symmetry breaking.

Whenever a global symmetry is broken, the theory will contain Nambu-Goldstone bosons (NGBs) with the same quantum numbers as the broken operators. If we assume that some global extension of the electroweak gauge group is broken at the 10 TeV scale, the Higgs can be realized as a NGB with the correct $SU(2)$ and $U(1)$ charges.

The idea of Little Higgs theories is to construct the symmetry breaking by gauge couplings in such a way that one-loop corrections to the Higgs mass are avoided. In this way, the Higgs can have a mass term at the EWSB scale even though global symmetry breaking occurs at the 10 TeV scale. This can be achieved if two or more copies of the electroweak group are gauged such that when only one copy is present, the Higgs would still be a massless NGB. This

mechanism is known as collective symmetry breaking.

In addition to gauge boson loops, the Higgs mass is also strongly affected by top quark loops, since the top Yukawa coupling is approximately one. Once again, a collective symmetry breaking mechanism is used to avoid quadratic contributions to the Higgs mass.

Little Higgs models do not aspire to explain the remaining hierarchy between the 10 TeV scale and the Planck scale, and have to be regarded as effective theories. To solve the problem of stabilizing the 10 TeV scale, a more fundamental theory is needed that remains valid for higher energy, i.e. "ultraviolet" (UV), degrees of freedom.

In chapter three, such a UV completion of the Littlest Higgs with T-Parity is constructed. This theory contains heavy copies of the $SU(2)_L$ and $U(1)_Y$ gauge bosons, as well as heavy versions of the fermions in the Standard Model. The particle content is therefore similar to the MSSM, except that here the heavy mirror particles have the same spin as their SM partners. In analogy to the supersymmetric model, an additional Z_2 symmetry (T-Parity) is introduced, which assures that the theory does not violate EW precision constraints. The lightest T-odd particle (LTP) is then stable and a possible dark matter candidate.

1.5 The Large Hadron Collider

At this moment, the largest energies that have been achieved in particle accelerators are 209 GeV for electron-positron beams at LEP and 1.96 TeV for proton-antiproton collisions at the Tevatron. Production of new particles at the Tevatron

is limited by the center of mass energy of the individual partons, and the cross section is dominated by strong interaction processes.

Because of this, the only information about electroweak symmetry breaking so far has been indirect. Measurements of e^+e^- collisions at the Z pole energy have been done at LEP and at SLC/SLD. The Tevatron has provided two crucial measurements: M_W with a higher precision than LEP, and the only measurement of $M_{\rm top}$. The top mass enters precision electroweak constraints at the one-loop level, but is very important because of the large Yukawa coupling constant. In addition to this, there are also a number of low-energy experiments (NuTeV, Møller scattering, atomic parity violation and others) that have provided relevant information for precision electroweak fits.

However, the most important piece of the puzzle is still missing, since no direct evidence for the Higgs boson has been found so far. The Large Hadron Collider is designed to collide protons at a center of mass energy of 14 TeV. If a Higgs boson with Standard Model–like couplings exists, the LHC will be able to produce it and detect its decay products, clarifying the mechanism of electroweak symmetry breaking.

Because of naturalness arguments, it is also anticipated that heavy colored particles will be found at energies accessible to the LHC. Furthermore, astrophysical and cosmological arguments point to the existence of dark matter at the EWSB scale. At the LHC, such dark matter particles could be produced directly via electroweak processes, or as decay products of the new colored states.

In chapter four, we discuss some of the possibilities and limitations of distinguishing between models of beyond the Standard Model physics that incorpo-

rate the proposed new particles. We consider a minimal scenario with a directly produced strongly interacting heavy quark partner and a weakly interacting, stable massive particle. Simulating a parameter point in the MSSM that corresponds to such a a spectrum, we attempt to fit the "data" to the wrong model, in this case a Little Higgs model. In this way, we investigate the amount of integrated luminosity at the LHC that would be necessay to exclude the incorrect model.

CHAPTER 2

A COLLIDER SIGNATURE OF THE SUPERSYMMETRIC GOLDEN REGION

Published in Journal of High Energy Physics (JHEP) **04**, 070 (2007).

2.1 Introduction

It is widely believed that physics at the TeV scale is supersymmetric. The simplest realistic implementation of this idea, the minimal supersymmetric standard model (MSSM) [2,3], is the most popular extension of the standard model (SM). However, null results of experimental searches for the superpartners and, especially, the Higgs boson, place non-trivial constraints on the parameters of the model. Furthermore, the requirement that the observed electroweak symmetry breaking (EWSB) occur without significant fine-tuning places an additional constraint. It is well known that there is a certain amount of tension between these two constraints [4]. Several authors have interpreted this tension as a motivation to extend the minimal model [5–10], or to question the conventional ideas about naturalness [11]. An alternative interpretation, which we will explore in this chapter, is that data and naturalness point to a particular "golden" region within the parameter space of the minimal model, where the experimental bounds are satisfied and fine-tuning is close to the minimum value possible in the MSSM. This minimal value itself depends on the messenger scale of supersymmetry breaking $\Lambda_{\rm mess}$, determined by dynamics outside of

the MSSM, in addition to the MSSM parameters[1]. However, for *any* $\Lambda_{\rm mess}$, the points in the golden region require *less* fine-tuning compared to the rest of the MSSM parameter space. Thus, independently of the model of SUSY breaking, nature seems to provide us with a hint about what the MSSM parameters might be[2]. In this chapter, we will discuss experiments at the Large Hadron Collider (LHC) which will be able to determine whether this hint is correct.

Both the Higgs mass bound and naturalness considerations probe the effective Higgs potential, which is primarily determined by the parameters of the Higgs and top sectors of the MSSM. (The quantum part of the potential is dominated by the top/stop loops due to a large value of the top Yukawa coupling.) It is therefore these sectors that are most directly constrained by data. We will focus on collider measurements probing these sectors.[3]

The golden region is characterized by relatively small values of the μ parameter and the stop soft masses m_{Q^3}, m_{u^3} (both are required to minimize fine-tuning of the Z mass), and a large stop trilinear soft term A_t (required to raise the Higgs mass above the LEP2 lower bound). The spectrum is then expected to contain light neutralinos and charginos with a substantial higgsino content, as well as two light (sub-TeV) stop mass eigenstates, $\tilde{t}_1$ and $\tilde{t}_2$, with a large (typically a few hundered GeV) mass splitting. A striking consequence of such a

[1]For example, it was claimed in Ref. [12, 13] that in models with "mirage mediation" of SUSY breaking [14] the scale $\Lambda_{\rm mess}$ can be as low as 1 TeV, resulting in fine-tuning of 20% or better. See Ref. [15] for a discussion of difficulties in realizing such a scenario, and Ref. [16] for an alternative implementation.

[2]An explicit model of supersymmetry breaking in a grand-unified framework which naturally generates SUSY breaking parameters in the golden region was constructed in [17, 18].

[3]Our approach is more model-independent than that of Kitano and Nomura in Ref. [19], which also considered collider signatures of the MSSM with parameters in the golden region. However, the signatures studied in [19] mainly probe the features of the superpartner spectrum dictated by a specific (mirage mediation) model of SUSY breaking [12, 13], rather than the direct consequences of data and naturalness.

"split stop" spectrum is that the decay

$$\tilde{t}_2 \to \tilde{t}_1 + Z \tag{2.1.1}$$

is kinematically allowed. Observing this decay at the LHC would provide clear evidence that the stop mass difference is larger than the Z mass, and studying the Z distributions would provide an approximate measurement of this quantity. In this chapter, we will argue that the decay (2.1.1) should be observable at the LHC, with realistic integrated luminosity, for the MSSM parameters in the golden region.

The experimental signature of the decay (2.1.1) depends on the decay pattern of the $\tilde{t}_1$. Since stops are almost always pair-produced at the LHC, it also depends on how the second $\tilde{t}_2$ decays. The details of both decay patterns depend on the superpartner spectrum. However, both $\tilde{t}_1$ and $\tilde{t}_2$ decay products always contain a b quark, produced either directly or through a top decay, as well as (under the usual assumptions of conserved R parity and weakly interacting lightest supersymmetric particle) large missing transverse energy. We therefore propose an inclusive final state

$$Z + 2j_b + \not{E}_T + X, \tag{2.1.2}$$

where Z is assumed to be reconstructed from leptonic decays and j_b denotes a b jet, as a signature of the $\tilde{t}_2\tilde{t}_2^*$ production followed by the decay (2.1.1).

Throughout the golden region of the MSSM, both the $\tilde{t}_2$ pair-production cross section and the branching fraction of the decay (2.1.1) are sizeable. Therefore, a null result of a search for a non-SM contribution in the channel (2.1.2) would provide a strong argument against this scenario. Unfortunately, a positive identification of non-SM physics in this channel would *not* necessarily imply that the stops are split. Indeed, in the MSSM, events in this channel may

appear even if the decay (2.1.1) is kinematically forbidden, since Z bosons may also be produced in decays of neutralinos and charginos [20, 21]. For example, a cascade

$$\tilde{b} \to b\chi_2^0, \quad \chi_2^0 \to Z\chi_1^0, \tag{2.1.3}$$

or a similar cascade with charginos replacing the neutralinos, gives the signature (2.1.2). Distinguishing these interpretations is difficult, and there is no single "silver bullet" observable that would remove this ambiguity. However, a variety of measurements can be used to shed light on this question (see Section 5), and combining all available evidence may allow one to build a convincing case for (or against) the interpretation of the signature (2.1.2) in terms of the decay (2.1.1).

The chapter is organized as follows. In Section 2, we review the fine-tuning and Higgs mass constraints in the MSSM, as well as other experimental results that determine the shape of the golden region. In Section 3, we define a benchmark point which is characteristic of the golden region and suitable for studying its collider phenomenology. Section 4 is dedicated to a detailed analysis of the observability of the $Z + 2j_b + \not{E}_T$ signature, including a study of the SM backgrounds. In Section 5, we discuss the alternative interpretations of this signature within the MSSM, and outline the measurements that would need to be performed to discriminate between these interpretations. Section 6 contains our conclusions, and outlines some possible directions for future work.

2.2 The Golden Region

In this section, we will discuss the constraints on the MSSM parameters imposed by current experimental data and naturalness, focusing on the Higgs and top sectors. Our goal is to understand the qualitative features of the MSSM golden region, rather than to determine the precise location of its boundaries which are in any case fuzzy due to an inherent lack of precision surrounding the concept of fine-tuning. With this motivation, we will make several approximations which greatly clarify the picture.

Phenomenological studies of the MSSM are complicated by the large number of free parameters. Typically, studies are performed within simplified frameworks, which assume certain correlations among the parameters motivated by high-scale unification and/or by specific models of SUSY breaking. However, the shape of the golden region is to a great extent independent of such assumptions. The Higgs sector of the MSSM is strongly coupled to the top sector, but couplings to the rest of the MSSM are weaker. One may therefore begin by considering the Higgs and top sectors in isolation; that is, the gauge and non-top Yukawa couplings are set to zero. In this approximation, physics is described in terms of the holomorphic Higgs mass μ and the six parameters appearing in the soft Lagrangian for the Higgs and top sectors:

$$\begin{aligned}\mathcal{L} \;=\; & -\, m_u^2 |H_u|^2 - m_d^2 |H_d|^2 - \left(b H_u^T H_d + \text{c.c.}\right) - m_{Q^3}^2 Q^{3\dagger} Q^3 - m_{u^3}^2 |u^3|^2 \\ & - \left(y_t A_t Q^{3\dagger} H_u u^3 + \text{c.c.}\right), \end{aligned} \tag{2.2.4}$$

where y_t is the MSSM top Yukawa coupling, $y_t = y_t^{\rm SM}/\sin\beta$. Since the model has to reproduce the known EWSB scale, $v = 174$ GeV, only six parameters are

independent. We choose the physical basis:

$$\tan\beta, \mu, m_A, \tilde{m}_1, \tilde{m}_2, \theta_t, \tag{2.2.5}$$

where m_A is the CP-odd Higgs mass, $\tilde{m}_1$ and $\tilde{m}_2$ are stop eigenmasses (by convention, $\tilde{m}_2 > \tilde{m}_1$) and θ_t is the stop mixing angle. We will analyze the fine-tuning and Higgs mass constraints in this approximation and map out the golden region in the six-parameter space (2.2.5).

Before proceeding, let us discuss the sizes of contributions to the relevant observables that are omitted in this approximation scheme. The leading contributions to the Higgs effective potential due to the $SU(3)$, $SU(2)$ and $U(1)_Y$ gauge interactions and the bottom Yukawa coupling[4] are expected to be of the order

$$\frac{g_3^2 M_3^2}{16\pi^2 \lambda_t^2 M_{\tilde{t}}^2}, \quad \frac{g_2^2 M_2^2}{\lambda_t^2 M_{\tilde{t}}^2}, \quad \frac{g_1^2 M_1^2}{\lambda_t^2 M_{\tilde{t}}^2}, \quad \frac{m_b^2 M_{\tilde{b}}^2 \tan^2\beta}{m_t^2 M_{\tilde{t}}^2}, \tag{2.2.6}$$

respectively, compared to the one-loop top sector contribution. Here g_i and M_i are the gauge couplings and (weak-scale) gaugino masses for each group, and $M_{\tilde{t}}$ is the stop mass scale, which can be conveniently taken as the average between the two stop eigenmasses. (The same definition can be made for $M_{\tilde{b}}$ if sbottoms are non-degenerate.) For a wide range of sensible superpartner spectra, these corrections are subdominant: this is the case if

$$M_1/M_{\tilde{t}} \lesssim 4, \quad M_2/M_{\tilde{t}} \lesssim 2, \quad M_3/M_{\tilde{t}} \lesssim 10, \quad M_{\tilde{b}} \lesssim \frac{35 M_{\tilde{t}}}{\tan\beta}. \tag{2.2.7}$$

The following discussion is valid for spectra obeying these constraints. If some of the above inequalities are violated, the analysis could be easily extended to include the corresponding effects; however, little additional insight would be gained.

[4]The corrections due to other Yukawa couplings are always negligible.

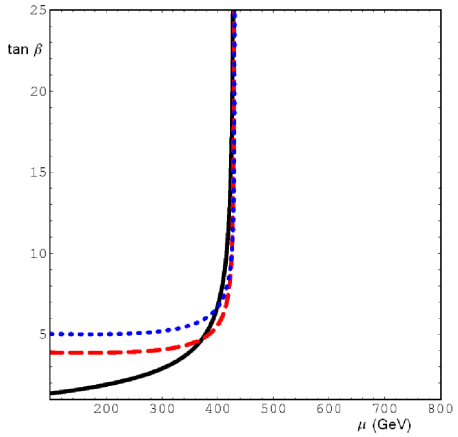

Figure 2.1: Contours of 1% fine-tuning in the $(\mu, \tan\beta)$ plane. The black (solid) contour corresponds to $m_A = 100$ GeV, but remains essentially unchanged for any value of m_A in the range between 100 and 1000 GeV. The red (dashed) and blue (dotted) contours correspond to $m_A = 1.5$ and 2 TeV, respectively.

2.2.1 Constraints on the Higgs Sector

At tree level, the Z mass in the MSSM is given by

$$m_Z^2 = -m_u^2\left(1 - \frac{1}{\cos 2\beta}\right) - m_d^2\left(1 + \frac{1}{\cos 2\beta}\right) - 2|\mu|^2\,, \tag{2.2.8}$$

where

$$\sin 2\beta = \frac{2b}{m_u^2 + m_d^2 + 2|\mu|^2}\,. \tag{2.2.9}$$

Following Barbieri and Guidice [22], we quantify fine-tuning by computing

$$A(\xi) = \left|\frac{\partial \log m_Z^2}{\partial \log \xi}\right|, \tag{2.2.10}$$

where $\xi = m_u^2, m_d^2, b, \mu$ are the relevant Lagrangian parameters. In terms of the physical parameters (2.2.5), we obtain

$$\begin{aligned}
A(\mu) &= \frac{4\mu^2}{m_Z^2}\left(1+\frac{m_A^2+m_Z^2}{m_A^2}\tan^2 2\beta\right), \\
A(b) &= \left(1+\frac{m_A^2}{m_Z^2}\right)\tan^2 2\beta, \\
A(m_u^2) &= \left|\frac{1}{2}\cos 2\beta + \frac{m_A^2}{m_Z^2}\cos^2\beta - \frac{\mu^2}{m_Z^2}\right| \times \left(1-\frac{1}{\cos 2\beta}+\frac{m_A^2+m_Z^2}{m_A^2}\tan^2 2\beta\right), \\
A(m_d^2) &= \left|-\frac{1}{2}\cos 2\beta + \frac{m_A^2}{m_Z^2}\sin^2\beta - \frac{\mu^2}{m_Z^2}\right| \times \left|1+\frac{1}{\cos 2\beta}+\frac{m_A^2+m_Z^2}{m_A^2}\tan^2 2\beta\right|,
\end{aligned} \tag{2.2.11}$$

where we assumed $\tan\beta > 1$. The overall fine-tuning Δ is defined by adding the four A's in quadruture; values of Δ far above one indicate fine-tuning. For concreteness, we will require $\Delta \leq 100$, corresponding to fine tuning of 1% or better. This requirement maps out the golden region in the space of $(\tan\beta, \mu, M_A)$, as illustrated in figure 2.1. (We do not plot $\mu < 100$ GeV, since this region is ruled out by LEP2 chargino searches.) The shape of this region is easily understood. In the limit of large $\tan\beta$, the parameters $A(m_u^2)$ and $A(m_d^2)$ are small, and $A(\mu)$ and $A(b)$ (considered separately) lead to constraints

$$\frac{\mu}{m_Z} < \frac{\Delta_{\max}^{1/2}}{2}, \quad \frac{m_A}{m_Z} < \frac{\Delta_{\max}^{1/2}}{2}\tan\beta\,, \tag{2.2.12}$$

which are clearly reflected in Fig. 2.1. As β approaches $\pi/4$, the factors of $1/\cos 2\beta$ and $\tan 2\beta$, present in all four A parameters, become large, and as a result the model is always fine-tuned for $\tan\beta \lesssim 2$.

2.2.2 Constraints on the Top Sector

Naturalness also constrains the size of the quantum corrections to the parameters in Eq. (2.2.8). The largest correction in the MSSM is the one-loop contribu-

tion to the m_u^2 parameter from top and stop loops:

$$\begin{aligned}\delta m_{H_u}^2 &\approx \frac{3}{16\pi^2}\left(y_t^2\left(\tilde{m}_{Q_3}^2+\tilde{m}_{t^c}^2\right)+y_t^2(A_t\sin\beta-\mu\cos\beta)^2\right)\\ &\quad\times\log\frac{2\Lambda^2}{\tilde{m}_{Q_3}^2+\tilde{m}_{t^c}^2}\\ &\approx \frac{3}{16\pi^2}\left(y_t^2\left(\tilde{m}_1^2+\tilde{m}_2^2-2m_t^2\right)+\frac{(\tilde{m}_2^2-\tilde{m}_1^2)^2}{4v^2}\sin^2 2\theta_t\right)\\ &\quad\times\log\frac{2\Lambda^2}{\tilde{m}_1^2+\tilde{m}_2^2}\,,\end{aligned} \tag{2.2.13}$$

where m_t is the top mass, Λ is the scale at which the logarithmic divergence is cut off, and finite (matching) corrections have been ignored. The correction induced by this effect in the Z mass is

$$\delta_t m_Z^2 \approx -\delta m_{H_u}^2\left(1-\frac{1}{\cos 2\beta}\right), \tag{2.2.14}$$

where we ignored the renormalization of the angle β by top/stop loops: the contribution of this effect scales as $1/\tan^2\beta$ and is subdominant for $\tan\beta \gtrsim 2$. To measure the fine-tuning between the bare (tree-level) and one-loop contributions, we introduce

$$\Delta_t = \left|\frac{\delta_t m_Z^2}{m_Z^2}\right|. \tag{2.2.15}$$

Choosing the maximum allowed value of Δ_t selects a region in the stop sector parameter space, $(\tilde{m}_1, \tilde{m}_2, \theta_t)$, whose shape is approximately independent of the other parameters.[5] This constraint is shown by the black (dashed) lines in Figs. 2.2, where we plot 5%, 3%, 1% and 0.5% tuning contours (corresponding to $\Delta_t = 20, 33.3, 100$, and 200, respectively) in the stop mass plane for several values of θ_t and $\tan\beta = 10$. Note that the particular values of Δ_t depend on the scale Λ; we choose it to be 100 TeV in this figure. However, the shape of the contours and the obvious trend for tuning to increase with the two stop masses is independent of Λ.

[5]Note that we choose not to combine the tree-level and quantum fine-tuning measures into a single tuning parameter; doing so would make the analysis less transparent without producing

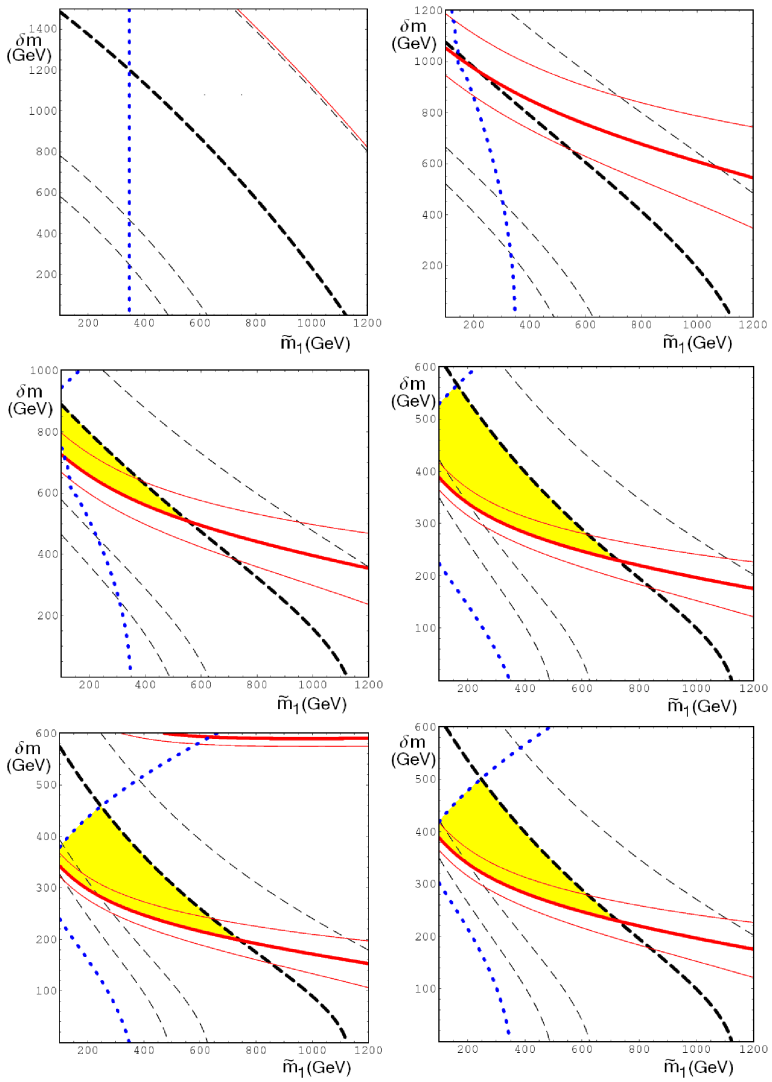

Figure 2.2: Fine-tuning (black/dashed contours), Higgs mass bound (red/colid contours), and ρ-parameter (blue/dotted contours) constraints in the ($\tilde{m}_1$, δm) plane. The six panels correspond to (starting from the upper-left corner, clockwise): $\theta_t = 0, \pi/25, \pi/15, \pi/6, \pi/4, \pi/3$. In all panels $\tan\beta = 10$. The yellow/shaded intersection of the regions allowed by the three constraints is the MSSM "golden" region.

The second constraint that determines the shape of the golden region is the LEP2 lower bound on the Higgs mass [23]. For generic MSSM parameter values,

additional physical insights.

the limit on the lightest CP-even Higgs is very close to that for the SM Higgs:

$$m(h^0) \gtrsim 114\,\mathrm{GeV}. \tag{2.2.16}$$

It is possible for a lighter Higgs (down to about 90 GeV) to be consistent with the negative results of the LEP2 searches; however, this requires precise coincidence between $m(h^0)$ and m_A, which should be regarded as additional source of fine-tuning. Thus, we will use the LEP2 bound for the SM Higgs [24], 114.4 GeV, as the lower bound on $m(h^0)$ in this analysis. At tree level, the MSSM predicts $m(h^0) \leq m_Z |\cos 2\beta|$, and large loop corrections are required to satisfy this bound. Extensive calculations of these corrections have been performed in the literature (for a recent summary of the status of these calculations, see Ref. [25]). Complete one-loop corrections within the MSSM are known. The dominant one-loop contribution is from top and stop loops; for $\tan\beta \gtrsim 35$, the sbottom loop contribution is also important. The two-loop corrections to these contributions from strong and Yukawa interactions are also known. Numerical packages incorporating these results are available [26–29]. For our purposes here, however, it is convenient to use a simple analytic approximation, due to Carena *et. al.* [30], which includes the one-loop and leading-log two-loop contributions from top and stop loops:

$$\begin{aligned} m^2(h^0) &= m_Z^2 \cos^2 2\beta \left(1 - \frac{3}{8\pi^2}\frac{m_t^2}{v^2}\, t\right) \\ &+ \frac{3}{4\pi^2}\frac{m_t^4}{v^2}\left[\frac{1}{2}X_t + t + \frac{1}{16\pi^2}\left(\frac{3}{2}\frac{m_t^2}{v^2} - 32\pi\alpha_3\right)\left(X_t t + t^2\right)\right] \end{aligned} \tag{2.2.17}$$

where α_3 is the strong coupling constant evaluated at the pole top quark mass M_t; $m_t = M_t/(1 + \frac{4}{3\pi}\alpha_3)$ is the on-shell top mass; and

$$\begin{aligned} X_t &= \frac{2(A_t - \mu\cot\beta)^2}{M_{\mathrm{susy}}^2}\left(1 - \frac{(A_t - \mu\cot\beta)^2}{12 M_{\mathrm{susy}}^2}\right), \\ t &= \log\frac{M_{\mathrm{susy}}^2}{M_t^2}. \end{aligned} \tag{2.2.18}$$

The scale $M^2_{\rm susy}$ is defined as the arithmetical average of the diagonal elements of the stop mass matrix. The expression (2.2.17) is valid when the masses of all superparticles, as well as the CP-odd Higgs mass m_A, are of order $M_{\rm susy}$. Additional threshold corrections may be required, for example, if $m_A < M_{\rm susy}$; for simplicity, we will ignore such corrections here. Eq. (2.2.17) agrees with the state-of-the-art calculations to within a few GeV for typical MSSM parameters [25]; while such accuracy is clearly inadequate for precision studies, it is sufficient for the present analysis.[6]

The contours in the stop mass plane corresponding to the LEP2 Higgs mass bound are superimposed on the fine-tuning contours in Figs. 2.2. The positions of these contours depend strongly on the top quark mass. We used $M_t = 171.4 \pm 2.1$ GeV [31], and plotted the constraint corresponding to the central value (thick red/solid lines), as well as the boundaries of the 95% c.l. band (thinner red/solid lines). The contours are approximately independent of $\tan\beta$ for $3 \lesssim \tan\beta \lesssim 35$; the golden region shrinks rapidly outside of this range of $\tan\beta$. We use $\tan\beta = 10$ in the plots. The overlap between the regions of acceptably low fine-tuning (for definiteness, we choose $\Delta_t = 100$) and experimentally allowed Higgs mass defines the golden region, shaded in yellow in Figs. 2.2.

[6] We also verified that the Higgs mass at the benchmark point used for the collider phenomenology analysis in this chapter satisfies the LEP2 bound with a more precise numerical calculation using `SuSpect`; see Section 3.

2.2.3 Collider Bounds, Precision Electroweak Constraints and Rare Decays

Apart from the Higgs mass bound, several other observables constrain the shape of the golden region.

First, direct collider bounds play a role in determining the boundary at low μ and $\tilde{m}_1$: LEP2 searches for direct production of charginos and stops constrain both μ and $\tilde{m}_1$ to be above ≈ 100 GeV, and are to a large extent independent of the rest of the MSSM parameters. (At large $\tan\beta$, it can be easily shown that $m(\chi_1^\pm) < |\mu|$ for any M_2.) The Tevatron stop searches yield a similar (though more model-dependent) bound on $\tilde{m}_1$. A sbottom search in the $b\chi_1^0$ channel (which is relevant because the $\tilde{b}_L$ mass is given by m_{Q^3}, and can be expressed in terms of $\tilde{m}_1$ and $\tilde{m}_2$) places a lower bound $m(\tilde{b}_L) \geq 200$ GeV. However, this bound will not be used in our analysis since it is highly sensitive to the neutralino mass and can be easily evaded if $m(\chi_1^0) > 80$ GeV.

Second, in the presence of a large A_t term, stop and sbottom loops may induce a significant correction to the ρ parameter. This correction is known at the two-loop level [32]; for our purposes, it suffices to use the one-loop result:

$$\begin{aligned}\Delta\rho &= \frac{3G_F}{8\sqrt{2}\pi^2}\Big(-\sin\theta_t^2\cos\theta_t^2 F_0(\tilde{m}_1^2,\tilde{m}_2^2) + \cos^2\theta_t F_0(\tilde{m}_1^2, m_{\tilde{b}_L}^2) \\ &\quad + \sin^2\theta_t F_0(\tilde{m}_2^2, m_{\tilde{b}_L}^2)\Big)\,, \end{aligned} \tag{2.2.19}$$

where

$$F_0(a,b) = a + b - \frac{2ab}{a-b}\log\frac{a}{b}. \tag{2.2.20}$$

Expressing $m_{\tilde{b}_L}$ in terms of $\tilde{m}_1$, $\tilde{m}_2$ and θ_t, and using the PDG value $\rho = 1.0002\ ^{+0.0004}_{-0.0007}$ [24], we obtain the 95% c.l. contours in the stop mass plane shown

by the blue/dotted lines in Figs. 2.2. This constraint eliminates a part of the parameter space with very low $\tilde{m}_1$ and large δm.

Finally, several low-energy measurements play a role in constraining the MSSM parameter space; among these, the $b \to s\gamma$ decay rate [33–36] and the anomalous magnetic moment of the muon, $g_\mu - 2$ [37], provide the most stringent constraints. The supersymmetric contribution to $g_\mu - 2$ depends sensitively on the slepton and weak gaugino mass scales, and only weakly on the parameters defining the golden region. On the other hand, since the golden spectrum contains light stops and higgsinos, we can expect a large contribution to the $b \to s\gamma$ rate from the $\tilde{t} - \tilde{H}$ loop. It is well known, however, that this can be cancelled by the contribution of the top-charged Higgs loop. A simplified analysis of this constraint based on the one-loop analytic formulas presented in Ref. [38] shows that for *any* values of the stop masses inside the golden region in Figs. 2.2, and for any value of μ between 100 and 500 GeV, one can find values of m_A in the 100-1000 GeV range for which this cancellation ensures consistency with experiment. (Recall that $m^2(H^\pm) = m_A^2 + m_W^2$.) For low $\tilde{m}_1$ and μ, however, the cancellation only occurs in a narrow band of m_A, which can be thought of as an additional source of fine tuning. A detailed analysis of this issue is outside the scope of this inquiry.

2.3 A Benchmark Point for Collider Studies

The analysis of Section 2 defined the golden region in the six-dimensional parameter space (2.2.5); its shape is approximately independent of the other MSSM parameters. This region has the following interesting qualitative features:

Table 2.1: The benchmark point: MSSM input parameters, defined at the weak scale. (All dimensionful parameters are in GeV.)

m_{Q^3}	m_{u^3}	m_{d^3}	A_t	μ	m_A	$\tan\beta$	M_1	M_2	M_3	$m_{\tilde{q}}$	$m_{\tilde{\ell}}$
548.7	547.3	1000	1019	250	200	10	1000	1000	1000	1000	1000

Table 2.2: The benchmark point: physical spectrum. All masses are in GeV. The masses of the superparticles not listed here are close to 1 TeV.

$\tilde{m}_1$	$\tilde{m}_2$	$m_{\tilde{b}_L}$	$m(\chi_1^0)$	$m(\chi_2^0)$	$m(\chi_1^\pm)$	m_{h^0}	m_{H^0}	m_A	$m_{H^\pm}$
400	700	552	243	253	247	128.6	201	200	250

- Both stops typically have masses below 1 TeV;
- A substantial mass splitting between the two stop quarks is required: typically,

  $\delta m \gtrsim 200$ GeV;
- The stop mixing angle must be non-zero: there is no intersection between the naturalness and Higgs mass constraints for $\theta_t = 0, \pi/2$.

The first feature implies that both $\tilde{t}_1$ and $\tilde{t}_2$ will be produced with sizeable cross sections at the LHC, so that the stop sector can be studied directly experimentally. The second feature implies that the decay mode $\tilde{t}_2 \to \tilde{t}_1 Z$ is kinematically allowed. The vertex responsible for this decay is given by

$$\frac{1}{2}\sin 2\theta_t \, \frac{g}{c_w}\left(\frac{1}{2} - \frac{4}{3}s_w^2\right), \tag{2.3.21}$$

where c_w and s_w are the cosine and sine of the SM Weinberg angle. The last of the three points above then guarantees that the vertex is non-zero, and the decay $\tilde{t}_2 \to \tilde{t}_1 Z$ indeed occurs.

The branching ratio of the $\tilde{t}_2 \to \tilde{t}_1 Z$ mode depends on which competing $\tilde{t}_2$ decay channels are available. The possible two-body channels are

$$t\tilde{g}, \quad t\tilde{\chi^0}, \quad b\tilde{\chi^+}, \quad \tilde{b}W^+, \quad \tilde{b}H^+, \quad \tilde{t}_1 h^0, \quad \tilde{t}_1 H^0, \quad \tilde{t}_1 A^0, \tag{2.3.22}$$

where $\tilde{\chi^0}$ and $\tilde{\chi^+}$ denote all the neutralinos and charginos that are kinematically accessible, and flavor-changing couplings are assumed to be negligible.

We would like to evaluate the prospects for observing the $\tilde{t}_2 \to \tilde{t}_1 Z$ decay mode at the LHC. For concreteness, we choose a benchmark point (BP) within the golden region, and perform a detailed analysis of the signal at this point (see Section 4). The BP is defined in terms of the weak-scale MSSM parameters. We assume that all soft parameters are flavor-diagonal. Further, we assume a common soft mass for the first and second generation squarks, $m_{\tilde{q}} = m_{Q^{1,2}} = m_{u^{1,2}} = m_{d^{1,2}}$, and for all sleptons, $m_{\tilde{\ell}} = m_{L^{1,2,3}} = m_{e^{1,2,3}} = m_{\nu^{1,2,3}}$. All A terms have been set to zero, with the exception of A_t. The parameters defining the BP are listed in Table 2.1. The top and Higgs sector parameters are chosen so that the BP is comfortably inside the golden region, well away from the boundaries, and is representative of this region. In particular, the lightest Higgs mass at the BP is well above the LEP bound. (The physical spectrum of the model at the BP was computed using the `SuSpect` software package [29] and is listed in Table 2.2.) Gaugino, slepton, and first and second generation squark masses are set at 1 TeV. Varying these parameters does not have a significant effect on the stop production rate and decay patterns, and thus the conclusions of the analysis in Section 4 are largely independent of these choices. Using `SuSpect`, we checked that the $b \to s\gamma$ branching ratio, the ρ parameter and the supersymmetric contribution to the muon anomalous magnetic moment at the BP are consistent with the current experimental constraints.

Table 2.3: The benchmark point: branching ratios of $\tilde{t}_2$ decay modes, in %.

$\tilde{t}_1 Z$	$\chi_1^0 t$	$\chi_2^0 t$	$\chi_1^+ b$	$\tilde{b} W^+$	$\tilde{t}_1 A$	$\tilde{t}_1 h^0$	$\tilde{t}_1 H^0$
31	19	13	18	15	3	3×10^{-3}	3×10^{-4}

The $\tilde{t}_2$ decay branching ratios at the BP were evaluated using the SDECAY package [39], and are listed in Table 2.3. The $\tilde{t}_2 \to \tilde{t}_1 Z$ mode has a substantial branching ratio, about 31%. Note that of the possible $\tilde{t}_2$ decay modes listed in Eq. (2.3.22), only the $t\tilde{g}$ channel is kinematically forbidden at the BP. If the gluino mass were lowered to allow this decay, the branching ratio of the $\tilde{t}_2 \to \tilde{t}_1 Z$ mode would be suppressed. However, this effect is not dramatic: we checked that if M_3 is varied between 300 and 1000 GeV, keeping all other MSSM parameters fixed at their values listed in Table 2.1, we still obtain $\mathrm{Br}(\tilde{t}_2 \to \tilde{t}_1 Z) \gtrsim 17\%$. This is an example of the robustness of the stop decay pattern with respect to the variations of the non-stop sector MSSM parameters, mentioned above.

2.4 Observability of the $Z + 2j_b + \not{E}_T + X$ Signature at the LHC

Stop pair production cross section at the LHC, computed using the MadGraph/MadEvent v4 software package [40], is shown in Fig. 2.3. At the benchmark point, we find $\sigma(pp \to \tilde{t}_2 \tilde{t}_2^*) = 0.05$ pb, corresponding to about 500 $\tilde{t}_2$ pairs per year at the initial design luminosity of 10 fb^{-1}/year. The produced $\tilde{t}_2$ decays promptly, with branching ratios listed in Table 2.3; in about 52% of the events, either one or both of the produced stops decays in the $\tilde{t}_1 Z$ mode. This

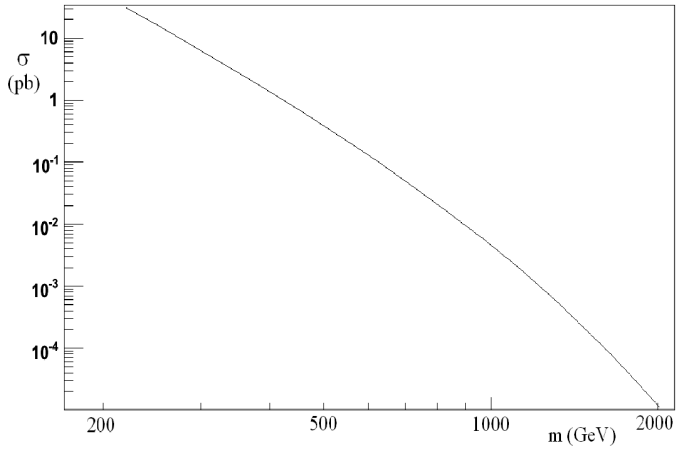

Figure 2.3: Cross section of the process $pp \to \tilde{t}\tilde{t}^*$ at the LHC, $\sqrt{s} = 14$ TeV, at tree level. Factorization and renormalization scales were set to $\mu = M_{\tilde{t}}$, and the CTEQ6L1 parton distribution function set [1] was used.

decay is followed by a cascade

$$\begin{aligned} \tilde{t}_1 \to \chi_1^+ b, \quad \chi_1^+ &\to u\bar{d}\chi_1^0 \,/\, c\bar{s}\chi_1^0, \\ &\to \ell^+\nu\chi_1^0, \end{aligned} \tag{2.4.23}$$

where the jets and leptons produced in the χ_1^+ decays are very soft due to a small chargino-neutralino mass splitting. The details of this cascade are particular to the chosen BP, and are quite model-dependent. There are, however, two model-independent features true for all $\tilde{t}_2$ and $\tilde{t}_1$ decays: the cascade always contains a b jet (produced either directly or via top decay), and it always ends with the lightest supersymmetric particle (LSP), the neutralino χ_1^0, giving a missing transverse energy signature. In order to make the analysis as model-independent as possible, we focus on an inclusive signature,

$$Z(\ell^+, \ell^-) + 2j_b + \not{E}_T + X, \tag{2.4.24}$$

where $Z(\ell^+, \ell^-)$ denotes a lepton pair ($\ell = e$ or μ) with the invariant mass at the Z peak. The presence of energetic leptons ensures that essentially all such events will be triggered on; we will assume a triggering probability of 1 for this analysis. Note that events with hadronic Z decays may in principle be triggered on due to large $\not{E}_T$; however, this sample would suffer from a severe background of purely QCD events with apparent $\not{E}_T$ due to jet energy mismeasurement, and it will not be used in our study. Note also that the requirement that both jets be b-tagged can be relaxed, as will be discussed below. While a cleaner sample is obtained if two b-tags are required, this sample is smaller due to the less-than-perfect tagging efficiency, which may be relevant since the signal rates are not large.

To assess the observability of the signature (2.4.24), we have simulated a statistically significant event sample for the signal and several SM background channels[7] using the `MadGraph/ MadEvent v4` software package [40]. This tool package allows us to generate both SM and MSSM processes, so that the signal and backgrounds can be treated uniformly. The parton level events generated by `MadEvent` were recorded in the format consistent with the Les Houches accord [41, 42]. These events were then passed on to the `Pythia` package [43, 44], which was used to simulate showering and hadronization, as well as the decays of unstable particles. Finally, the `Pythia` output was processed by the PGS 3.9 package [45], which provides a simple and realistic simulation of the response of a "typical" particle detector. (A more detailed analysis of the detector effects using complete ATLAS and CMS detector simulation packages would clearly be interesting, but is outside the scope of this study.) The final output was analyzed

[7] At the chosen benchmark point, the events containing $\tilde{t}_2 \to \tilde{t}_1 Z$ are the only non-SM source of the signature (2.4.24), so there are no "signal backgrounds". Possible alternative interpretations of this signature in the general MSSM context are discussed below in Section 2.5.

with ROOT, using only detector level information for event reconstruction.

The following SM backgrounds have been considered in detail:

- $jjZZ$, which can produce the signature (2.4.24) if one Z decays invisibly and the other one is reconstructed in $\ell^+\ell^-$;
- $t\bar{t}Z$, with $Z \to \ell^+\ell^-$ and one or both tops decaying leptonically (with $\not{E}_T$ due to neutrinos), or both tops decaying hadronically (with $\not{E}_T$ due to jet energy mismeasurement).
- $t\bar{t}$, with both tops decaying leptonically and the invariant mass of the two leptons accidentally close to m_Z.

The total production cross sections (with $p_{T,\text{jet}}^{\text{min}} = 50$ GeV for the $jjZZ$ channel) and the size of the event sample used in our analysis for each channel are listed in the first two rows of Table 2.4. To identify the events matching the signature (2.4.24), we impose the following set of requirements on the event sample:

1. Two opposite-charge same-flavor leptons must be present with $\sqrt{s(\ell^+\ell^-)} = M_Z \pm 2$ GeV.
2. Two hard jets must be present, with $p_T > 125$ GeV for the first jet and $p_T > 50$ GeV for the second jet;
3. At least one of the two highest-p_T jets must be b-tagged;
4. The boost factor of the Z boson, $\gamma(Z) = 1/\sqrt{1 - v_Z^2}$, reconstructed from the lepton pair, must be larger than 2.0;
5. A missing E_T cut, $\not{E}_T > 225$ GeV.

Table 2.4: Summary of the analysis of observability of the supersymmetric golden region signature (2.4.24). First row: Production cross section for the signal and background processes at the LHC. Second row: Number of Monte Carlo events used in the analysis. Rows 3–8: Cut efficiencies, in%. Last row: The expected number of events for an integrated luminosity of 100 fb^{-1}.

	signal: $\tilde{t}_2\tilde{t}_2^*$	$jjZZ$	$t\bar{t}Z$	$t\bar{t}$	jjZ
$\sigma_{\rm prod}$(pb)	0.051	0.888	0.616	552	824
total simulated	9964	159672	119395	3745930	1397940
1. leptonic Z(s)	1.4	4.5	2.6	0.04	2.1
2(a). $p_t(j_1) > 125$ GeV	89	67	55	21	41
2(b). $p_t(j_2) > 50$ GeV	94	93	92	76	84
3. b-tag	64	8	44	57	5
4. $\gamma(Z) > 2.0$	89	66	69	26	68
5. $\not{E}_T > 225$ GeV	48	2.2	4.4	1.7	< 0.9 (95% c.l.)
$N_{\rm exp}(100\ fb^{-1})$	16.4	2.8	10.8	8.8	< 177 (95% c.l.)

e

The efficiencies of these cuts are given in Table 2.4, and the $\not{E}_T$ distribution of the events passing cuts 1–4 is shown in Figure 2.4. While the overall rate of the SM background processes is much higher than the signal rate, the cuts 1-5 are quite effective in discriminating signal from background. Assuming that the search is statistics-limited, we estimate that a 3-sigma observation would require 75 fb^{-1} of data, while a definitive 5-sigma discovery is possible with 210 fb^{-1}. Note that one important contribution to the background, from the $t\bar{t}$ channel, can be effectively measured from data by measuring the event rates with dilepton invariant masses away from the Z peak and performing shoulder subtraction. This procedure is likely to be statistics-limited. However, systematic uncertainties in other background contributions could play a role in limiting the reach, and should be studied carefully with a more detailed detector simulation.

We also briefly considered several other irreducible SM backgrounds which are expected to be less significant than the ones listed in Table 2.4, but might

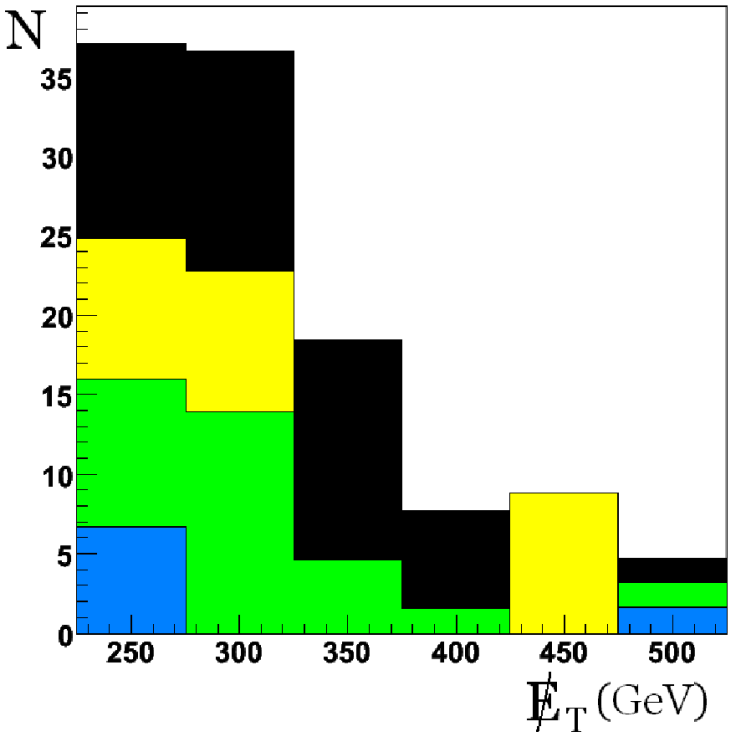

Figure 2.4: Missing E_T distribution of the events passing cuts 1–4. Signal is shown in black; $jjZZ$, $t\bar{t}Z$ and $t\bar{t}$ backgrounds are shown in blue/dark-gray, green/gray, and yellow/light-gray, respectively. The normalization corresponds to an integrated luminosity of 300 fb^{-1} at the LHC.

nevertheless be relevant. The most important one of these is $t\bar{t}j$, where j is a hard jet. The cross section for this channel is suppressed compared to $t\bar{t}$, but the presence of the additional hard jet increases the probability that the events will pass the jet p_T cut (cut 2). We find a parton-level cross section $\sigma(t\bar{t}j, p_T^j > 125\ \mathrm{GeV}) = 65$ pb. Assuming conservatively that all these events pass the cut 2, and that the efficiencies of all other cuts are the same as for the $t\bar{t}$ sample, we expect that this background would add at most about 50% to the $t\bar{t}$ rate. As in the $t\bar{t}$ case, this contribution can be subtracted using data away from the Z peak in the lepton invariant mass distribution. Assuming that the statistical error

dominates this subtraction, the net effect would be an increase in the integrated luminosity required to achieve the same level of significance by at most about 10%.[8] Other backgrounds we considered are three vector boson channels ZZZ, ZZW, and ZWW; as well as channels with single top production, tZj and $\bar{t}Zj$. Combining the parton-level cross sections for these channels with the branching ratios of decays producing the signature (2.4.24) results in event rates that are too small to affect the search.

While the SM processes considered above genuinely produce the signature (2.4.24), other SM processes may contribute to the background due to detector imperfections. We expect that the dominant among these is the process jjZ, with $Z \to \ell^+\ell^-$ and apparent $\not{E}_T$ due to jet energy mismeasurement or other instrumental issues. We conducted a preliminary investigation of this background by generating and analyzing a sample of 1.4×10^6 jjZ events with $p_{T,\mathrm{jet}}^{\mathrm{min}} = 50$ GeV (see the last column of Table 2.4). None of the events in this sample pass the cuts 1-5. This allows us to put a 95% c.l. bound on the combined efficiency of this set of cuts for the jjZ sample of about 2×10^{-6}, corresponding to a background rate about 10 times larger than the signal rate. However, we expect that the actual jjZ background rate is well below this bound, since all 349 events in our sample that pass the cuts 1–4 in fact have $\not{E}_T$ below 50 GeV. We find that the $\not{E}_T$ distribution of these 349 events can be fit with an exponential, $N \propto e^{-0.10\not{E}_T}$, where $\not{E}_T$ is in units of GeV. Assuming that this scaling adequately describes the tail of the distribution at large $\not{E}_T$, we estimate that the rate of jjZ events passing all 5 cuts is completely negligible and that this background should not present a

[8] The $t\bar{t}j$ background may be suppressed very effectively by requiring that *the hardest* jet be b-tagged (as oppossed to one of the two hardest jets in our main analysis), since the extra jet is always initiated by a gluon or a light quark. However this would also reduce the signal and all other backgrounds by about a half due to the lower probability of tagging a single jet, resulting in lower significance.

Table 2.5: Same as Table 2.4, with an alternative set of requirements including 2 b-tagged jets.

	signal: $\tilde{t}_2\tilde{t}_2^*$	$jjZZ$	$t\bar{t}Z$	$t\bar{t}$	jjZ
$\sigma_{\rm prod}$(pb)	0.051	0.888	0.616	552	824
total simulated	9964	159672	119395	3745930	1397940
1. leptonic Z(s)	1.4	4.5	2.6	0.04	2.1
2(a). $p_t(j_1) > 125$ GeV	89	67	55	21	41
2(b). $p_t(j_2) > 50$ GeV	94	93	92	76	84
3. 2 b-tags	22	0.4	6	9	0.3
4. $\not{E}_T > 225$ GeV	56	< 2	< 5	< 3	< 10 (95% c.l.)
$N_{\rm exp}(100\ fb^{-1})$	7	< 2.4	< 2.7	< 8.8	< 177 (95% c.l.)

problem. This conclusion is of course rather preliminary, and this issue should be revisited once the performance of the LHC detectors is understood using real data. Note that the necessity to understand the shape and normalization of the large apparent $\not{E}_T$ tail from SM processes with large cross sections is not unique to the signature discussed here, but is in fact crucial for most SUSY searches at the LHC.

As an alternative, we considered a variation of the analysis where the cuts 1, 2, and 5 are unchanged, cut 4 is eliminated, and *two* b-tagged jets are required. The cut efficiencies for this analysis are summarized in Table 2.5. Unfortunately, the Monte Carlo samples used in our analysis are not large enough to reliably estimate the efficiencies of this set of cuts applied to the backgrounds, since only one event out of all background samples passes the cuts. Therefore we list the 95% c.l. upper bounds on the efficiencies, and on the number of background events expected for a 100 fb^{-1} event sample, in the table. It is clear that while the second b-tag is quite efficient in improving the S/B ratio, this search suffers from low statistics, with only 7 signal events expected in a 100 fb^{-1} data sample.

To summarize, our analysis indicates that, for the MSSM parameters at the benchmark point, the signature (2.4.24) of the split-stop spectrum can be discovered at the LHC. The chosen BP is typical of the golden region, and this conclusion should generally hold as the MSSM parameters are varied away from the BP, scanning this region. There are, however, several exceptional parts of the parameter space where the observability of this signature could be substantially degraded. These include:

- Large $\tilde{m}_2$ region: The $\tilde{t}_2$ production cross section drops rapidly with its mass, see Fig. 2.3, suppressing the signal rates;
- Small θ_t region: While non-zero θ_t is required in the golden region, values as small as $\theta_t = \pi/15$ are allowed (see Fig. 2.2). The branching ratio Br($\tilde{t}_2 \to Z\tilde{t}_1$) is proportional to $\sin^2 2\theta_t$, see Eq. (2.3.21), and the event rate is suppressed at small θ_t;
- Small $\tilde{t}_1$-LSP mass difference: The absence of hard jets in this case would make the signal/background discrimination more difficult.

In these special regions, observing the signature (2.4.24) may not be feasible at the LHC. These limitations should be kept in mind when theoretical interpretation of a search for the signature (2.4.24) is given.

2.5 Alternative Interpretations of the $Z + 2j_b + \not{E}_T + X$ Signature

Unfortunately, observing an excess of events in the channel (2.4.24) at the LHC does not prove that the decay $\tilde{t}_2 \to \tilde{t}_1 Z$ is occuring. Even within the MSSM,

this is not the only possible interpretation of such an excess. The simplest alternative interpretation is stop or sbottom production, followed by a cascade decay containing a b quark and a Z boson from a neutralino or chargino decay: $\chi_j^0 \to \chi_i^0 Z$ (due to the higgsino components of the neutralinos) or $\chi_2^\pm \to \chi_1^\pm Z$. Can this alternative interpretation be ruled out based on data?

One useful input for discriminating between these two interpretations is whether a signal is observed in a search identical to the one presented in Section 2.4, but requiring that the jets *not* be b-tagged. If the signal is due to $\tilde{t}_2 \to \tilde{t}_1 Z$, all signal events contain energetic b quarks, and the number of events in this search would be zero if b tagging were perfect. The actual number of expected events under realistic conditions can be deduced from the error rate in b tagging, which can be measured elsewhere. If the signal is due to $\chi_j^0 \to \chi_i^0 Z$ or $\chi_2^\pm \to \chi_1^\pm Z$, it does not have to be associated preferentially with third-generation squark production, and the number of events without b tags could be substantially larger than this expectation. This argument could be used to rule out the $\tilde{t}_2 \to \tilde{t}_1 Z$ interpretation. Unfortunately, however, it cannot be used to confirm it: the pattern consistent with the $\tilde{t}_2 \to \tilde{t}_1 Z$ interpretation may also appear if the events are actually due to chargino or neutralino decays, provided that the first two generations of squarks are substantially heavier than their counterparts of the third generation and their production cross section is suppressed. A direct measurement of the squark masses could break this degeneracy. If the first two generations of squarks were found to be light, but no signal is seen in $Z + 2j + \not\!\!E_T$ with non-b jets, the "split stop" interpretation of the signal (2.4.24) would be preferred.

A more direct way to discriminate between the two interpretations would be

Figure 2.5: Cascade decays in the MSSM leading to the $Z + 2j + \not{E}_T$ signature: (a) the chain characteristic of the golden region; (b) an alternative chain.

to study the distribution of the events as a function of the Z-jet invariant mass $s_{jZ} \equiv (p_j + p_Z)^2$. This strategy is the same as the recently proposed method of discriminating between SUSY and alternative theories with same-spin "superpartners" [46–48], but in this case it is applied to distinguishing two processes within the MSSM. Consider the Feynman diagrams corresponding to the two interpretations of the signal, shown in Figure 2.5. In the case of $\tilde{t}_2 \to \tilde{t}_1 Z$ decays, the Z and the jet are separated by a scalar (stop) line, and their directions are uncorrelated. In the case of chargino or neutralino decays, the Z and the jet are separated by a fermion line, and spin correlations between their directions are possible. Unfortunately, in the neutralino case, no such correlations occur, because of the non-chiral nature of the $\chi_i^0 \chi_j^0 Z$ coupling [48]. In the chargino case, however, the coupling has the form [2]

$$-\frac{g}{2c_w}\,\bar{\tilde{\chi}}_i \gamma^\mu \left[C_{ij}^L(1-\gamma_5) + C_{ij}^R(1+\gamma_5)\right] \tilde{\chi}_j\,, \tag{2.5.25}$$

where

$$\begin{aligned} C_{ij}^L &= V_{i1}V_{j1}^* + \frac{1}{2}V_{i2}V_{j2}^*\,, \\ C_{ij}^R &= U_{i1}^* U_{j1} + \frac{1}{2}U_{i2}^* U_{j2}\,. \end{aligned} \tag{2.5.26}$$

Here, U and V are the rotations of the negatively-charged and positively-charged charginos, respectively, required to diagonalize the chargino mass matrix. Since in general $U \neq V$, the couplings (2.5.25) are generically chiral. The stop-bottom-chargino coupling is also generically chiral: it has the form

$$\bar{b}(A^L_{ij}P_R + A^R_{ij}P_L)\tilde{\chi}^c_i\tilde{t}_j, \tag{2.5.27}$$

which can be equivalently rewritten as

$$\bar{\tilde{\chi}}_i(A^L_{ij}P_R + A^R_{ij}P_L)b^c\tilde{t}_j. \tag{2.5.28}$$

Here

$$\begin{aligned} A^L_{ij} &= gV_{i1}R^t_{j1} + \frac{y_t}{s_\beta}V_{i2}R^t_{j2}\,, \\ A^R_{ij} &= \frac{y_b}{c_\beta}U_{i2}R^t_{j1}\,, \end{aligned} \tag{2.5.29}$$

where R^t is the matrix diagonalizing the stop masses: $(\tilde{t}_1, \tilde{t}_2)^T = R^t(\tilde{t}_L, \tilde{t}_R)^T$. Squaring the matrix element $\mathcal{M}$ for the decay $\tilde{t}_j \to b + Z + \chi_1^+$, see Fig. 2.5 (b), and summing over the final-state polarizations yields

$$\sum_{\text{pol}} |\mathcal{M}|^2 \propto (|A^L_{j2}|^2 - |A^R_{j2}|^2)\,(|C^L_{12}|^2 - |C^R_{12}|^2)\,s_{bZ} + \text{const}, \tag{2.5.30}$$

where the constant terms do not depend on s_{bZ}, narrow-width approximation for $\chi_2^\pm$ has been used, and the b quark mass was neglected. The charge-conjugate decay $\tilde{t}^*_j \to \bar{b} + Z + \chi_1^-$ has the same asymmetry. Observing a linear dependence of the event rate on s_{bZ} would provide clear evidence against the interpretation of the signal in terms of the process in Fig. 2.5 (a). Of course, in a real experiment, the asymmetry would be partially washed out by combinatoric backgrounds, as well as possible non-chiral decay chains containing the same final state. A detailed analysis of the observability of the correlation in Eq. (2.5.30) is beyond the scope of this study.

While our analysis so far focused on the decay $\tilde{t}_2 \to \tilde{t}_1 Z$ as a signature of the MSSM golden region, there are two other, closely related decays that are also characteristic of this region:

$$\tilde{t}_2 \to \tilde{b}_L W^+, \quad \tilde{b}_L \to \tilde{t}_1 W^-. \tag{2.5.31}$$

For example, at the benchmark point used for the analysis in Section 4, these two decays have branching ratios of 15% and 43%, respectively. Stop or sbottom pair-production followed by these decays leads to a signature

$$W + 2j_b + \not{E}_T + X. \tag{2.5.32}$$

This signature is complementary to the $Z + 2j_b + \not{E}_T + X$ signature studied above. On the one hand, it suffers from higher backgrounds, since the W cannot be fully reconstructed in purely leptonic channels. On the other hand, its interpretation within the MSSM is somewhat cleaner. The leading alternative interpretation of the signature (2.5.32) is that the W's are produced in chargino $\to$ neutralino decays. But the chargino-neutralino coupling is chiral, and the directions of the W and the associated jet are correlated. If the W is sufficiently boosted, this will result in an observable linear dependence of the cross section on $s_{\ell j} \equiv (p_\ell + p_j)^2$, where ℓ is the lepton daughter of the W [48]. If, on the other hand, the W is produced in decays of scalars, such as the processes (2.5.31), the distribution of events in $s_{\ell j}$ should be flat.

To summarize, even if the MSSM is assumed to be the underlying model, the interpretation of events with vector bosons associated with jets and missing E_T is not unambiguous. Careful comparisons of the rates with and without b jets, as well as the distribution of events in vector boson-jet invariant masses, would be required to remove the ambiguity. This may take considerably more data than the discovery of an excess over the SM backgrounds in these channels.

If the MSSM is *not* assumed from the beginning, the question of interpretation becomes even more confusing. For example, in the Littlest Higgs model with T-parity [49–52], Z bosons can be produced in the decay $W_H^3 \to ZB_H$, due to the mixing between the $SU(2)$ and $U(1)$ heavy gauge bosons. A similar decay involving the Kaluza-Klein states of the $SU(2) \times U(1)$ gauge bosons can occur in models with universal extra dimensions (UED) [53, 54]. Again, a careful study of spin correlations would be necessary to disentangle these possibilities. Understanding the nature of such correlations in various models is an interesting direction for future work.

2.6 Conclusions

In this chapter, we discussed an LHC signature of the MSSM characteristic of the "golden region" in the model parameter space. The advantage of this signature is that it directly probes the features of the stop spectrum that are dictated by naturalness and the Higgs mass bound. Experimentally, the signature is not straightforward, but the results of our simulations indicate that it should be within reach at the LHC.

Given the strong theoretical motivation for the signature discussed here, we encourage experimental collaborations to perform a more detailed study of its observability. The analysis of this chapter relied on a set of simple rectangular cuts, and no systematic procedure to optimize the cuts was employed. It is very likely that a better algorithm for signal/background discrimination, perhaps using modern data analysis tools such as neural networks or decision trees, would significantly enhance the reach. On the other hand, it should be noted that we

ignored systematic uncertainties on the background rates in our reach estimates, and that no fully realistic detector simulation was attempted.

If the first round of the LHC results points towards an MSSM-like theory, obtaining experimental information about the stop spectrum, and in particular testing whether the "golden region MSSM" hypothesis is correct, will become an important priority for the LHC experiments. An indirect, complimentary way to shed some light on this issue by identifying the stop loop contributions to the Higgs production cross section and mass has been recently proposed by Dermisek and Low [55]. It would be interesting to explore other experimental consequences of the golden region hypothesis.

CHAPTER 3

A WEAKLY COUPLED ULTRAVIOLET COMPLETION OF THE LITTLEST HIGGS WITH T-PARITY

Published in Physical Review D **79**, 035014 (2009).

3.1 Introduction

One of the most pressing issues facing particle theory is the little hierarchy problem. On the one hand, electroweak precision measurements at LEP and the Tevatron seem to indicate the existence of a weakly coupled light (below 200 GeV) Higgs boson. This Higgs would be unstable against large radiative corrections, and one would expect new physics at or below the TeV scale to stabilize the Higgs potential. On the other hand, the same electroweak precision measurements have failed to provide any indirect evidence for such physics. For the case of supersymmetry (SUSY), a natural minimal model should have already been discovered at LEP2 or the Tevatron: null results of superpartner and Higgs searches imply that a fine-tuning of order 1% or worse is required to accommodate the data, which is the particular incarnation of the little hierarchy problem for SUSY.

The motivation for Little Higgs (LH) models is to solve this issue by pushing the scale of new physics that solves the "large" (weak/Planck) hierarchy problem up to 10 TeV, and provide a rationale for the cancelation of the remaining quadratic divergences in the Higgs mass between 1 TeV and 10 TeV. This is achieved by interpreting the Higgs as an approximate Goldstone boson corre-

sponding to a spontaneously broken global symmetry of the electroweak sector. Gauge and Yukawa couplings of the Higgs must break the global symmetry explicitly; however, if this breaking is "collective" (meaning that no single coupling breaks all of the symmetry responsible for keeping the Higgs light), the extended theory can remain perturbative until the 10 TeV scale without fine-tuning [56, 57]. Several explicit realizations of this idea have appeared in the literature [52, 58]. Models with T-parity are especially promising, since they can be consistent with precision electroweak constraints without need for fine tuning in the Higgs mass [59, 60]. In this thesis, we will focus on the Littlest Higgs model with T-parity (LHT) [49], which is a fully realistic example of this class.

Like all existing Little Higgs models, the LHT has been constructed as an effective field theory, valid below the cutoff scale of order 10 TeV. This is sufficient to discuss the model's consistency with precision electroweak data [51, 61], its signatures at the Tevatron [62] and the LHC [50, 63], and the dark matter candidate that naturally emerges in this model [50, 61, 64, 65]. However, in order to really complete the program outlined above one needs to find the ultraviolet (UV) completion of these models, i.e. embed it into a more fundamental theory valid at higher scales, possibly all the way up to the scale of grand unification (GUT) or the Planck scale. The main aim of this chapter is to present such a construction. As with most BSM models, there are two possibilities. The UV completion may be a strongly coupled theory, which happens to produce the LHT as its effective theory below the confinement scale of 10 TeV, or the UV completion remains perturbative, and the LHT emerges as a low-energy description of a renormalizable weakly coupled gauge theory. Here we choose to follow the second possibility, that is we present a linear UV completion of the LHT. In this approach, one needs to introduce supersymmetry to stabilize the hierarchy

between the 10 TeV scale and the GUT/Planck scale; however, since SUSY is broken at 10 TeV, the model is free of the fine-tuning plaguing the MSSM. Alternatively one can have a Kaluza-Klein (KK) tower of a warped extra dimension starting at 10 TeV, which would also stabilize the large hierarchy. Our model explains the appearance and radiative stability of the global symmetry structure of the LHT, which at first sight appears rather unnatural. Furthermore, the model is manifestly free of anomalies, including both the familiar gauge/gravitational anomalies and the anomalies involving T-parity. Thus, the anomaly-induced T-parity violating operators, which recently received some attention in the literature [66, 67], are completely absent in our model and T-parity is an exact symmetry, at least as long as gravitational effects can be ignored. This illustrates the point that the existence of these operators depends crucially on the nature of the ultraviolet completion of the LH model. This has also been emphasized very recently in [68], where it was also pointed out the UV completions with anomalous T-parity are unlikely to have the correct vacuum alignment. The model constructed here does not exhibit gauge coupling unification. Construction of a unified model is outside the scope of this work.

Before presenting our model, let us briefly comment on its relation to previous work in this area. UV completions of the Littlest Higgs model have been until now based on either a strongly interacting theory or equivalently a warped extra dimension at the 10 TeV scale. Models without T-parity have been constructed [69,70], while recently an attempt to incorporate a discrete parity based on two throats of warped dimensions was presented in [71]. Our model is based on conventional, four-dimensional and perturbative physics, making it much easier to incorporate T-parity and to analyze anomalies. Supersymmetric ultraviolet completions of an alternative LH model, the "simplest" little Higgs, have

also appeared in the literature [8, 9, 72, 73]. However, in those models the electroweak precision constraints are so strong that one has to assume that SUSY is broken at the weak scale, and the LH scale is much higher. The role of the Little Higgs mechanism is to solve the little hierarchy problem within SUSY. In contrast, in our model the LH partners appear first, and SUSY is irrelevant until the 10 TeV scale. At the LHC, our model would look like the familiar LHT, with a few extra states. We will also present an extra dimensional model that is reminiscent of the structure of the minimal composite Higgs (MCH) models of [74], in which the Higgs will appear as the zero mode of the A_5 bulk gauge fields, which will pick up a finite radiatively generated potential. The main difference between the model presented here and the MCH models is that we will have the T-odd little Higgs partners appearing at the 1 TeV scale, which will allow us to push the KK mass scale of the theory to 10 TeV without fine-tuning. Thus the KK tower only plays a role of UV completing the theory above 10 TeV and stabilizing the hierarchy between 10 TeV and the Planck scale, but it is not used to cut off the 1-loop quadratic divergences between 1 and 10 TeV.

The chapter is organized as follows. We first construct a four-dimensional, non-supersymmetric, renormalizable model which reduces to the LHT (plus a few extra states) below the 10 TeV scale. We discuss the bosonic (gauge and scalar) sector of the model in section 3.2, and show how to incorporate fermions in section 3.3. In section 3.4, we extend the model to achieve complete anomaly cancelation, including anomalies involving T-parity. In section 3.5, we discuss how the hierarchy between the 10 TeV scale and the Planck scale can be stabilized by either supersymmetrizing the model or embedding it into a theory with a warped fifth dimension à la Randall and Sundrum [75]. In section 3.6, we estimate the precision electroweak constraints on the model, and show that

the model is realistic. In section 3.7, we show by an explicit diagrammatic calculation how the little Higgs cancelations occur in our renormalizable model. Finally, section 3.8 contains our conclusions.

3.2 The Scalar/Gauge Sector for $SU(5) \times SU(2) \times U(1)$

The bosonic (scalar and gauge) degrees of freedom of the LHT model are described by a gauged non-linear sigma model (nlσm). The scalars are the Goldstone bosons of the global symmetry breaking $SU(5) \to SO(5)$. The symmetry-breaking vev (or condensate) is in the symmetric representation **15** of the $SU(5)$. The symmetry breaking scale f_S is assumed to be about 1 TeV. To incorporate the gauge degrees of freedom, an $[SU(2) \times U(1)]^2$ subgroup of the $SU(5)$ is gauged; for the fundamental representation, the gauged subgroup of $SU(5)$ is spanned by the generators

$$Q_1^a = \left(\begin{array}{c|c|c} \tau^a & & \\ \hline & 0 & \\ \hline & & 0 \end{array}\right), \qquad Y_1 = \frac{1}{10}\left(\begin{array}{c|c|c} 3 & & \\ \hline & -2 & \\ \hline & & \begin{array}{cc} -2 & \\ & -2 \end{array} \end{array}\right) \tag{3.2.1}$$

$$\text{and} \quad Q_2^a = \left(\begin{array}{c|c|c} 0 & & \\ \hline & 0 & \\ \hline & & -\tau^{aT} \end{array}\right), \qquad Y_2 = \frac{1}{10}\left(\begin{array}{c|c|c} 2 & & \\ \hline & 2 & \\ \hline & & \begin{array}{cc} -3 & \\ & -3 \end{array} \end{array}\right) \tag{3.2.2}$$

where $\tau^a = \sigma^a/2$. Below f_S, the gauge symmetry is reduced to the diagonal $SU(2) \times U(1)$, which is identified with the Standard Model (SM) electroweak gauge group $SU(2)_L \times U(1)_Y$. Under this group, the physical (uneaten) Goldstones decompose into a weak doublet, identified with the SM Higgs, and a weak triplet. The Higgs mass is protected from a one-loop quadratic divergence by the collective symmetry breaking mechanism. The nlσm is an effective theory valid up to the scale $\Lambda \sim 4\pi f_S \sim 10$ TeV. For a more detailed description of the LHT model, see Refs. [49–51].

The first step to a weakly coupled UV completion of the LHT is to replace the nlσm with a *linear* sigma model with the same symmetry breaking structure. This model contains a single scalar field S, transforming as **15** of $SU(5)$, which is assumed to get a vev

$$\langle S \rangle \;=\; f_S \begin{pmatrix} & & \mathbb{1} \\ & 1 & \\ \mathbb{1} & & \end{pmatrix}, \tag{3.2.3}$$

where $f_S \sim 1$ TeV. The Lagrangian is simply

$$\mathcal{L}_{\rm lin} = \tfrac{1}{8}|D_\mu S|^2 \;-\; V(S)\,, \tag{3.2.4}$$

where D_μ is the covariant derivative, and the renormalizable potential $V(S)$ is assumed to lead to an S vev of the form (3.2.3). We will not need to specify this and other scalar potentials explicitly here, for an example of a possible potential for S see eq. (3.7.3). The excitations around the vacuum (3.2.3) can be parametrized as

$$S = \langle S \rangle \;+ i \begin{pmatrix} \phi_S & \sqrt{2}\, h_S & \chi_S + \frac{\eta_S}{\sqrt{5}} \\ \sqrt{2}\, h_S^T & -\frac{4\eta_S}{\sqrt{5}} & \sqrt{2}\, h_S^\dagger \\ \chi_S^T + \frac{\eta_S}{\sqrt{5}} & \sqrt{2}\, h_S^* & \phi_S^\dagger \end{pmatrix} + (\text{radial modes})\,, \tag{3.2.5}$$

where χ_S is a hermitan, complex 2×2 matrix, η_S a real singlet, ϕ_S a complex, symmetric 2×2 matrix and h_S a complex doublet, which will be identified with the SM Higgs. These fields are pseudo-Goldstone bosons (they would be exact Goldstone bosons, if the gauge couplings were taken to zero). They contain 14 degrees of freedom, corresponding to the number of $SU(5)$ generators broken by the S vev. The other 16 degrees of freedom in S, the "radial" modes, obtain masses $\sim cf_S$, where c are order-one numbers determined by the coupling constants in $V(S)$. Integrating out the radial modes reproduces the nlσm description of the LHT, independent of the details of $V(S)$. This is guaranteed by the Coleman-Wess-Zumino theorem [76, 77]. In particular, the crucial feature of the LHT nlσm is the special structure of the Higgs coupling to gauge fields, which guarantees the absence of a quadratic divergence in the Higgs mass at one loop. In section 3.7, we show by an explicit calculation how this structure emerges from the linear sigma model.

The model defined by eq. (3.2.4) is of course renormalizable, and can be valid up to an arbitrarily high scale, for example the Planck scale. In this sense, it is a viable UV completion of (the bosonic sector of) the LHT. However, it has two significant shortcomings:

- The symmetry structure of this model is *very unnatural*. Because gauge interactions break the global $SU(5)$ explicitly, renormalization-group evolution generates $SU(5)$-violating operators in the Lagrangian. In the LHT model, the global $SU(5)$ has to be a good symmetry at the 10 TeV scale. This would require the linear model to contain a very special combination of $SU(5)$-violating terms at the Planck scale, finely tuned just so that the $SU(5)$ is miraculously restored at 10 TeV.

- SM fermions *cannot* be incorporated in this model in a way consistent with T-parity. T-parity requires that for every field transforming under one of the two $SU(2) \times U(1)$ gauge groups of the LHT model, there must be another field transforming in the same way under the other $SU(2) \times U(1)$. Since the SM weak group is the diagonal combination of the two $SU(2)$ factors, this means that the model must have an even number of weak doublets of the same hypercharge and color charge. Therefore this model cannot lead to the chiral fermion content of the SM in the low energy limit.

To avoid the first problem, we would like to start at high energies with a model in which the full $SU(5)$ is promoted to a *gauge* symmetry. Further, to incorporate chirality, we must enlarge the gauge structure to contain an odd number of gauged $SU(2)$ factors. The most obvious and easiest choice is to add one extra gauge $SU(2)$. As we will see below, obtaining the correct hypercharge assignments for all SM fermions also requires an additional $U(1)$ gauge group.

Thus, the full gauge group of our model, at high energies, is

$$SU(5) \times SU(2)_3 \times U(1)_3, \tag{3.2.6}$$

where we labeled the extra $SU(2) \times U(1)$ factor with a subscript "3" to distinguish it from the $[SU(2) \times U(1)]^2$ subgroup of the $SU(5)$ that survives below 10 TeV. To break the $[SU(2) \times U(1)]^3$ subgroup to the SM electroweak gauge group, we also need additional bifundamental scalars under $SU(5) \times SU(2)_3$, K_1 and K_2, which will acquire the appropriate vevs (see eq. (3.2.9)).

To reproduce the symmetries of the LHT model at low energies, we introduce a set of scalar fields, summarized in Table 3.1. At the 10 TeV scale, the Φ

Table 3.1: Scalar fields and their gauge charge assignments.

	$SU(5)$	$SU(2)_3$	$U(1)_3$
$\Phi_{1,2}$	Adj	1	0
S	$\square\square$	1	0
K_1	$\square$	$\square$	$-1/2$
K_2	$\overline{\square}$	$\square$	$-1/2$

fields get vevs of the form

$$\langle\Phi_1\rangle = f_\Phi \begin{pmatrix} -3 & & & & & \\ & -3 & & & & \\ & & 2 & & & \\ & & & 2 & & \\ & & & & 2 & \\ & & & & & 2 \end{pmatrix}, \quad \langle\Phi_2\rangle = f_\Phi \begin{pmatrix} 2 & & & & & \\ & 2 & & & & \\ & & 2 & & & \\ & & & -3 & & \\ & & & & -3 & \\ & & & & & -3 \end{pmatrix} \tag{3.2.7}$$

where $f_\Phi \sim 10$ TeV. These vevs break the $SU(5)$ down to $[SU(2) \times U(1)]^2$, the gauge group of the LHT model, and leave the $SU(2)_3 \times U(1)_3$ unbroken. If the scalar potential has the form

$$V = V(\Phi_1, \Phi_2) + V(S, K_1, K_2)\,, \tag{3.2.8}$$

so that there are no direct couplings between Φ's and other scalars, the model will possess an $SU(5)$ global symmetry below 10 TeV, broken only by gauge interactions. This is the idea that was first emplyed in the context of $SU(6)$ GUT models in [78–80], and also in the "simplest little Higgs" model in [81,82]. With this assumption, the full gauge/global symmetry structure of the LHT is reproduced. Of course, this construction is only natural, if there is a symmetry reason for the absence of direct potential couplings between Φ's and the other scalars. In section 3.5, we will show that the Φ-vevs can be stabilized at the 10 TeV scale, either by supersymmetrizing the model or by embedding it into

a five-dimensional model with warped geometry. In both cases, the couplings between Φ and the other scalars can be naturally suppressed.

At the 1 TeV scale, the field S gets a vev given in eq. (3.2.3), while the bifundamental fields get vevs

$$\langle K_1 \rangle = f_K \begin{pmatrix} 1 & & \\ & 1 & \\ & & \\ & & \end{pmatrix}, \quad \langle K_2 \rangle = f_K \begin{pmatrix} & & \\ & & \\ 1 & & \\ & 1 & \end{pmatrix}, \tag{3.2.9}$$

where $f_K \sim 1$ TeV. Together, these vevs break the $[SU(2) \times U(1)]^3$ gauge symmetry down to a single $SU(2) \times U(1)$, identified with the SM. The unbroken generators are simply $Q_D^a = Q_1^a + Q_2^a + Q_3^a$ and $Y_D = Y_1 + Y_2 + Y_3$.

The global symmetry breaking by the K-vevs results in additional pseudo-Goldstone bosons. We will assume that the tree-level scalar potential does not contain direct couplings between the fields: $V = V(S) + V(K_1, K_2)$. With this assumption, the Goldstones contained in different fields do not mix. Most of the Goldstones are not protected by the collective symmetry breaking mechanism. They will therefore receive quadratically divergent masses at the one-loop level from gauge loops, and their masses are in the TeV range. The only exceptions are the SM Higgs h_S, and a set of three real Goldstones transforming as a real triplet under the SM $SU(2)$ gauge group. Two of these triplets are eaten by the heavy $SU(2)$ gauge bosons, while the third one remains physical. The physical mode is a linear combination of the Goldstones coming from S, K_1 and K_2. In fact, one can think of our model below 10 TeV as a three-site deconstruction of a five-dimensional model, with the moose diagram shown in Fig. 3.1. In this pic-

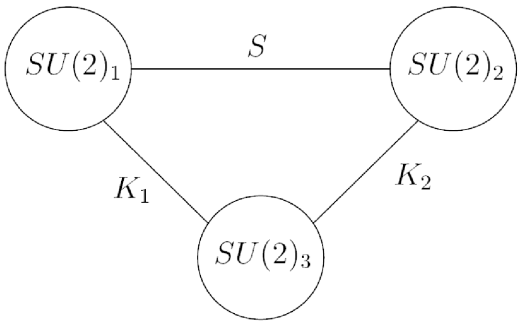

Figure 3.1: The gauge symmetries and scalar field content of the model below the 10 TeV scale.

ture, the light triplet mode is simply the counterpart of A_5, and can only receive a mass from non-local effects due to compactification. However, the Yukawa couplings of our model (discussed in the following section) do not have such an "extra-dimensional" structure, and the triplet mass is *not* protected from the one-loop diagrams involving the Yukawas. Thus, this mode will also receive a TeV-scale mass. The only pseudo-Goldstone protected by the collective symmetry mechanism is the SM Higgs.

In addition to the gauge symmetries, we impose that the model is invariant under a discrete T-parity, which acts on the gauge and scalar fields as follows:

$$\begin{aligned} W_{SU(5)} &\rightarrow \Omega(W_{SU(5)})\Omega^\dagger\,, \\ W_{SU(2)} &\rightarrow \omega(W_{SU(2)})\omega^\dagger = W_{SU(2)}\,, \\ B_{U(1)} &\rightarrow B_{U(1)}\,, \\ \Phi_1 &\leftrightarrow \Omega\Phi_2\Omega^\dagger\,, \\ S &\rightarrow \Omega S^\dagger\Omega^T\,, \\ K_1 &\leftrightarrow \Omega K_2\omega^T\,, \end{aligned} \tag{3.2.10}$$

where $W_{SU(5)}$, $W_{SU(2)}$ and $B_{U(1)}$ are the SU(5), SU(2)$_3$ and U(1)$_3$ gauge fields,

respectively, and

$$\Omega = \begin{pmatrix} & & -\mathbb{1} \\ & 1 & \\ -\mathbb{1} & & \end{pmatrix} \quad \text{and} \quad \omega = -\mathbb{1}. \tag{3.2.11}$$

Note that $\Omega \in SU(5)$ and $\omega \in SU(2)$. The kinetic terms are automatically invariant under this parity, while the scalar potential must be restricted to the terms consistent with it. The vevs in eqs. (3.2.3), (3.2.7) and (3.2.9) do not break T-parity. It is easy to check that the T-parity defined in this way acts in the desired way on the fields of the LHT model: the two $SU(2) \times U(1)$ factors inside the $SU(5)$ are interchanged, the Higgs boson h_S is T-even, while the weak triplet is T-odd, as required by precision electroweak fits.

Now, let us discuss the spectrum of the bosonic states. Sixteen out of the 24 $SU(5)$ gauge bosons get masses at the 10 TeV scale. These states are too heavy to have any phenomenological consequences, and we will not discuss them further. Below 10 TeV, we have three sets of $SU(2)$ gauge bosons:

$$\begin{aligned}
&m^2_{W_{SM}} = 0: && W_{SM} = \tfrac{1}{\sqrt{2g_3^2+g_5^2}}[g_3(W_1+W_2)+g_5 W_3] \\
&m^2_{W_{\text{even}}} = \tfrac{g_5^2+2g_3^2}{4} f_K^2: && W_{\text{even}} = \tfrac{1}{\sqrt{2g_5^2+4g_3^2}}[g_5(W_1+W_2)-2g_3 W_3] \\
&m^2_{W_{\text{odd}}} = \tfrac{g_5^2}{4}(2f_S^2+f_K^2): && W_{\text{odd}} = \tfrac{1}{\sqrt{2}}[W_1 - W_2]\,,
\end{aligned} \tag{3.2.12}$$

as well as three $U(1)$ bosons:

$$\begin{aligned}
&m^2_{B_{SM}} = 0: && B_{SM} = \tfrac{1}{\sqrt{2{g'_5}^2+{g'_3}^2}}[g'_3(B_1+B_2)+g'_5 B_3] \\
&m^2_{B_{\text{even}}} = \tfrac{{g'_5}^2+2{g'_3}^2}{4} f_K^2: && B_{\text{even}} = \tfrac{1}{\sqrt{2{g'_5}^2+4{g'_3}^2}}[g'_5(B_1+B_2)-2g'_3 B_3] \\
&m^2_{B_{\text{odd}}} = \tfrac{{g'_5}^2}{100}(10f_S^2+f_K^2): && B_{\text{odd}} = \tfrac{1}{\sqrt{2}}[B_1 - B_2].
\end{aligned} \tag{3.2.13}$$

Here g_5, g_3 and g'_3 are the $SU(5)$, $SU(2)_3$ and $U(1)_3$ coupling constants, respectively, and in proper normalization $g'_5 = \sqrt{5/3}\, g_5$.

Note that the model contains a set of T-even gauge bosons at the TeV scale, due to the presence of an extra $SU(2) \times U(1)$ gauge factor, which is T-even. These states can be problematic for electroweak precision constraints, but are inevitable in our model. However, they do not participate in the cancelation of the quadratic divergences in the Higgs boson mass. Therefore, they can be substantially heavier than the T-odd states, without spoiling naturalness. This occurs if $g_3', g_3 \gg g_5$; if the T-odd states are at 1 TeV, requiring that $g_3', g_3 \sim$ 3-5 g_5 is sufficient to avoid precision electroweak constraints, and the model remains weakly coupled, but for these parameters, the Weinberg angle is fixed at a wrong value: $\sin^2\theta_W = 5/8$ in the limit $g_3', g_3 \gg g_5$. However, as we will discuss in section 3.3.2, reproducing the top sector of the LHT from a renormalizable model will require introduction of additional scalar vevs at the TeV scale, which will affect the gauge boson spectrum. It turns out that in the full model the correct value of the Weinberg angle can be easily reproduced without conflict with precision electroweak data, as we will show in detail in section 3.6.

3.3 The Fermion Sector

In this section we describe the fermion sector of our model that contains the SM fermions plus a number of heavier states. Our convention is to write all fermion fields as left-handed two-component spinors.

Table 3.2: Fermion fields required to incorporate one generation of SM quarks, and their gauge charge assignments. Here $Y = 1/6$ is the SM quark doublet hypercharge. For a generation of leptons, the same set of fields is required, except $d_R \to e_R$, u_R is omitted if the neutrino is Majorana (or $u_R \to \nu_R$ if it is Dirac), and $Y = -1/2$.

	$SU(5)$	$SU(2)_3$	$U(1)_3$
Ψ_1	$\overline{\square}$	1	$Y + 1/2$
Ψ_2	$\square$	1	$Y + 1/2$
ψ_3	1	$\square$	$-Y$
$\psi_{4,5}$	1	$\square$	$-Y - 1$
$U_{R1,2}$	1	1	$-Y - 1/2$
u_R	1	1	$-Y - 1/2$
d_R	1	1	$-Y + 1/2$

3.3.1 The SM fermions

It is straightforward to include the SM $SU(2)_L$ singlets as T-even fermionic singlets, u_R, d_R and e_R. (The SM generation index will be omitted throughout this chapter.) For each SM doublet, we introduce two fermions in the representations **5** and $\overline{\mathbf{5}}$ of $SU(5)$

$$\Psi_1 = \begin{pmatrix} \psi_1 \\ U_{L1} \\ \chi_1 \end{pmatrix} \text{ and } \Psi_2 = \begin{pmatrix} \chi_2 \\ U_{L2} \\ \psi_2 \end{pmatrix}. \tag{3.3.1}$$

A linear combination of ψ_1 and ψ_2 will become the SM doublet. To decouple the extra components, we need 5 extra fermions: ψ_3, ψ_4 and ψ_5 are $SU(2)_3$ doublets, and U_{R1} and U_{R2} are singlets. We also need two extra scalar fields, $F_1 \in \mathbf{5}$ and $F_2 \in \overline{\mathbf{5}}$ of $SU(5)$. Both are uncharged under $SU(2)_3 \times U(1)_3$. Under T-parity,

$$
\begin{aligned}
\Psi_1 &\leftrightarrow \Omega^\dagger \Psi_2 \\
\psi_3 &\rightarrow \omega \psi_3 \\
\psi_4 &\leftrightarrow \omega \psi_5 \\
U_{R1} &\leftrightarrow U_{R2} \\
u_R &\rightarrow u_R \\
d_R &\rightarrow d_R \\
F_1 &\leftrightarrow \Omega F_2.
\end{aligned}
\tag{3.3.2}
$$

The Yukawa couplings allowed by gauge symmetries and T-parity are:

$$
\begin{aligned}
\mathcal{L}_{\text{Yuk}} = \kappa_1 \left[\Psi_1 K_1 \psi_3 + \Psi_2 K_2 \psi_3\right] + \kappa_2 \left[\Psi_1^\dagger K_2 \psi_4^\dagger + \Psi_2^\dagger K_1 \psi_5^\dagger\right] \\
+\kappa_3 \left[\Psi_1 F_1 U_{R1} + \Psi_2 F_2 U_{R2}\right] + \text{ h.c.}.
\end{aligned}
\tag{3.3.3}
$$

The invariance under T-parity can be easily shown using $\Omega^\dagger \Omega = \mathbb{1}$ and $\omega^\dagger \omega = \mathbb{1}$. This form of the Yukawas, together with the requirement of the correct hypercharges for the SM fields, unambiguously fixes the $U(1)_3$ charges for all fermions. The gauge quantum numbers of the fermions are summarized in Table 3.2.

The fundamental scalars get vevs consistent with T-parity:

$$
\langle F_1 \rangle = \langle F_2 \rangle = (0, 0, f_F, 0, 0)^T , \tag{3.3.4}
$$

where $f_F \sim$ TeV. These vevs break Y_1 and Y_2 seperately, but leave $Y_1 + Y_2 + Y_3$ unbroken, so that no gauge symmetries not already broken by S and K vevs are broken.

For each SM doublet, our model contains five massive Dirac fermions at the TeV scale[1], three T-odd and the other two T-even. Their masses are $m_{1-} =$

[1]Note that the T-odd fermion masses are bounded from above by constraints on four-fermion operators [51], and cannot be much heavier than a TeV.

$\sqrt{2}\kappa_1 f_K$, $m_{2\pm} = \kappa_2 f_K$ and $m_{3\pm} = \kappa_3 f_F$, where the signs denote the T-parity of each state. There is one massless T-even doublet, $\psi_{SM} = \frac{1}{\sqrt{2}}(\psi_1 - \psi_2)$, which is identified with the SM quark or lepton doublet. In the next subsection, we will explain how the SM Yukawa couplings can be generated in this model.

3.3.2 The Yukawa couplings

We will start with the top Yukawa. Due to the large value of this coupling in the SM, naturalness requires it to be implemented in a way that only breaks the global symmetries of the LHT collectively. It is straightforward to incorporate the top Yukawas of the LHT model in our linear model. For the third generation quarks, we use the set of fields listed in Table 3.2. In addition to the terms in (3.3.3), we include the following operators:[2]

$$\mathcal{L}_{\mathrm{t}} \,=\, \lambda_1 \frac{1}{M}\left[\epsilon^{ijk}\epsilon^{xy}\Psi_{1i}S^{\dagger}_{jx}S^{\dagger}_{ky} + \epsilon_{i'j'}\epsilon_{x'y'z'}\Psi_2^{x'}S^{y'i'}S^{z'j'}\right] u_R + \text{ h.c.} \tag{3.3.5}$$

where we restrict the summation to $i,j,k \in \{1,2,3\}$, $x,y \in \{4,5\}$ and $i',j' \in \{1,2\}$, $x',y',z' \in \{3,4,5\}$ and M is the mass scale suppressing this dimension-5 operator. Note that eq. (3.3.5) is T-parity invariant, although this is not immediately manifest; taking the T-parity transformation of the first term yields

$$\begin{aligned}
\epsilon^{ijk}\epsilon^{xy}\Psi_{1i}S^{\dagger}_{jx}S^{\dagger}_{ky} \to{}& \epsilon^{ijk}\epsilon^{xy}(\Omega^{\dagger}\Psi_2)_i(\Omega^{\dagger}S\Omega^*)_{jx}(\Omega^{\dagger}S\Omega^*)_{ky} \\
&= \left[\epsilon^{ijk45}\Omega^{\dagger}_{ix'}\Omega^{\dagger}_{jy'}\Omega^{\dagger}_{kz'}\Omega^{\dagger}_{41}\Omega^{\dagger}_{52}\right]\left[\epsilon^{123xy}\Omega^*_{41}\Omega^*_{52}\Omega^*_{33}\Omega^*_{i'x}\Omega^*_{j'y}\right] \\
&\quad \Psi_2^{x'}S^{y'i'}S^{z'j'} \\
&= \left[\epsilon_{x'y'z'}\det\Omega^{\dagger}\right]\left[\epsilon_{i'j'}\det\Omega^*\right]\Psi_2^{x'}S^{y'i'}S^{z'j'},
\end{aligned} \tag{3.3.6}$$

[2]By convention fundamental $SU(5)$ indices are upper, antifundamental are lower. SU(2) indices are raised and lowered with ϵ^{ab} and ϵ_{ab} as usual.

which together with $\det \Omega = 1$ gives exactly the second term in eq. (3.3.5). The expansion to summing over 1 to 5 (and then restricting again to partial summation as in eq. (3.3.5)) in this derivation is possible due to the special structure of Ω. After the S field gets a vev and the radial modes are integrated out, eq. (3.3.5) reduces to the top Yukawa term of the usual nlσm LHT model (see e.g. [50, 51, 59]). These Yukawa couplings incorporate the collecitve symmetry breaking mechanism, which protects the Higgs mass from large renormalization by top loops.

We now want to obtain the operators in eq. (3.3.5) from an $SU(5)$-invariant, renormalizable Lagrangian. To restore $SU(5)$ invariance, let us introduce two scalar fields,

$$A_1 \in \overline{\mathbf{10}}\,, \quad A_2 \in \mathbf{10}\,, \tag{3.3.7}$$

with T-parity action

$$A_1 \leftrightarrow \Omega^\dagger A_2 \Omega^*. \tag{3.3.8}$$

These fields get vevs

$$\langle A_1 \rangle = f_A \begin{pmatrix} 0 & & \\ & 0 & \\ & & \varepsilon \end{pmatrix}, \quad \langle A_2 \rangle = f_A \begin{pmatrix} \varepsilon & & \\ & 0 & \\ & & 0 \end{pmatrix}, \quad \text{where } \varepsilon = \begin{pmatrix} 0 & 1 \\ -1 & 0 \end{pmatrix}. \tag{3.3.9}$$

These vevs do not break T-parity or the gauged $SU(2)$s, but break the Y_1 and Y_2 gauged generators. So, the A's need to be charged under $U(1)_3$ with charges chosen such that the broken linear combinations are orthogonal to the one identified with hypercharge, $Y_1 + Y_2 + Y_3$. This requires $Q_3(A_1) = Q_3(A_2) = -1$. In addition to their role in the top sector, the antisymmetric fields also help resolve the problem with the correct value of the Weinberg angle mentioned earlier. For a disussion of this issue, see section 3.6.

Eq. (3.3.5) can now be thought of as the low-energy limit of the following ($SU(5)$-invariant, but still non-renormalizable) Lagrangian:

$$\mathcal{L}_{\rm t} \propto \left[\epsilon^{abcde}\Psi_{1a}S^{\dagger}_{bx}S^{\dagger}_{cy}(A_1)_{de}(A_1^*)^{xy} + \epsilon_{abcde}\Psi_2^a S^{bx}S^{cy}(A_2)^{de}(A_2^*)_{xy}\right] u_R + \text{ h.c.}, \tag{3.3.10}$$

where the summations are no longer restricted and run from 1 to 5.

One possible way to obtain a renormalizable model is to introduce four scalar fields, η, η', ξ, and ξ'. These are uncharged under $SU(2)_3 \times U(1)_3$, and transform under $SU(5)$ as follows:

$$\eta \in \square, \;\; \eta' \in \overline{\square}, \;\; \xi, \xi' \in \text{ Adj.} \tag{3.3.11}$$

T-parity acts in by-now familiar way:

$$\eta \leftrightarrow \Omega\eta' \,, \quad \xi \leftrightarrow \Omega^{\dagger}\xi'\Omega \,. \tag{3.3.12}$$

The renormalizable Lagrangian is then given by

$$\begin{aligned}\mathcal{L}_{\rm t} \propto \; & \Psi_{1a}\eta^a u_R + \epsilon^{abcde}\eta^{\dagger}_a S^{\dagger}_{bx}\xi^x{}_c(A_1)_{de} + m_0(\xi^{\dagger})_x{}^c S^{\dagger}_{cy}(A_1^*)^{xy} \\ & + \Psi_2^a\eta'_a u_R + \epsilon_{abcde}\eta'^{\dagger a}S^{bx}(\xi'^{\dagger})_x{}^c(A_2)^{de} + m_0\xi'^x{}_c S^{cy}(A_2^*)_{xy} + \text{ h.c.}\end{aligned} \tag{3.3.13}$$

plus mass terms for the scalars. Assuming that the scalars are heavier than f, integrating them out reproduces eq. (3.3.10).

With the above quantum numbers there is no Yukawa coupling possible for the leptons and the down quarks, which resembles the top Yukawa in eq. (3.3.5). However, it is possible to write down a dimension-6 operator to generate these Yukawa couplings. For the down quarks, this operator has the form

$$\mathcal{L}_{\rm d} \sim \frac{\lambda}{M_d^2}\left(\epsilon_{ijk}\epsilon_{xy}\Psi_2^x K_1^{ia}K_{1\,a}^{j}S^{ky} + \epsilon^{i'j'}\epsilon^{x'y'z'}\Psi_{1i'}K^a_{2x'}K_{2y'a}S^{\dagger}_{z'j'}\right) d_R + \text{ h.c.}, \tag{3.3.14}$$

where the summation is restricted to $i,j,k \in \{1,2,3\}$, $x,y \in \{4,5\}$ and $i',j' \in \{1,2\}$, $x',y',z' \in \{3,4,5\}$, and M_d is the mass scale at which this operator is

generated. The lepton Yukawas are of the same form. In complete analogy to the top sector, the desired operators can be obtained from a renormalizable and $SU(5)$ invariant lagrangian by introducing new heavy states (scalars or fermions) and integrating them out.

3.3.3 A non $SU(5)$ invariant theory

One might wonder if the rich structure of the model we built is just due to the requirement of $SU(5)$ gauge invariance at high energies. If one is willing to assume that the $SU(5)$ global symmetry accidentally emerges at the 10 TeV scale, a model with ungauged $SU(5)$ can be considered. Could this dramatically simplify the particle content needed to reproduce the LHT? A detailed look at the previous section reveals that only very few states could actually be omitted in such a non-$SU(5)$ invariant model:

- We could use incomplete $SU(5)$ representations in (3.3.1) and omit the states $\chi_{1,2}$.
- We would not need the scalars $F_{1,2}$ to give mass to the $U_{L1,2}$ states.
- We would not need the scalars $A_{1,2}$, whose role is to make the coupling (3.3.5) $SU(5)$ invariant.
- Fewer massive scalars would be necessary to obtain the top Yukawas (3.3.5) from a renormalizable theory.

In total one would end up with a slightly smaller particle content, but overall the model would not simplify significantly.

3.4 Anomaly Cancellation

While the model presented above suffers from gauge anomalies, in this section we will present a simple extension of the model which is anomaly free. Furthermore, we will show that T-parity is an anomaly free symmetry of the quantum theory.

3.4.1 Gauge anomalies

First, we examine the gauge anomalies of the model. The chiral fermion content of a single generation is summarized in Table 3.2, where $Y = 1/6$ for quarks and $Y = -1/2$ for leptons. Note that the $SU(5)$ group is vectorlike, while $SU(2)$ representations are real, so all anomalies involving only these two groups vanish. However, anomalies involving U(1)$_3$ are *not* canceled with this fermion content. The simplest way to achieve anomaly cancelation is to extend the model in such a way that it contains a sector which is vectorlike under the full $SU(5) \times SU(2)_3 \times U(1)_3$ gauge group, plus a sector which is chiral under $SU(2)_3 \times U(1)_3$, but with charges identical to one generation of the SM fermions. This guarantees anomaly cancelation as in the SM. Since at low energies the matter content of our model coincides with the SM, this is in fact possible. In order to achieve this, we need to introduce mirror partners for all fields that don't already have SM quantum numbers. In particular for the quark sector we introduce the mirror partners Q'_1, Q'_2, q'_4, q'_5, U'_{R1}, U'_{R2} and *two* fields q'_3, q''_3. The two q_3 partners are necessary in order to exactly reproduce the chiral SM matter content under $SU(2)_2 \times U(1)_3$, guaranteeing complete anomaly cancelation. The total anomaly-free fermion content in the quark sector is summarized in

Table 3.3: The quark sector (single generation) and the gauge charge assignments for the anomaly-free version of the model.

	$SU(5)$	$SU(2)_3$	$U(1)_3$		$SU(5)$	$SU(2)_3$	$U(1)_3$
Q_1	$\bar{\square}$	1	$+2/3$	Q'_1	$\bar{\square}$	1	$-2/3$
Q_2	$\square$	1	$+2/3$	Q'_2	$\square$	1	$-2/3$
q_3	1	$\square$	$-1/6$	q'_3, q''_3	1	$\square$	$+1/6$
q_4	1	$\square$	$-7/6$	q'_4	1	$\square$	$+7/6$
q_5	1	$\square$	$-7/6$	q'_5	1	$\square$	$+7/6$
U_{R1}	1	1	$-2/3$	U'_{R1}	1	1	$+2/3$
U_{R2}	1	1	$-2/3$	U'_{R2}	1	1	$+2/3$
u_R	1	1	$-2/3$				
d_R	1	1	$+1/3$				

Table 3.4: The lepton sector (single generation) and the gauge charge assignments for the anomaly-free version of the model.

	$SU(5)$	$SU(2)_3$	$U(1)_3$
L_1	$\bar{\square}$	1	0
L_2	$\square$	1	0
ℓ_3	1	$\square$	$+1/2$
ℓ_4	1	$\square$	$-1/2$
ℓ_5	1	$\square$	$-1/2$
E_{R1}	1	1	0
E_{R2}	1	1	0
e_R	1	1	$+1$
$(\nu_R$	1	1	0)

Table 3.3.

The additional states acquire TeV-scale masses through a Lagrangian of the form

$$\mathcal{L} \propto Q'_1 K_2^* q'_3 + Q'_2 K_1^* q''_3 + {Q'_1}^\dagger K_1^* {q'_4}^\dagger + {Q'_2}^\dagger K_2^* {q'_5}^\dagger + Q'_1 F_1 U'_{R1} + Q'_2 F_2 U'_{R2}\,. \quad (3.4.1)$$

Note that this is almost the same as eq. (3.3.3), except that the presence of the

Table 3.5: The chiral matter content for one generation of the anomaly-free version of the model.

	$SU(5)$	$SU(3)_c$	$SU(2)_3$	$U(1)_3$
q_3''	1	$\square$	$\square$	$+1/6$
u_R	1	$\bar{\square}$	1	$-2/3$
d_R	1	$\bar{\square}$	1	$+1/3$
ℓ_5	1	1	$\square$	$-1/2$
e_R	1	1	1	$+1$

two *different* fields q_3' and q_3'' guarantees that there is no light mode.

For the lepton sector with $Y = -1/2$ in Table 3.2 we automatically have a charge assignment that produces the SM chiral matter content under $SU(2)_3 \times U(1)_3$, so no additional mirror fields are needed. The matter content in the lepton sector is summarized in Table 3.4.

The chiral matter content of one generation of the model is summarized in Table 3.5. Here $SU(3)_c$ denotes the color gauge group. As anticipated above, the quantum numbers of these fermions under $SU(3)_c \times SU(2)_3 \times U(1)_3$ are exactly the same quantum numbers as for the usual SM fermions under $SU(3)_c \times SU(2)_L \times U(1)_Y$. Hence all gauge and gravitational anomalies cancel.

The above construction should be viewed as a proof of principle, showing that it is possible to add a set of spectator fermions to our model to cancel all gauge and gravitational anomalies, and to give them large masses in a way consistent with the symmetries. The particular set of spectators chosen here is rather large, but has the advantage that the anomalies cancel in exactly the same way as in the SM. Its disadvantage is that the QCD β-function will become very large and the theory would rapidly develop a Landau pole. The exact location

of the pole depends on the values chosen for the Yukawa couplings and vevs in eqs. (3.4.1) and (3.3.3). In the supersymmetric version of this model, which we will describe in section 3.5.1, this implies that once the Landau pole is hit an appropriate Seiberg duality [83] has to be performed and the theory will be a cascading gauge theory as in [84]. It would be interesting to see if a more minimal anomaly-free matter content can be found.

3.4.2 T-parity anomalies

Whenever physical Goldstone bosons appear in a theory, one has to check whether the global symmetries whose spontaneous breaking produces the Goldstones are anomalous. The presence of such anomalies would produce new couplings for the Goldstones, of the general form

$$\frac{1}{f}\pi^a \partial_\mu J^{a\mu} \,. \tag{3.4.2}$$

If the global current $J^{\mu a}$ is anomalous with respect to a gauge symmetry, then

$$\partial_\mu J^{a\mu} = \frac{A g^2}{16\pi^2} \mathrm{Tr} F \tilde{F} \,, \tag{3.4.3}$$

where F is the gauge field, and the anomaly coefficient A can be calculated from the triangle diagrams involving fermion loops. In the low energy effective theory after the fermions are integrated out, a term involving the light gauge fields and the Goldstones has to be present, whose variation reproduces the anomalies of the global current. This is the Wess-Zumino-Witten (WZW) term [85, 86], whose coefficient can be found by matching to the triangle diagrams in the high energy theory. This WZW term may break discrete symmetries of the Goldstone sector. The canonical example is the $\pi^a \to -\pi^a$ symmetry of the pseudoscalar

octet of QCD. The effect of the $SU(2)_A^2\ U(1)_{em}$ anomaly in the quark picture will imply the presence of the $\pi_0 F\tilde{F}$ coupling in the effective low-energy theory, which breaks the $\pi \to -\pi$ reflection symmetry. Using similar arguments Hill and Hill [66] argued that T-parity will also be broken in a similar way in little Higgs models. They have discussed several examples based both on more complicated versions of the $SU(3) \times SU(3) \to SU(3)_D$ breaking pattern, as well as the $SU(5) \to SO(5)$ and other little Higgs-type models, and have calculated the form of the Wess-Zumino-Witten terms in a variety of examples. However, whether these T-parity breaking terms are ultimately present in the low-energy effective theory or not depends on the UV completion of the theory. If the global symmetries (and T-parity itself) are not anomalous, then the coefficient of the Wess-Zumino term vanishes, and T-parity remains a good symmetry at the quantum level. Therefore, in a complete model with T-parity one has to show that T-parity is not broken by any of the global anomalies present in the theory. While in an effective low-energy theory one may only speculate whether such anomalies are present or not, our UV completion allows us to address this issue straightforwardly. Since the $SU(5)$ global symmetry responsible for producing the Goldstones is also gauged, it has to be anomaly free. Indeed we have shown above that it is possible to choose the matter content such that all anomalies involving $SU(5)$ will disappear. Therefore there can be no Wess-Zumino-Witten term from $SU(5)$ anomalies present in this theory that would give rise to T-parity violation.

A final worry might be that the T-parity itself as a discrete symmetry might be anomalous. However, as we have seen before, T-parity is a combination of an $SU(5) \times SU(2)_3$ gauge transformation element with a discrete exchange symmetry. We have seen that the gauge transformations are anomaly free, but what

about the exchange symmetry (which is a symmetry similar to charge conjugation)? Could that possibly be anomalous? The answer is clearly negative. The exchange symmetry in the path integral language merely corresponds to a relabeling of the integration variables. The integration measure is invariant under this relabeling. So, if the Lagrangian is invariant under the exchange symmetry, then the whole path integral is invariant. Therefore we do not expect T-parity violating anomalous terms to show up anywhere in the model.

3.5 Solutions to the Large Hierarchy Problem

We constructed a weakly coupled, four-dimensional UV completion of the LHT model, with T-parity exact at the quantum level. However, the model assumes a large hierarchy between the scale of scalar vevs (1 or 10 TeV), and the Planck scale. This hierarchy needs to be stabilized. In this section, we will explore two possible ways this can be achieved: by embedding the model into a supersymmetric theory above 10 TeV, and by promoting it to a warped-space five-dimensional model with the Planck scale at the infrared (IR) boundary of order 10 TeV.

3.5.1 A supersymmetric version

It is straightforward to supersymmetrize our model by promoting all fields to superfields, and assuming that the components that do not appear in our model receive soft masses at the 10 TeV scale. In addition, one needs to introduce a superfield $\bar{S}$, which has the same quantum numbers as $S^\dagger$. This fields gets inter-

changed with S under T-parity in the familiar way $S \leftrightarrow \Omega \bar{S} \Omega^T$. It ensures that it is possible to write down a superpotential that allows for the vev in eq. (3.2.3) and generates the Yukawa couplings (3.3.13). We assume the superpotential of the form

$$W = W_\Phi(\Phi_1, \Phi_2) \, + \, W_{\rm Yuk}(S, \bar{S}, K_1, K_2, \ldots) \, , \tag{3.5.1}$$

where W_Φ generates $SU(5)$ breaking vevs as in eq. (3.2.7) without breaking SUSY, and $W_{\rm Yuk}$ includes the Yukawa couplings of our model. This superpotential allows for the adjoint vevs in Eq. (3.2.7), with $\langle \sigma \rangle = 0$. At the same time, since the Yukawa couplings do not contain the Φ fields, it does *not* lead to direct couplings between Φ and the other fields in the F-term scalar potential. As a result, the global SU(5) symmetry below the scale $f_\Phi \sim 10$ TeV is preserved at this level. Note that this structure of the F-term potential is technically natural, due to the standard non-renormalization theorems of SUSY.

The scalar potential also receives a D-term contribution. Since both Φ and the other scalar fields, including S and $\bar{S}$, are charged under SU(5), the D-term potential will in general couple them, violating the global SU(5). This can give a large contribution to the Higgs mass, potentially of order $g_5 f_\Phi$. However, it can be shown that this effect is suppressed in the limit when the soft masses for the adjoint fields are small compared to f_Φ, and the Higgs mass can remain at the weak scale without fine-tuning.

The argument is based on the following observation [87, 88]: In the limit of unbroken SUSY, the effective theory below the scale f_Φ is a supersymmetric theory with reduced gauge symmetry. This SUSY theory does *not* contain any D-terms for S or $\bar{S}$ corresponding to the broken generators, and does not contain any Φ fields as they are either eaten or get masses at the scale f_Φ. So, in this limit

we are only left with D-terms for S and $\bar{S}$ corresponding to the unbroken subgroup. These terms do not generate a tree-level S or $\bar{S}$ mass, and moreover they break the SU(5) in exactly the same pattern as the unbroken gauge symmetries themselves. In particular, the Higgs (contained in S and $\bar{S}$) would still remain a Goldstone if only one of the two $SU(2)$ subgroups was gauged. Thus, in the unbroken-SUSY limit, the D-terms do not spoil the symmetries responsible for keeping the Higgs light.

Let us see explicitly how this works. Since for the protection of the higgs mass only the interactions between $S, \bar{S}$ and $\Phi_{1,2}$ are relevant, we will only focus on these fields on the following discussion. Above f_Φ, the D-term potential has the form

$$\begin{aligned} V_D &= \frac{g_5^2}{2}\sum_a (D_\Phi^a + D_S^a + ...)^2, \\ \text{with} \quad D_\Phi^a &= \sum_i \mathrm{Tr}\,\Phi_i^\dagger [T^a, \Phi_i]\,, \quad D_S^a \,=\, 2\,\mathrm{Tr}\,S^\dagger T^a S - 2\mathrm{Tr}\bar{S}^\dagger T^{aT}\bar{S}\,. \end{aligned} \tag{3.5.2}$$

After the Φ's get vevs, this potential includes $SU(5)$ symmetry breaking terms for S and $\bar{S}$. However, to obtain the correct low-energy potential, we have to carefully integrate out the heavy "radial" modes of the Φ fields. The important radial modes are $R^{\hat{a}}$ along the generators $T^{\hat{a}}$ broken by $\langle\Phi_{1,2}\rangle$. These modes are the real parts of the superfield containing the Goldstones, and as such they must be F-flat directions.[3] But since the Goldstones are eaten by the broken gauge bosons, the $R^{\hat{a}}$ fields will get masses from the D-terms, which must be precisely equal to the gauge boson masses in order to preserve SUSY. Furthermore, they are the only radial modes that receive a mass from the D-terms. The scalar

[3]Non-linearly realized Goldstones are completely F-flat. If realized linearly, however, one will encounter quartic and higher interactions in the F-term potential.

potential has the form

$$V_{\text{SUSY}} = F^* F + \frac{g^2}{2} D^a D^a = \frac{1}{2} \sum_{\hat{a}} (M_{\hat{a}} R^{\hat{a}} + ... + g_5 D_S^{\hat{a}})^2 + ... \,, \tag{3.5.3}$$

where $\hat{a}$ labels the broken generators, $M_{\hat{a}}$ are the gauge boson masses and the dots denote terms that do not contain either $D_S^{\hat{a}}$ or $R^{\hat{a}}$. The equations of motion yield

$$R^{\hat{a}} = -\frac{g_5 D_S^{\hat{a}}}{M_{\hat{a}}} \,, \tag{3.5.4}$$

which exactly cancels the unwanted D-terms for S and $\bar{S}$ corresponding to the broken generators.

In a realistic model, SUSY must be broken. Consider a situation when the SUSY-breaking soft masses for the Φ fields are lower than the $SU(5)$ breaking scale f_Φ. Assume that the soft breaking are of the form

$$V_{\cancel{SUSY}} = \frac{1}{2} \sum_{\hat{a}} m_{\hat{a}}^2 {R^{\hat{a}}}^2 + \ldots \,, \tag{3.5.5}$$

with $m_{\hat{a}} \ll f_\Phi$, and dots denote terms not containing $R^{\hat{a}}$. The important feature of these soft terms is that they do not contain a linear term in $R^{\hat{a}}$, and thus only affect the SUSY cancellation of the D-terms at subleading order in $m_{\hat{a}}/M_{\hat{a}}$. The equations of motion for $R^{\hat{a}}$ now yield

$$R^{\hat{a}} = -\frac{g_5 D_S^{\hat{a}} M_{\hat{a}}}{M_{\hat{a}}^2 + m_{\hat{a}}^2} + ... \approx -\frac{g_5 D_S^{\hat{a}}}{M_{\hat{a}}} \left(1 + \frac{m_{\hat{a}}^2}{M_{\hat{a}}^2} + ...\right) . \tag{3.5.6}$$

The resulting low-energy potential has the form

$$V_{\text{eff}} \sim \sum_{\hat{a}} \frac{m_{\hat{a}}^2}{M_{\hat{a}}^2} \left(g_5 D_S^{\hat{a}}\right)^2 + \ldots \tag{3.5.7}$$

where the dots denote terms of higher order in $m_{\hat{a}}/f_\Phi$. This potential gives a mass to the Goldstones in S and $\bar{S}$ (including the SM Higgs) of the order

$$m_h^2 \sim \frac{m_{\hat{a}}^2}{M_{\hat{a}}^2} f_S^2 \,. \tag{3.5.8}$$

This is phenomenologically acceptable as long as $m_{\hat{a}}/M_{\hat{a}} \lesssim 0.1$. One possibility is that $f_\Phi \sim M_{\hat{a}} \sim 10$ TeV as previously assumed, but the soft masses for Φ are an order of magnitude smaller than the other soft masses in the theory, $m_{\hat{a}} \sim 1$ TeV. This small mass hierarchy would be radiatively stable. Another possibility is that $m_{\hat{a}} \sim 10$ TeV along with the other soft masses, but $f_\Phi \sim 100$ TeV. In this case, all quadratic divergences are still cut off at 10 TeV due to SUSY, but SU(5)-violating logarithmic corrections are enhanced by running between 10 and 100 TeV scales. This leads to an additional contribution to the Higgs mass of order $\sim \frac{g^2}{16\pi^2} f_S^2 \log \frac{100 \text{ TeV}}{10 \text{ TeV}}$, which is of the same order as the top contribution.

The above discussion is completely general and does not depend on any particular representation of the $SU(5)$ breaking fields and their vevs, the specific form of the superpotential W_Φ, or the soft breaking potential $V_{\not{SUSY}}$. As an example consistent with our model, we can use a T-parity invariant superpotential of the form

$$W = \kappa\sigma(\mathrm{Tr}\,\Phi_1\Phi_1 + \mathrm{Tr}\,\Phi_2\Phi_2 - 60 f_\Phi^2) \; + \; W_{\text{Yuk}}(S, \bar{S}, K_1, K_2, \ldots), \tag{3.5.9}$$

with σ a gauge-singlet chiral superfield, and the soft breaking terms

$$V_{\not{SUSY}} = M_\Phi^2 \left(\mathrm{Tr}\,\Phi_1^\dagger \Phi_1 + \mathrm{Tr}\,\Phi_2^\dagger \Phi_2 \right) + M_\sigma^2 |\sigma|^2. \tag{3.5.10}$$

This potential has an extended $SU(5)^2$ global symmetry, and thus not all Goldstone bosons are eaten by the heavy gauge field. However, the uneaten Goldstones will receive a contribution to their mass of order $\frac{f_\Phi}{4\pi}$ at one loop, which is of order $1 - 10$ TeV.

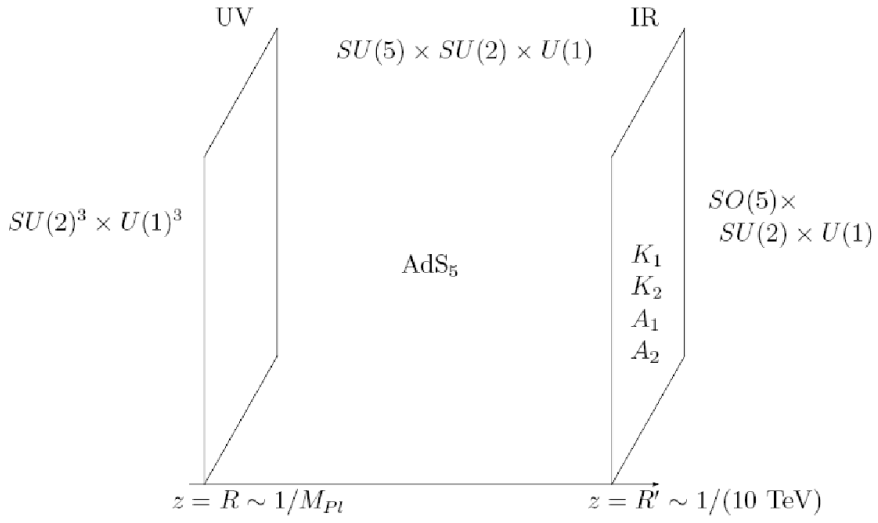

Figure 3.2: Geometric setup, gauge symmetries and matter content of the five-dimensional model.

3.5.2 A five-dimensional version

A popular alternative to supersymmetry for solving the weak/Planck hierarchy problem is the warped-space five-dimensional (5D) setup pioneered by Randall and Sundrum [75]. It is straightforward to embed our model into such a setup.[4]

The five-dimensional version of the model is illustrated in Fig. 3.2. We assume that the extra dimension has a warped AdS_5 gravitational background given by the metric

$$ds^2 = \left(\frac{R}{z}\right)^2 \left(\eta_{\mu\nu} dx^\mu dx^\nu - dz^2\right), \tag{3.5.11}$$

The extra dimension is an interval bounded at $z = R$ by the "ultraviolet" (UV) boundary (or brane), and at $z = R'$ by the "infrared" (IR) brane. The AdS curvature R is assumed to be $1/R \sim \mathcal{O}(M_{Pl})$, while $1/R'$ is of order a few TeV.

The 5D theory should reproduce at $\sim$ 1 TeV the T-odd particle spectrum

[4] A 5D version of the original Littlest Higgs model was given in [70].

necessary for the little Higgs mechanism. The cutoff scale of the 4D little Higgs theory is usually at around 10 TeV. In the 5D theory this will be identified with the scale m_{KK} where the additional KK resonances appear, thus UV completing the theory above 10 TeV. The cutoff scale of the 5D theory can be estimated via NDA to be of the order $\Lambda_{5D} \sim 24\pi^3/(g^2 R' \log R'/R)$, while the scale f is given by $f = 2/(gR'\sqrt{\log R'/R})$. In our case we want $f \sim 1$ TeV, then the cutoff scale is of order 100 TeV, while the KK mass scale is $m_{KK} \sim 2/R' \sim 10$ TeV.

The best handle for finding the right setup is to use the dictionary of the AdS/CFT correspondence. From that point of view we would be looking for the dual of a CFT with an $SU(5)$ global symmetry, where the $SU(2)^2 \times U(1)^2$ subgroup is gauged. As we discussed in this chapter, this symmetry needs to be extended to $SU(5) \times SU(2)_3 \times U(1)_3$, with $[SU(2) \times U(1)]^3$ gauged, in order to incorporate T-parity in the (chiral) fermion sector. So, the 5D setup we start with is an $SU(5) \times SU(2)_3 \times U(1)_3$ bulk gauge group. The action of T-parity on the gauge bosons is again given by eq. (3.2.10). We assume that the gauge symmetry is broken by boundary conditions (BC's) for the gauge fields, as in [89, 90]: on the UV brane,

$$SU(5) \times SU(2) \times U(1) \to [SU(2) \times U(1)]^3 \quad (\mathrm{UV})\,, \tag{3.5.12}$$

while on the IR brane

$$SU(5) \times SU(2) \times U(1) \to SO(5) \times SU(2) \times U(1) \quad (\mathrm{IR}). \tag{3.5.13}$$

In the language of the 4D model, this is equivalent to placing the $\Phi_{1,2}$ fields on the UV brane and the S field on the IR brane, and integrating out the radial models of these fields after they get vevs. (Note that this geometric separation of Φ and S automatically guarantees the absence of the direct potential couplings between them, as needed in our model.) These BC's result in an unbro-

ken $[SU(2) \times U(1)]^2$ gauge group at low energies and leave T-parity unbroken. The gauge fields in $[SU(2) \times U(1)]^3$ which are only broken by BC's on the IR brane will get a mass of order $f \sim 1$ TeV. These fields correspond to the T-odd gauge bosons of the LHT model. As discussed above, the full Kaluza-Klein (KK) tower starts at the somewhat higher scale $m_{KK} \sim 10$ TeV.

To reduce the group further (down to just the SM) we will assume that the scalars K_1, K_2 live on the IR brane, getting vevs of order $m_{KK} \sim 10$ TeV. Furthermore, to incorporate fermion masses in an $SU(5)$ invariant way, we also add the scalars A_1, A_2 on the IR brane,with vevs of order m_{KK}. (We will not need to introduce the scalars $F_{1,2}$ to give masses to $U_{L1,2}$.) Note that $m_{KK} \sim 10$ TeV is the natural scale for the vevs on the IR brane. It is an order of magnitude larger than the vevs for these fields in the 4D version of the model. However, these larger vevs do not lead to larger masses for the corresponding massless gauge bosons: in fact, their contribution to the masses is at most of order $gf \sim 1$ TeV. This can be seen by observing that the limit of very large vevs is equivalent to breaking gauge symmetries by BC's on the IR brane, which produce masses of order gf.

The A_5 components of the gauge fields corresponding to the broken $SU(5)/SO(5)$ generators develop zero modes. These modes, which are scalars from the 4D point of view, include the weak doublet identified with the SM Higgs. The Higgs mass is protected by the collective symmetry breaking mechanism. To see this, consider a variation of the symmetry breaking pattern in eqs. (3.5.12), (3.5.13), with $SU(5)$ broken down to a *single* $SU(2) \times U(1)$ subgroup on the UV brane. This theory possesses an $SU(3)$ global symmetry, broken down to $SU(2)$ by the BC's on the IR brane. The A_5 components identi-

fied with the Higgs are the Goldstone bosons of this global symmetry breaking, and as such are exactly massless. Thus, the Higgs can only get a mass if *both* $SU(2) \times U(1)$ factors in $SU(5)$ are unbroken at the UV brane. That is, zero modes for at least two different gauge fields must enter into any diagram contributing to the Higgs mass. Just as in the 4D LHT, this implies cancelation of the quadratic divergence in the Higgs mass between the SM gauge bosons and their T-odd counterparts at scale f. The remaining logarithmic divergence is canceled by the KK states at the scale of order $1/R' \sim 10$ TeV, and a finite Higgs mass is generated, as guaranteed by non-locality and 5D gauge invariance. Note that there may be additional light states among the A_5 modes due to the large vevs of $K_{1,2}$, $A_{1,2}$ on the IR brane. However, those would not be protected by the collective breaking mechanism, but only by the 5D non-locality, so their masses would be of the order of $m_{KK}/4\pi \sim 1$ TeV, rather than the 100 GeV range for the doubly protected physical Higgs.

It is useful to compare this structure to that of the "minimal" holographic composite Higgs model of Agashe, Contino and Pomarol [74]. In that model, *all* divergences in the Higgs mass are canceled at the same scale, the KK scale $1/R'$. Precision electroweak (PEW) constraints push this scale up to at least 3 TeV, and some amount of fine-tuning is needed to obtain consistent EWSB. In contrast, in our theory, the quadratic divergence is canceled at the 1 TeV scale by the Little Higgs mechanism, without any tension with PEW constraints thanks to T parity. This allows us to push the KK scale to 10 TeV without fine-tuning. At this scale, the KK states themselves are completely safe from PEW constraints. Thus, the tension between fine-tuning and PEW constraints is eliminated. Of course, the price to pay is a larger symmetry group and matter content.

In principle, the fermion content of the five-dimensional model could be simplified compared to the 4D $SU(5)$-invariant model, if one were to take advantage of the symmetry breaking BC's and simply project out some of the unwanted zero modes for the fermions (such as, for example, U_i and χ_i components of the Ψ_i fields) instead of introducing new states for them to marry. However, one needs to be careful with this, if T-parity is to be maintained as an exact symmetry. 5D theories are automatically anomaly free in the sense that every bulk fermion is actually a 4D Dirac fermion, and so the theory is always vectorlike. However, once orbifold projections are introduced, *localized* anomalies can be generated on the boundaries, which would be locally canceled by an anomaly flow corresponding to the bulk Chern-Simons (CS) term [91]. These bulk CS terms would contain the A_5 field and thus could violate T-parity similarly to the WZW operators in the 4D case. In order to avoid such terms, we need to make sure that there are no localized anomalies in our theory. The most obvious way of achieving this is by putting a separate bulk fermion field for every field in Tables 3.3 and 3.4, with a zero mode forming a complete $SU(5)$ representation. This would imply that we pick a $(+,+)$ boundary condition for all the left handed components, and a $(-,-)$ BC for all the right handed components. This choice ensures that all localized anomalies cancel in the same way as in the 4D theory (see section 3.4), and there would be no bulk CS term appearing. The terms corresponding to the Lagrangian in eqs. (3.3.3) and (3.4.1) can then be mimicked by brane localized Yukawa terms involving the K_1, K_2 fields on the IR brane, and via UV brane localized mass terms of the form $U_{L1}U_{R1} + U_{L2}U_{R2}$ (remember that on the UV brane $SU(5)$ is broken and so these mass terms are not violating gauge invariance, so we do not need to introduce $F_{1,2}$). If we were to try to simplify the spectrum by using $(-,+)$ type boundary conditions for

some of the fermions (and introducing fewer bulk fields), we would end up with a consistent theory, but with a bulk CS-term breaking T-parity.

In order to obtain Yukawa couplings, we need to make sure that the zero modes for the right-handed quarks also partly live in the right-handed component of $U_{L1,2}$. This can be achieved via the IR brane localized scalars corresponding to η, η', ξ, ξ' in eq. (3.3.11). A Lagrangian corresponding to eq. (3.3.13) can be also added to the IR brane, except for adding mass terms along the pattern of the $\langle S \rangle$ instead of the complete S field (which is allowed due to the symmetry breaking BC's). The effect of those boundary terms will be to partially rotate the u_R zero mode into Q_1, and thus generate our effective Yukawa coupling. Note, that since all global $SU(3)_{1,2}$ violating effects are non-local (as they need to involve both branes), the radiatively generated Higgs potential will be completely finite. We leave the detailed study of the EWSB and the phenomenology of the holographic T-parity models to future investigations.

3.6 Constraints from the Weinberg Angle, Precision Electroweak Fits, and Dark Matter

The model constructed in sections 3.2 and 3.3 correctly reproduces the particle content of the SM at low energies. At the TeV scale, the model reproduces the particle content and couplings of the LHT. This sector eliminates the little hierarchy problem, and is consistent with precision electroweak fits as long as $f_S \geq 500$ GeV, and the T-odd partners of the SM fermion doublets are not too far above the TeV scale [51]. In addition, our model contains a number of states at the TeV scale that were *not* present in the LHT. These states can produce ad-

ditional contributions to precision electroweak observables. While a detailed analysis of the resulting constraints is outside the scope of this study, we would like to briefly discuss the most salient constraint and show that it can be satisfied.

Most TeV-scale non-LHT states in our model are vectorlike fermions, and their contributions to PEW observables are small. The dominant new contribution is from the massive T-even gauge bosons. As discussed in section 3.2, these states can be significantly heavier than the T-odd gauge bosons, if the gauge couplings of the $SU(2)_3 \times U(1)_3$ gauge groups are stronger than that of the $SU(5)$ group. Since the SM Higgs does not couple to the $SU(2)_3 \times U(1)_3$ gauge bosons, the little hierarchy problem is still solved in this limit, provided that the T-odd gauge bosons remain sufficiently light. However, as mentioned at the end of section 3.2, the potential problem with this limit is the Weinberg angle prediction: the SM coupling are related to the $SU(5) \times SU(2)_3 \times U(1)_3$ gauge couplings via

$$\frac{1}{g^2} = \frac{2}{g_5^2} + \frac{1}{g_3^2} \quad \text{and} \quad \frac{1}{g'^2} = \frac{6}{5g_5^2} + \frac{1}{g_3'^2}\,, \tag{3.6.1}$$

so that $\sin^2\theta = 5/8$ in the limit $g_3', g_3 \gg g_5$. Is it possible to satisfy precision electroweak constraints and at the same time reproduce the experimental value of the Weinberg angle, $\sin^2\theta_{\text{exp}} \approx 0.2315$?

The spectrum of the TeV-scale gauge bosons has been discussed in section 3.2, see eqs. (3.2.12) and (3.2.13). However, these equations did not take into account the effect of the additional breaking of the $U(1)$ gauge bosons by the vevs of $A_{1,2}$ and $F_{1,2}$. Including these vevs, the $U(1)$ gauge boson masses are

$$m^2_{B_{\text{even}}} = \tfrac{g_5'^2+2g_3'^2}{4}(f_K^2+16f_A^2) \quad \text{and} \quad m^2_{B_{\text{odd}}} = \tfrac{g_5'^2}{100}(10f_S^2+f_K^2+16f_A^2+32f_F^2)\,, \tag{3.6.2}$$

(where $g_5' = \sqrt{5/3}\, g_5$),while the $SU(2)$ gauge boson masses are still given by eq. (3.2.12). It is convenient to rewrite the gauge boson spectrum and the Weinberg angle in terms of dimensionless ratios:

$$\begin{aligned}
\sin^2\theta &= \left[1 + \frac{1}{5}\cdot\frac{6+5/r'}{2+1/r}\right]^{-1} \\
\frac{m^2_{W_{\text{even}}}}{m^2_{W_{\text{odd}}}} &= \frac{1+2r}{1+2r_S} \\
\frac{m^2_{B_{\text{odd}}}}{m^2_{W_{\text{odd}}}} &= \frac{1+10r_S+16r_A+32r_f}{60(1+2r_S)} \\
\frac{m^2_{B_{\text{even}}}}{m^2_{W_{\text{odd}}}} &= \left[\frac{5}{3}+2r'\right]\frac{1+16r_A}{1+2r_S},
\end{aligned} \tag{3.6.3}$$

where the ratios are defined as

$$r = g_3^2/g_5^2,\ r' = g_3'^2/g_5^2,\ r_S = f_S^2/f_K^2,\ r_A = f_A^2/f_K^2,\ r_F = f_F^2/f_K^2. \tag{3.6.4}$$

Tree-level shifts in precision electroweak observables can be computed in terms of the T-even gauge boson masses and the coupling constant ratios, r and r'. For example, taking the Z mass, the Fermi constant G_F and the fine structure constant α as inputs, the shift in the W boson mass with respect to the reference value is given by

$$\Delta m_W \equiv m_W - c_w^{\text{ref}} m_Z = \frac{m_W}{4}\,\frac{\pi\alpha}{c_w^2 - s_w^2}\left(\frac{1}{r}\frac{v^2}{m^2_{W_{\text{even}}}} + \frac{5}{3}\frac{1}{r'}\frac{v^2}{m^2_{B_{\text{even}}}}\right), \tag{3.6.5}$$

where c_w^{ref} is the reference value of the cosine of the Weinberg angle, and $v \approx 246$ GeV is the Higgs vev. The structure of corrections to *all* observables is the same as in eq. (3.6.5): the contributions of the heavy $SU(2)$ states are proportional to $r^{-1}m^{-2}_{W_{\text{even}}}$, while those due to the heavy $U(1)$ states are proportional to $r'^{-1}m^{-2}_{B_{\text{even}}}$. This is because both the light-heavy gauge boson mixing, and the couplings of the heavy gauge bosons to light fermions, are inversely proportional to $\sqrt{r}$ or $\sqrt{r'}$.

This structure can be exploited to find the region of parameter space where the corrections are suppressed without fine-tuning. To avoid large corrections to the Higgs mass from the $SU(2)$ sector, the W_{odd} gauge bosons should be light, preferably around 1 TeV or below. At the same time, the W_{even} can be much heavier, if the parameter r is large. In this regime, the contribution to precision electroweak observables from the $SU(2)$ sector is suppressed both by the W_{even} mass and by its small mixing and couplings to the SM fermions, as noted above. The PEW constraint on the mass of an extra $SU(2)$ boson with SM-strength couplings (such as the KK gauge bosons in models with extra dimensions) is typically around 3 TeV. Using this value and assuming $m_{W_{\text{odd}}} = 1$ TeV and $f_S = f_K$, we estimate that the $SU(2)$ contributions in our model are sufficiently suppressed if $r \gtrsim 2$. The r parameter is limited from above by the requirement that the $SU(2)_3$ not be strongly coupled:

$$\frac{g_3^2}{4\pi} \lesssim 0.3 \quad \Leftrightarrow r \lesssim 5\,. \tag{3.6.6}$$

There is a wide rage of values where the model is perturbative and consistent with data.

Once r is fixed, the requirement of getting the correct Weinberg angle fixes r'; the range $2 < r < 5$ corresponds to $0.14 \lesssim r' \lesssim 0.16$, so that the $U(1)$ mixing angle is essentially fixed. Thus, the B_{even} boson *cannot* be decoupled by assuming large g_3'. Moreover, the couplings of the heavy $U(1)$ gauge boson to the SM fermions are actually enhanced compared to the SM hypercharge coupling. However, its mass is essentially a free parameter, and it can be heavy provided that $f_A \gg f_S, f_K$. For example, assuming again $m_{W_{\text{odd}}} = 1$ TeV and $f_S = f_K$, the value of $f_A = 3f_S$ gives $m_{B_{\text{even}}} \approx 10$ TeV, which should be completely safe for precision electroweak fits even with the enhanced coupling. At the same time, for the same parameters and $f_F = f_S$, the T-odd $U(1)$ boson B_{odd} has a mass

just above 1 TeV, so that the Higgs mass divergence is still canceled at 1 TeV and there is no fine-tuning. Thus, we estimate that in the region

$$2 \lesssim r \lesssim 5\,, \quad r' \approx 0.15\,, \quad r_A \gtrsim 10\,, \tag{3.6.7}$$

and all other dimensionless ratios of order one, our model should be consistent with precision electroweak data without fine-tuning in the Higgs mass.

An interesting phenomenological feature of the spectrum needed to satisfy the constraints is that the $B_{\rm odd}$ boson is not necessarily the lightest T-odd particle (LTP), in contrast to the situation typical in the original LHT model. Cosmological considerations require that the LTP not be strongly interacting or electrically charged. In our model, the T-odd partner of the SM neutrino can also play the role of the LTP. The T-odd neutrino LTP has not been considered in the previous studies of Little Higgs dark matter, which focused on the $B_{\rm odd}$ as the dark matter candidate. Our model provides a motivation to analyze this alternative possibility.

In addition to the gauge bosons, several new scalar states appear at the TeV scale in our model. These include pseudo-Goldstone bosons which receive a mass at the one-loop order, as well as the radial excitations of the fields S and $K_{1,2}$. Several of these states are triplets with respect to the SM weak SU(2). If allowed by T-parity and hypercharge conservation, gauge interactions will generate terms of the form $h^\dagger \phi_i h$, where ϕ_i are the triplets, in the one-loop Coleman-Weinberg potential. Such terms do indeed arise for some of the triplets in our model. Those triplets are forced to acquire vevs, which can give large corrections to precision electroweak observables. For example, this effect played an important role in constraining the original littlest Higgs model without T-parity [92]. In our model, the triplet vevs are not directly related to the magni-

tude of the Higgs quartic coupling, as was the case in the LH without T-parity. We expect that it should be possible to find phenomenologically consistent regions of parameter space where the triplet vevs are small.

3.7 Little Higgs Mechanism in the Linear Sigma Model

A key feature of little Higgs models is the protection of the SM Higgs mass from quadratic divergence at the one-loop level through collective symmetry breaking. We argued in sections 3.2 and 3.3 that, since our model below the 10 TeV scale reproduces the nlσm LHT, the same cancelations will occur. While our model has extra states at the TeV scale, the symmetric scalar field S, which contains the SM Higgs, has no direct couplings to those states. (It is uncharged under the extra gauge group $SU(2)_3 \times U(1)_3$ and has no Yukawa couplings other than the top Yukawa already present in the LHT.) Thus, no new one-loop quadratic divergences arise. This argument ensures that in our model the little hierarchy problem is resolved in exactly the same manner as in the LHT. Nevertheless, it is interesting and instructive to see explicitly how the little Higgs cancelations occur in our weakly-coupled, UV-complete model. We will do so in this section.

First, let is consider the renormalization of h_S mass by gauge boson loops. We will focus on the $SU(2)$ gauge bosons; the analysis for the $U(1)$ bosons is essentially identical. In our model, the Higgs coupling to the gauge bosons includes the terms

$$\mathcal{L} \supset \tfrac{1}{8} h_S^\dagger h_S \left(g_1^2 W_1^1 + g_2^2 W_2^2 \right), \tag{3.7.1}$$

where g_i denotes the gauge coupling to the $SU(2)_i$ subgroup of $SU(5)$ (which are

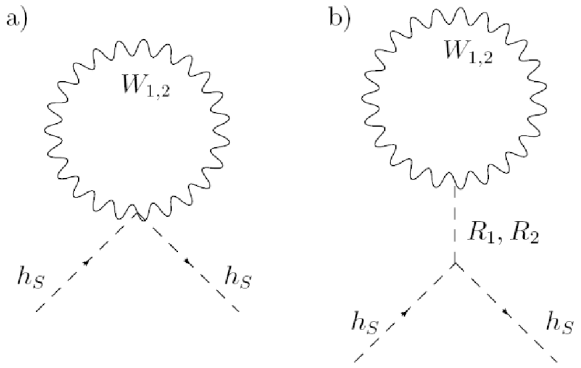

Figure 3.3: The Feynman diagrams contributing to the effective gauge couplings of the Higgs boson at low energies.

the same in our model, but potentially different in the original Littlest Higgs). These terms arise from the covariant derivative in eq. (3.2.4) and are required by gauge invariance. These couplings produce a quadratic divergence in the Higgs mass via the "bow-tie" diagrams in Fig. 3.3 (a). Recall that in the Littlest Higgs model, the structure of the four-point Higgs-gauge boson coupling is different [93]:

$$\mathcal{L}_{\rm LHT} \supset \tfrac{1}{4} g_1 g_2 W_1 W_2 (h^\dagger h), \tag{3.7.2}$$

which does not lead to a quadratic divergence at one loop. Since our model must reduce to the LHT below the 10 TeV scale, there seems to be a contradiction.

This issue is resolved when the full set of diagrams contributing to the Higgs mass at one-loop in our linearlized model is included. Specifically, the relevant diagrams are the ones involving two radial (heavy) modes of S, coupling to the Higgs and the gauge bosons. These diagrams are shown in Fig. 3.3 (b). Let us assume that a potential for S has the form

$$V = -M^2 \,\mathrm{Tr}\, SS^\dagger + \lambda_1 (\mathrm{Tr}\, SS^\dagger)^2 + \lambda_2 \,\mathrm{Tr}\, SS^\dagger SS^\dagger, \tag{3.7.3}$$

where $M^2 = 2(5\lambda_1 + \lambda_2)f_S^2$. This potential produces the desired pattern of symmetry breaking at scale f_S. It leads to the following pieces in the Lagrangian containing the heavy radial modes R_1 and R_2 (amongst others):

$$\begin{aligned}\mathcal{L} \supset & -\tfrac{1}{2}M_{R_1}^2 R_1^2 - \tfrac{1}{2}M_{R_2}^2 R_2^2 + \tfrac{1}{\sqrt{5}f_S}\left(\tfrac{3}{2}M_{R_1}^2 R_1 + 2M_{R_1}^2 R_2\right) h_S^\dagger h_S \\ & + \frac{f_S}{4\sqrt{5}}(R_1 - 2R_2)\left(g_1^2 W_1^2 + g_2^2 W_2^2 - 2g_1 g_2 W_1 W_2\right) ,\end{aligned} \tag{3.7.4}$$

where the radial modes have masses $M_{R_1}^2 = 32\lambda_2 f_S^2$ and $M_{R_2}^2 = 32(5\lambda_1 + \lambda_2)f_S^2$. Note that the couplings of the radial modes to $h_S^\dagger h_S$ are proportional to their masses. The effective Lagrangian below the scale f_S is obtained by integrating out the radial modes $R_{1,2}$ in eq. (3.7.4). The resulting Lagrangian contains terms that exactly cancel the gauge-Higgs four-point couplings in eq. (3.7.1). The remaining coupling has the form

$$\mathcal{L}_{\text{eff}} \supset \tfrac{1}{4}g_1 g_2 W_1 W_2 (h_S^\dagger h_S), \tag{3.7.5}$$

which exactly matches the non-linear Littlest Higgs Lagrangian and does not lead to quadratic divergences at one loop. Note that this result is independent of the couplings $\lambda_{1,2}$, as expected from the Coleman-Wess-Zumino theorem.

In a completely analogous way, one can show that the diagrams for canceling the top loop divergence are generated by integrating out R_1, R_2 properly. These diagrams are shown in Fig. 3.4. Especially, we also recover the sum rule from [94] for the Yukawa coupling of the top quark with itself λ_t and with its heavy partner λ_T

$$\frac{M_T}{f_S} = \frac{\lambda_t^2 + \lambda_T^2}{\lambda_T}, \tag{3.7.6}$$

which ensures that the one-loop quadratic divergence due to the top quark cancel.

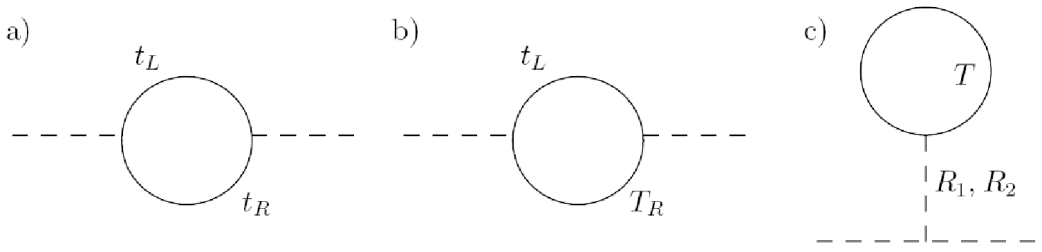

Figure 3.4: The Feynman diagrams contributing to the effective top couplings of the Higgs boson at low energies.

3.8 Conclusions and Outlook

In this chapter, we constructed a weakly coupled, renormalizable theory which reproduces the structure of the LHT model below the 10 TeV scale. This structure includes collective symmetry breaking mechanism to protect the Higgs mass from one-loop quadratic divergences, resolving the little hierarchy problem. The model is manifestly free of anomalies, and T-parity is an exact symmetry of the quantum theory. This leads to an exactly stable lightest T-odd particle, which can be either the T-odd hypercharge gauge boson or the partner of the neutrino. This particle can play the role of dark matter, and provide a missing energy signature at colliders. In addition, our model contains a few T-even extra states at the TeV scale, which can however be made sufficiently heavy to avoid conflict with precision electroweak data, without any fine tuning. Above the 10 TeV scale, our model can be embedded into either a supersymmetric theory or a five-dimensional setup with warped geometry, stabilyzing the large hierarchy between 10 TeV and the Planck scale. A remaining concern regarding the fully anomaly free matter content is that due to the large numbers of states required for anomaly cancelation a Landau pole in the QCD gauge coupling would rapidly develop. It would be very interesting to find a smaller anomaly

canceling matter content that can avoid this issue.

In a weakly coupled UV completion of the LHT, a number of issues can be addressed which could not be analyzed in the original effective theory. One issue is gauge coupling unification, since in our model renormalization group evolution of all couplings is calculable within perturbation theory above 10 TeV. Unfortunately, in the explicit anomaly-free models constructed here, the range of validity of perturbation theory is limited by the rapid increase in the gauge couplings above 10 TeV. In these models, no gauge coupling unification occurs within the perturbative regime. If consistent UV completions with smaller matter content are found, the issue of gauge unification should be reexamined.

Another important issue is flavor physics, in particular flavor-changing neutral currents (FCNCs). There are two sources of FCNCs in the LHT model. The first one is the effects generated by loops of heavy T-odd quarks and leptons, calculable within the effective theory. These effects have been considered in [95–98]. The second class are the effects generated at or above the cutoff scale of the effective theory. These effects should be represented by local operators in the effective theory, with coefficients obtained by matching to the UV completion at the cutoff scale. If the UV completion does not contain any flavor structure, one expects such operators to appear suppressed by powers of the cutoff scale, with order-one coefficients. In the LHT, the cutoff scale is 10 TeV, so several of these operators would strongly violate experimental bounds on the FCNCs. This indicates that additional flavor structure (e.g. flavor symmetries) is a necessary part of the UV completion of the LHT. It would be interesting to extend out model to obtain realistic flavor physics.

CHAPTER 4

MODEL DISCRIMINATION AT THE LHC: A CASE STUDY

Published in Physical Review D **79**, 075024 (2009).

4.1 Introduction

Theoretical arguments strongly indicate that the Standard Model (SM) picture of electroweak symmetry breaking is incomplete, and numerous extensions of the SM at the electroweak scale have been proposed. It is expected that at least some of the new particles and interactions predicted by such extended theories will be discovered and studied at the LHC. The ultimate goal of the experiments is, of course, to determine the correct theory of physics at the TeV scale. This task may be quite complicated. In particular, it is quite likely that nature is described by one of the several models possessing the following features:

- Physics at the TeV scale is weakly coupled, and there is a light Higgs (as motivated by precision electroweak data);
- A number of new states are present at the TeV scale, and new particles can be paired up with the known SM states, with states in the same pair carrying identical gauge charges;
- New states carry a parity quantum number distinct from their SM counterparts, implying that the lightest new particle (LNP) is stable;
- The LNP is weakly interacting (as motivated by cosmological constraints on stable particles).

The best known model of this class is the minimal supersymmetric standard model (MSSM). Other contenders include models with universal extra dimensions (UED) and Little Higgs models with T parity. Broadly speaking, all these theories share the same LHC phenomenology: the new physics production is dominated by the colored states, which are pair-produced, and then decay down to the LNP and SM states. The interesting final states then involve jets in association with missing transverse energy and possibly leptons and photons. Only by studying the detailed properties of these objects can one hope to discriminate among the models.

The most convincing way to discriminate between supersymmetry and its competitors is to measure the spin of the new particles: in the Little Higgs and UED models the new states and their SM partners have the same spin[1], while in SUSY models their spins differ by 1/2. Measuring spin at the LHC, however, is notoriously difficult. Almost all existing proposals rely on the observation that, if the produced strongly interacting state decays via a cascade chain, angular correlations between the particles emitted in subsequent steps in the cascade carry information about spin. (See Refs. [46–48, 99–103], as well as a recent review [104].) The availability of cascade decays with the right properties for this to work, however, depends on the spectrum and couplings of the model, and is by no means guaranteed. Moreover, a large amount of data is typically needed to alleviate combinatoric and other backgrounds.

If unambiguous spin measurments are unavailable, the experiments can still attempt a more modest task of model discrimination, *i.e.* determining which of two or more specific theoretical models provides a better fit to the available

[1]Robust discrimination between the Little Higgs and UED would require observing or ruling out the excited level-2 and higher KK excitations of the UED model, absent in the Little Higgs.

data. Unlike a direct spin measurement, which would rule out the entire *class* of models with the wrong spin assignment, this approach can only discriminate between *specific* models. For example, if it is found that the minimal Littlest Higgs with T-parity (LHT) model cannot fit the data, it does not exclude the possibility that another model of the Little Higgs class could provide a better fit. Still, this approach can provide valuable information, and is well worth pursuing at the LHC, especially at the early stages.

The goal of our study is to estimate the prospects for model discrimination with the CMS detector. As a test case, we consider a very simple scenario: We assume that the *only* new physics process observable at the LHC is pair-production of new color-triplet particles, followed by their decay into a quark and an LNP. This process occurs at the LHC at a significant rate over large parts of the parameter space of the MSSM, LHT, and UED models. Its detector signature is two hard jets (plus possibly additional jets from gluon radiation and showering) and missing transverse energy. Our assumption that no other signatures are observed allows us to focus on this channel alone, and to understand in detail the issues important for model discrimination. It would be straightforward to repeat our exercise with more complicated models for the exotic particle production (e.g. including color octet pair-production channels) and decay (e.g. including cascade chains involving leptons and/or weak bosons).

The main motivation for our study comes from the work of Barr [105], who showed that the angular distributions of leptons from the decay of lepton partners produced directly (via electroweak processes) in hadron collisions carry information about the lepton partner spin. This example is particularly simple since the lepton partners are always produced in s-channel quark collisions, and

their angular distribution in the production frame is almost unambiguously determined by their spin. However, its utility is somewhat limited by the small cross section of the direct lepton partner process. For quark partners, the cross sections are larger, but the production mechanism is more complicated: both quark-initiated and gluon-initiated processes need to be included, and in both cases there are both s-channel and t-channel diagrams. Still, as we will show, the model-dependence of the matrix elements can be sufficiently strong to yield observable differences between the models. Crucially, the differences cannot be removed by simply varying the free parameters of the model with the wrong spin assignments: to demonstrate this, we performed a scan over the parameter space of the "untrue" model. (A recent model-discrimination study of Hubisz *et. al.* [106], which studied a situation similar to our test case, also noted the significant differences in jet distributions between models with different spins, but was restricted to a single benchmark point in each model's parameter space. The importance of scanning over parameters in model-discrimination studies has been recently emphasized in Refs. [103, 107].)

The rest of the chapter is organized as follows: In section 2, we give a description of the minimally supersymmetric and Little Higgs models used in our study, including input parameters and particle spectra as well as the relevant production processes and decay chains. We discuss the dominant standard model backgrounds and the selection cuts that were applied to isolate signal events. We then define our observables and describe the statistical analysis. Section 3 contains the results of our model scan, including exclusion plots for 200 pb^{-1}, 500 pb^{-1}, 1 fb^{-1} and 2 fb^{-1} of integrated luminosity. We summarize our conclusions in section 4. Finally, the appendix includes a list of formulas for error estimates, a description of our method to calculate covariances, as well as

Table 4.1: Cross sections of squark pair-production processes at the LHC at the study point of Eq. (4.2.1). Here $q = u, d, s, c$. Factorization and renormalization scales are set to 500 GeV. The CTEQ6L1 parton distribution functions are used. The matrix elements are evaluated at tree level using `MadGraph/MadEvent`, and no K-factors are applied.

final state	$\tilde{u}_L\tilde{d}_L$	$\tilde{q}_{L,R}\tilde{q}^*_{L,R}$	$\tilde{u}_L\tilde{u}_L$	$\tilde{u}_R\tilde{d}_R$	$\tilde{u}_R\tilde{u}_R$	$\tilde{d}_L\tilde{d}_L$ $\tilde{u}_L\tilde{d}^*_R$ $\tilde{u}_R\tilde{d}^*_L$	$\tilde{u}_L\tilde{u}^*_R$ $\tilde{u}_R\tilde{u}^*_L$	$\tilde{d}_R\tilde{d}_R$ $\tilde{d}_R\tilde{d}^*_L$ $\tilde{d}_L\tilde{d}^*_R$	$\tilde{u}^*_L\tilde{d}_R$ $\tilde{u}^*_R\tilde{d}_L$
σ(fb)	600	400	300	230	170	80	65	40	30

an example of the angular distribution of jets at an excluded LHT model point.

4.2 Setup

We will focus on the discrimination between the minimal versions of the MSSM and the Littlest Higgs with T-parity (LHT) [49–51, 59]. Both models have been extensively studied in the literature; for reviews, see Refs. [3, 52]. Each model contains color-triplet massive partners for each SM quark: squarks in the MSSM and T-odd quarks, or TOQs, in the LHT. Also, each model contains a stable weakly-interacting particle: the neutralino of the MSSM and the "heavy photon" (the T-odd partner of the hypercharge gauge boson) of the LHT. We will assume that these are the only particles that play a role in the LHC phenomenology; the rest of the new states in each model are too heavy to be produced. Note that the two minimal models have important differences in their particle content: for example, the minimal LHT does not have a color-octet heavy particle, a counterpart of the gluino; while the MSSM does not have a T-even partner of the top quark present in the LHT [94,108]. In our scenario, however, neither of these particles is observed. This null result does not help with model discrimination,

since we don't know whether the particles don't exist or are simply beyond the LHC reach. Model discrimination must rely on the observed properties of the produced exotic particles or their decay products.

Our strategy is to simulate a large sample of events corresponding to one of the models (we will choose the MSSM) with fixed parameters, and treat this sample as "data". The question is then, how well can this data be fitted with the alternative model, in this case the LHT? It should be emphasized that the predictions of the LHT model are not unique, but depend on the LHT parameters. So, when fitting data, one should look for the point in the LHT parameter space that provides the *best fit*. The LHT can be said to be disfavored by data only to the extent that this best-fit point is disfavored.

4.2.1 "Data"

For our case study, we assume that the MSSM is the correct underlying theory, with the following parameters:

$$\begin{aligned} m(\tilde{Q}_L^{1,2}) &= m(\tilde{u}_R^{1,2}) = m(\tilde{d}_R^{1,2}) = 500 \text{ GeV} \ ; \\ m(\tilde{Q}_L^{3}) &= m(\tilde{u}_R^{3}) = m(\tilde{d}_R^{3}) = 1 \text{ TeV} \ ; \\ m(\tilde{L}_L^{1,2,3}) &= m(\tilde{e}_R^{1,2,3}) = 1 \text{ TeV} \, ; \quad A_{Q,L}^{1,2,3} = 0; \\ M_1 &= 100 \text{ GeV} \, ; \quad M_2 = 1 \text{ TeV} \, ; \quad M_3 = 3 \text{ TeV} \, ; \\ M_A &= 1 \text{ TeV} \, ; \quad \mu = 1 \text{ TeV} \, ; \quad \tan\beta = 10 \, . \end{aligned} \tag{4.2.1}$$

All parameters are defined at the weak scale, and no unification or other high-scale inputs are assumed. The parameter choices are driven by the desire to study a point with very simple collider phenomenology: the new physics production at the LHC is completely dominated by pair-production of the first two

generations of squarks. The total squark pair-production cross section is 5.0 pb. Table 4.1 lists the 22 leading squark pair-production processes, which together account for over 98% of the total. Associated squark-gluino production is strongly suppressed by the high gluino mass; the cross section (summed over squark flavors) is only 11 fb. Associated squark-neutralino production is larger, with the total cross section of about 290 fb. However, these events have only a single hard jet, and will not pass the analysis cuts (see section 4.2.4). Production of third generation squarks is also strongly suppressed, with a total cross section of only 17 fb. Thus, in our analysis we will simulate the processes listed in Table 4.1, and ignore all other SUSY production channels.

Another simplification that occurs at the chosen parameter point is in the decay pattern of the produced squarks: they decay into quarks and the lightest neutralino (essentially a bino) with a 100% probability. This means that in this model, the only place where strong evidence for new physics would show up at the LHC is the two jets+missing energy channel. We will limit our study to this channel.

The "data" event sample has been generated in the following way. First, we simulate a sample of parton-level events using the `MadGraph/MadEvent` package [40, 109]. The production processes included in this simulation, and their cross sections, are listed in Table 4.1. The squark decays are also handled by `MadGraph/MadEvent`, using the narrow-width approximation. The sample size corresponds to 10 fb^{-1} of integrated luminosity at the LHC. The resulting events are stored in a format compatible with the Les Houches accord, and then passed on to `PYTHIA` [43, 44] to simulate showering and hadronization. The `PYTHIA` output is then passed on to the detector simulation code. We

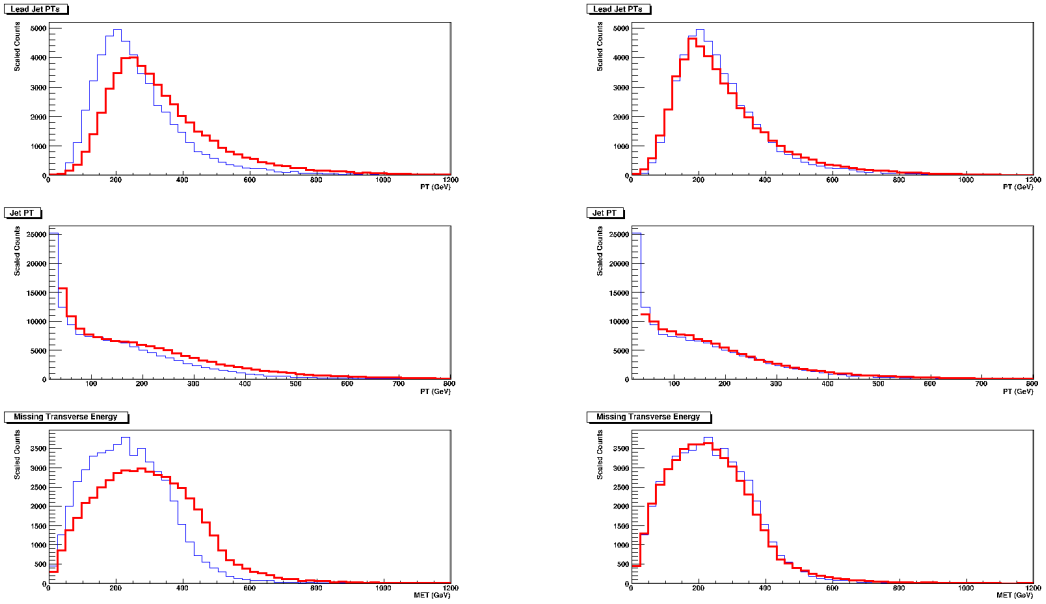

Figure 4.1: Jet p_T and missing transverse energy distributions in the MSSM, obtained with PGS (red/thick line histograms) and full CMS simulation (blue/thin line histograms). Left panel: Uncorrected PGS. Right panel: A jet energy scale correction factor has been applied to the PGS output.

use a modified version of the PGS code to perform fast (parametrized) detector simulation. The drastic speed-up of the event simulation provided by PGS (compared to full CMS detector simulation) allows us to scan the LHT parameter space, generating a statistically significant event sample for each point in the scan. To calibrate PGS to the CMS detector, we have generated two calibration event samples (one in the MSSM and one in the LHT) using the full CMS detector simulation, and compared them to the PGS output for the same two underlying models. On the basis of this comparison, we determined that the energy and angular distributions of the PGS jets are in excellent agreement with the full CMS simulation, once the jet energy has been appropriately corrected. This is clear from Fig. 4.1, which shows the jet p_T and missing transverse en-

ergy distributions in the MSSM, obtained with PGS (red histograms) and full CMS simulation (black histograms). For jets satisfying the selection criteria of our analysis (in particular, $p_T^{\min} = 100$ GeV), the correction factor is essentially the same as the one appearing in translation from parton-level jet energy to the energy reconstructed by the detector [110] (i.e., the PGS output in this p_T range essentially corresponds to parton-level jets). We have applied this correction factor to the PGS output throughout our analysis.

4.2.2 Little Higgs Model

If the only evidence for new physics is in the two jets+missing energy channel, it is natural to try to fit the data with the LHT model, assuming the dominant production process

$$pp \to U_i' \bar{U'}_i \,, \tag{4.2.2}$$

where U_i' is the TOQ of flavor i. We will assume that four flavors of TOQs, $i = u, d, s, c$, are degenerate at mass M_Q and are within the reach of the LHC, with the other two flavors being too heavy to play a role. Once produced, TOQs promptly decay via

$$U_i' \to q_i B', \quad \bar{U'}_i \to \bar{q}_i B' \,, \tag{4.2.3}$$

giving a 2 jets+MET signature. Here B' is the lightest T-odd particle (LTP), the heavy photon of mass M_B. The LHT predictions in this channel are sensitive to only two model parameters, M_Q and M_B, which allows us to scan the parameter space with realistic computing resources. The counterpart of the process (4.2.2), (4.2.3) in the pp collisions at the Tevatron was considered in Ref. [62]. The Tevatron experiments exclude a region in the $M_Q - M_B$ plane: roughly, they place a lower bound of $M_Q \gtrsim 350$ GeV for light B', $M_Q - M_B \gtrsim 250$ GeV, and

Table 4.2: Signal and Background cross sections (in pb), where σ_n denotes the cross section after cuts 1 to n (see text for description). Also listed are the total number of events simulated for our study.

	σ_{tot}	σ_1	σ_2	σ_3	σ_6	σ_7	N_{sim}
Signal (SUSY)	5.00	4.98	4.10	2.91	2.06	0.65	10,037
$(Z \to \nu\nu) + jj$	271.54	259.73	94.05	64.34	10.21	0.20	543,080
$(W \to \nu\ell) + jj$	55.80	52.58	19.30	12.89	6.27	0.37	111,602
$(W \to \nu\tau) + j$	138.27	92.67	12.18	2.49	0.52	0.04	276,540
$t\bar{t}$	398.52	384.14	27.85	13.89	1.62	0.04	797,039
total BG	864.13	789.11	153.37	93.61	18.62	0.65	1,728,261

somewhat weaker bounds for heavier B'. (There is no bound if $M_Q - M_B \lesssim 50$ GeV.)

To assess how well the data can be fitted with the LHT model, we perform a scan in the (M_Q, M_B) plane. We have picked 125 points in the LHT parameter space, uniformly scanning in the ranges

$$\begin{aligned} M_Q &= [500, 950]\ \text{GeV}\,, \\ M_B &= [100\ \text{GeV}\,, M_Q]\,. \end{aligned} \tag{4.2.4}$$

For each point in the scan, we generate an event sample using the procedure outlined in section 4.2.1 above. Each sample corresponds to 10 fb^{-1} of integrated luminosity at the LHC.

4.2.3 Backgrounds

Several Standard Model processes contribute to the jets + missing energy final state. The following background processes are dominant:

- Z+2 jets, with Z decaying invisibly (irreducible background);
- W+2 jets, with W decaying leptonically and the charged lepton misidentified or undetected;
- W+1 jet, with W decaying to $\tau\nu_\tau$, the τ decaying hadronically and misidentified as a jet
- $t\bar{t}$, with at least one of the top quarks decaying leptonically and the charged lepton(s) misidentified or undetected.

The cross sections for each process are listed in Table 4.2. (For the Z/W+jets channels, we list the parton-level $Z/W+2$ jets cross sections with $p_T^j \geq 100$ GeV.) We simulated two independent Monte Carlo samples for each process. One of the samples is mixed with the SUSY events to obtain the "data" sample, while the other one is mixed with the LHT events and used to fit the data. The size of each sample corresponds to 2 fb^{-1} of LHC data. All samples have been simulated following the same simulation path as for the signal: parton-level simulation with `MadGraph/MadEvent`, followed by showering and hadronization simulation with `PYTHIA` and a parametrized detector simulation with the modified `PGS`. It should be kept in mind that some of the CMS detector performance parameters which affect the background rates, such as lepton misidentification probabilities, may not be realistically modeled by `PGS`. In principle one could normalize these parameters using full CMS detector simulation, as we did for the jet-energy corrections. However, given the preliminary nature of our study, we did not attempt such normalization.

In addition to the processes listed above, pure QCD multi-jet events with mismeasured jets leading to apparent missing energy are expected to make an

important contribution to the background. However, until the detector is calibrated with real data, it is difficult to predict this background. We have not included it in this preliminary analysis.

4.2.4 Triggers and Selection Cuts

Throughout the analysis, we impose the following cuts:

1. At least two reconstructed jets in the event
2. $p^T(j_1) \geq 150$ GeV
3. $p^T(j_2) \geq 100$ GeV
4. $\eta(j_1) \leq 1.7$
5. $\eta(j_2) \leq 1.7$
6. No identified leptons (e,μ or τ) in the event
7. $\not{E}_T \geq 300$ GeV

where the jets are labeled according to their p_T, in descending order. We do not impose any explicit cuts on jet seperation, since jet reconstruction in PGS effectively acts as a minimum separation cut. The LHC data samples will correspond to certain trigger paths, in our case to the $\not{E}_T$ trigger and to jet triggers. Using simple parametrizations for the trigger efficiencies [111] we expect them to be essentially 100% efficient, given our selection cuts.

The signal and background cross sections passing each of the selection cuts are listed in Table 4.2. After the cuts are applied, we obtain

$$S/B = 1.0, \quad S/\sqrt{B} = 36 \quad (2\ \text{fb}^{-1}) \tag{4.2.5}$$

for the SUSY signal. The S/B value is not as good as those obtained in some existing studies of SUSY search prospects (see, for example, Refs. [106, 112]). The reason is that in those analyses gluinos are assumed to be light, around 500 GeV, which greatly increases the signal cross section and also yields three or more hard jets in the final state in most events, allowing to further suppress the background. Still, the relatively large new physics cross section implies that if reasonably accurate predictions of the background rate are available, the presence of new physics can be convincingly established. In particular, using the 10 observables listed below and the assumptions about the systematic and statistical errors described in Appendix 4.3, we estimate that the existence of new physics in this channel will be established at the level of 2.5, 4.2, and 4.9 sigma, with analyzed data samples of 200 pb^{-1}, 500 pb^{-1}, and 1 fb^{-1}, respectively. The discovery is dominated by shape observables: if the total rate, which may suffer from large uncertainties in the MC predictions, is removed from the fit completely, the confidence levels are only marginally lower.

4.2.5 Observables

Our analysis uses the following observables:

- $\sigma_{\rm eff}$: The cross section, in pb, of events that pass the analysis cuts. Experimentally, this quantity is inferred from the measured event rate using $N_{\rm obs} = \mathcal{L}_{\rm int}\sigma_{\rm eff}$, where $N_{\rm obs}$ is the number of events passing the cuts in a sample collected with integrated luminosity $\mathcal{L}_{\rm int}$. It is related to the total production cross section by $\sigma_{\rm eff} = \sum_i \sigma_i E_i$, where the sum is over all processes (signal and background) which contribute to the sample, and

σ_i and E_i are the total cross section and combined trigger/cuts efficiency, respectively, for channel i.

- $\langle p_T \rangle$: The average transverse momentum of all jets with $p_T > 100$ GeV in a given data sample that pass the analysis cuts. This variable is tightly correlated with the mass difference between TOQ and the LTP, $M_Q - M_B$.
- $\langle \ |\Sigma\eta| \ \rangle$: The average of the absolute value of the sum of the pseudo-rapidities of the two leading (highest-p_T) jets in the event.
- $\langle H_T \rangle$: The average of the scalar sum of the transverse momenta of all jets in the event plus the missing transverse energy

$$H_T = \sum_{\text{jets}} p_T^{(i)} + \not{E}_T.$$

- $\langle \not{E}_T \rangle$, the average of the missing transverse momentum in the events that pass the selection cuts.
- *Beam Line Asymmetry (BLA):* This observable is defined as $(N_+ - N_-)/(N_+ + N_-)$, where N_+ and N_- are the numbers of events with $\eta_1\eta_2 > 0$ and $\eta_1\eta_2 < 0$.
- *Directional Asymmetry (DA):* The same as above, where N_+ (N_-) are now the numbers of events where $\vec{p}_1 \cdot \vec{p}_2$ is positive (negative).[2]. A plot showing the distribution of relative angles between the two hardest jets can be found in Fig.4.5 in the appendix.
- *Transverse momentum asymmetry (PTA):* The ratio N^+/N^- of the number of jets with p_T larger than $\langle p_T \rangle$ and the number of jets with p_T smaller than $\langle p_T \rangle$.

[2]For a recent analysis using BLA and DA in a context similar to ours, see Ref. [113]

Table 4.3: Correlation matrix of observables in the SUSY plus SM background "data" sample, generated from 2 fb^{-1} of simulated events with 50 subsamples and 10,000 iterations. A description of the procedure used to calculate this matrix can be found in appendix 4.3.

	$\langle p_T \rangle$	$\langle H_T \rangle$	$\langle \not{E}_T \rangle$	$\langle \lvert\Sigma\eta\rvert \rangle$	BLA	DA	PTA	R_1	R_2
$\langle p_T \rangle$	1	0.86	0.42	-0.08	-0.03	-0.37	0.30	0.88	0.00
$\langle H_T \rangle$	0.86	1	0.66	-0.10	-0.05	-0.34	0.22	0.76	-0.06
$\langle \not{E}_T \rangle$	0.42	0.66	1	-0.04	-0.04	-0.06	0.05	0.35	-0.11
$\langle \lvert\Sigma\eta\rvert \rangle$	-0.08	-0.10	-0.04	1	0.64	0.50	-0.01	-0.07	0.02
BLA	-0.03	-0.05	-0.04	0.64	1	0.41	-0.02	-0.02	-0.00
DA	-0.37	-0.34	-0.06	0.50	0.41	1	-0.21	-0.38	-0.16
PTA	0.30	0.22	0.05	-0.01	-0.02	-0.21	1	0.22	0.64
R_1	0.88	0.76	0.35	-0.07	-0.02	-0.38	0.22	1	0.14
R_2	0.00	-0.06	-0.11	0.02	-0.00	-0.16	0.64	0.14	1

- *Transverse momentum bin ratios:* We distribute the jets in the event into three fixed bins, depending on their transverse momentum. The first bin corresponds to 100 GeV$< p_T <$300 GeV (N_1 events), the second to 300 GeV$< p_T <$500 GeV (N_2 events), and the third to $p_T >$500 GeV (N_3 events). We then define two bin count ratios, $R_1 = N_2/N_1$ and $R_2 = N_3/N_1$.

We compute the "measured" values of these observables using the "data" sample. For each LHT point in the scan, we compute the expected central values of the observables using the corresponding MC sample. We then use the standard χ^2 technique to estimate the quality of the fit between the expected and measured values. The observables are assumed to be Gaussian distributed, with the variances including statistical and systematic errors added in quadruture. The correlation matrix between observables for each LHT point is obtained from the generated Monte Carlo sample; the details of the procedure and error analysis are described in Appendix 4.3. As an example, we show the correlation

matrix for our susy "data" sample in Table 4.3. The quality of the fit to data at each LHT point is quantified by the χ^2 value, which can in turn be converted into probability that the observed disagreement between the measured and expected values of the observables is the result of a random fluctuation. (If this probability is close to one, the fit is perfect; if it approaches zero, the fit is very poor.) As a sanity check to validate our statistical procedure, we simulated a large number of independent subsamples of SUSY and SM background events, and confirmed that the distribution of χ^2 values agrees with statistical fluctuations.

4.3 Error estimates

Our estimates for the significance level of model exclusion rely on correct evaluation of statistical and systematic errors. We therefore include a summary of formulas used in our analysis. We use three fundamentally different types of observables. The first class consists of averages of measured quantities like the mean jet p_t and the mean H_t of events. Secondly, asymmetries in event shapes, as well as bin ratios, are obtained by counting events that do or do not fulfill certain conditions. Finally, the cross section is calculated from the total number of signal and background events after cuts.

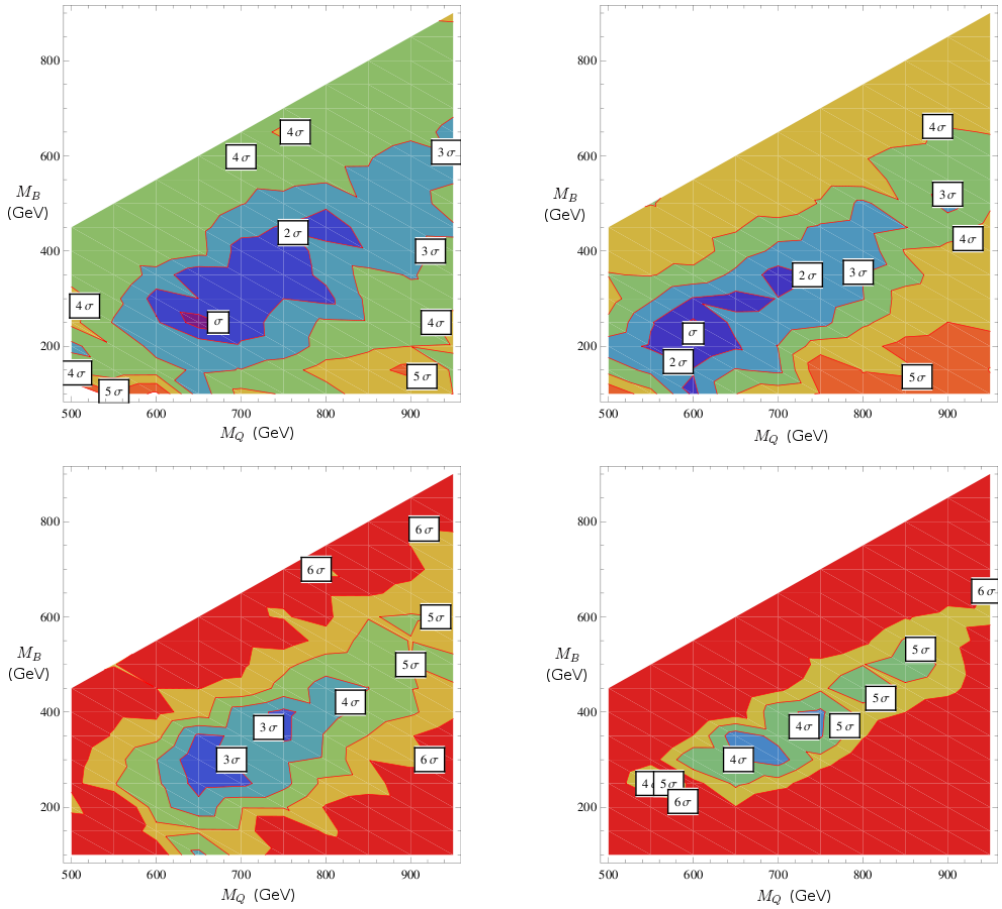

Figure 4.2: Exclusion level of the LHT hypothesis, based on the combined fit to the ten observables discussed in the text. Top left panel: with integrated luminosity of 200 pb^{-1} at the LHC. Top right panel: same, with integrated luminosity of 500 pb^{-1}, Bottom left panel: integrated luminosity of 1 fb^{-1}, Bottom right panel: 2 fb^{-1}.

4.3.1 Mean value observables

The error in transverse momentum p_T of individual jets is estimated using the parameterization given in [112].

$$\sigma_{p_T} = \left(\frac{5.6}{p_T^{\text{PGS}}} + \frac{1.25}{\sqrt{p_T^{\text{PGS}}}} + 0.033 \right) p_T^{\text{meas}}$$

where all momenta are in GeV, p_T^{PGS} is the transverse momentum obtained from PGS, and p_T^{meas} is the rescaled momentum as in [110].

The average transverse momentum observable $\langle p_T \rangle$ is calculated by taking the mean of all jets with a minimum p_T of 100 GeV in the events that pass our selection cuts.

The missing transverse energy as given by PGS has to be corrected to account for the change in jet energy scales. The modified missing transverse energy is

$$\not{E}_{T\,\text{meas}} = \not{E}_{T\,\text{PGS}} + \sum_{i=1}^{N_{\text{jets}}} \left(p_T^{\text{PGS}} - p_T^{\text{meas}} \right),$$

where the sum is a vector sum in the transverse plane.

The error in the missing transverse energy $\not{E}_T$ is estimated as

$$\sigma^2_{\not{E}_T} = (3.8\,\text{GeV})^2 + 0.97^2\,\text{GeV}\,\not{E}_T + (0.012\,\not{E}_T)^2$$

as given in [112].

The observable $\langle H_T \rangle$ is given by the scalar sum of the transverse momentum of all objects plus the missing energy in the event. The error of this quantity is calculated by adding the errors of each object and the missing energy in quadrature.

Given a list of individual measurements of the jet p_T, $\not{E}_T$, or H_T, the statistical error of the mean value is given by

$$\sigma^2_{\text{stat}} = V/N,$$

where V is the variance of the distribution and N is the number of entries. The systematic error is given by

$$\sigma^2_{\text{syst}} = \nu^2/N,$$

where ν is the mean value of the distribution.

For the average sum of leading jet pseudorapidities $\langle|\Sigma\eta|\rangle$ the statistical error is estimated as above, while the systematic error is calculated from

$$\sigma^2_{\text{syst}} = \frac{w_c^2}{2N},$$

where the η cell width w_c is 0.087.

4.3.2 Counting type observables

Given two bins of events N^+ and N^-, we define the asymmetry as

$$A = \frac{N^+ - N^-}{N^+ + N^-}.$$

We assume purely statistical errors given by

$$\sigma^+ = \sqrt{N^+}, \quad \sigma^- = \sqrt{N^-},$$

which leads to an asymmetry error of

$$\sigma^2_A = \frac{4N^+N^-}{(N^+ + N^-)^3}.$$

Given the same two bins, we define the event ratio as

$$R = \frac{N^+}{N^-}.$$

The statistical error is then given by

$$\sigma^2_R = \frac{N^+N^- + (N^+)^2}{(N^-)^3}.$$

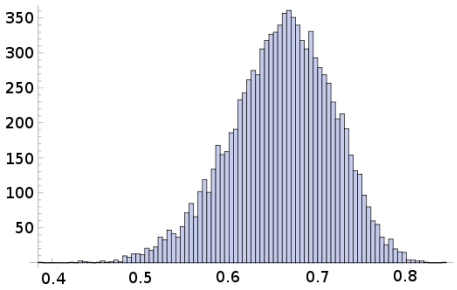

Figure 4.3: Histogram of the N_{repeat} values of the correlation between $\langle H_T \rangle$ and $\langle \not{E}_T \rangle$ obtained by applying the bootstrapping procedure on 2 fb^{-1} of SUSY plus background events, with $N_{\text{sub}} = 20$ and $N_{\text{repeat}} = 10,000$. The mean value of the distribution is 0.66, as given in Table 4.3.

4.3.3 Cross Section

The cross section after cuts σ_{eff} is given by

$$\sigma_{\text{eff}} = N_{\text{obs}} / \mathcal{L}_{\text{int}},$$

where $\mathcal{L}_{\text{int}}$ is the integrated luminosity and N_{obs} the observed number of events. The statistical error is given by

$$\sigma_{\text{stat}} = \frac{\sigma_{\text{eff}}}{\sqrt{N_{\text{obs}}}}$$

and the systematic error is estimated as 30 percent,

$$\sigma_{\text{syst}} = 0.3\, \sigma_{\text{eff}}.$$

4.3.4 Covariance Matrix Estimate

Preserving information about the expected correlations of observables can considerably increase or decrease χ^2 values, depending on the relative signs of ob-

served deviations from the expected mean values. It is therefore highly desireable to estimate the elements of the covariance matrix in a consistent way.

Since it is not possible to calculate the covariances of all observables $\mathcal{O}_i$ analytically, we have to rely on an estimate based on a sample of Monte Carlo simulations.

In an ideal world, we would simulate a full sample corresponding to the desired luminosity at each Little Higgs model point (including standard model backgrounds) N_S times and estimate the covariance matrix from

$$V_{ab} = \langle (\mathcal{O}_a - \langle \mathcal{O}_a \rangle) \, (\langle \mathcal{O}_b - \langle \mathcal{O}_b \rangle) \rangle,$$

where $\langle\rangle$ denotes the mean over the N_S sets. Because of limited computing resources, this is not feasible and we have to estimate the correlations from existing subsets of events for each data point. We use a bootstrapping procedure, where we randomly select N_{sub} subsamples from 2 fb^{-1} of signal plus background events. We calculate the correlation matrix from those subsamples, repeat the procedure N_R times and then calculate the mean values of the correlation matrix elements,

$$C_{ab} = \frac{1}{N_R} \sum_{i=1}^{N_R} \frac{V_{ab}^{(i)}}{\sigma_a^{(i)} \sigma_b^{(i)}},$$

where $V^{(i)}$ and $\sigma^{(i)}$ are the covariance and standard deviations obtained from the N_{sub} subsamples in iteration i. Those average matrix elements are then assumed to be the correct correlations of the observables in the full sample. A histogram of results obtained by this procedure is shown in Fig. 4.3.

Finally, we assume that the correlation is independent of the sample size, and extrapolate to find the covariances for the full set of events

$$V_{ab} = C_{ab} \sigma_a \sigma_b,$$

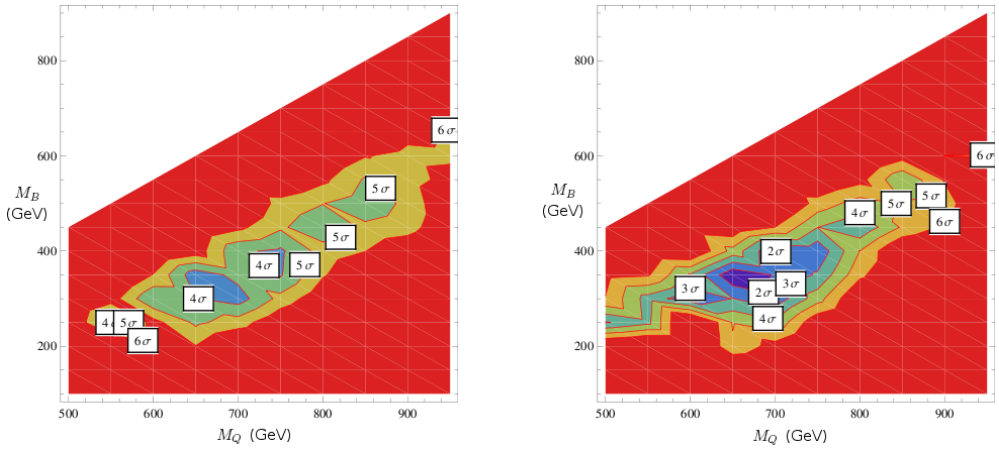

Figure 4.4: Exclusion level of the LHT hypothesis, based on the combined fit to the ten observables discussed in the text at 2 fb^{-1}. Left: As in Fig. 4.2, including correlations between observables as determined by the bootstrapping procedure. Right: Assuming that all observables in the Little Higgs model are uncorrelated.

where the standard deviations for the two observables σ_a and σ_b are now calculated from the full sample and include both statistical and systematic errors.

We verified that this procedure produces the correct χ^2 probability distribution function for the model distance between subsample and full sample observables.

Since the selection of subsample events that have passed our cuts is randomized, no information about the correlation of the cross section with the other observables can be obtained by this method, and we assume that the cross section is uncorrelated.

Fig. 4.4 illustrates the importance of including correlation information. Assuming uncorrelated observables, a small fraction of points in the LHT parameter space are found to be excluded at a higher confidence level. However, the ex-

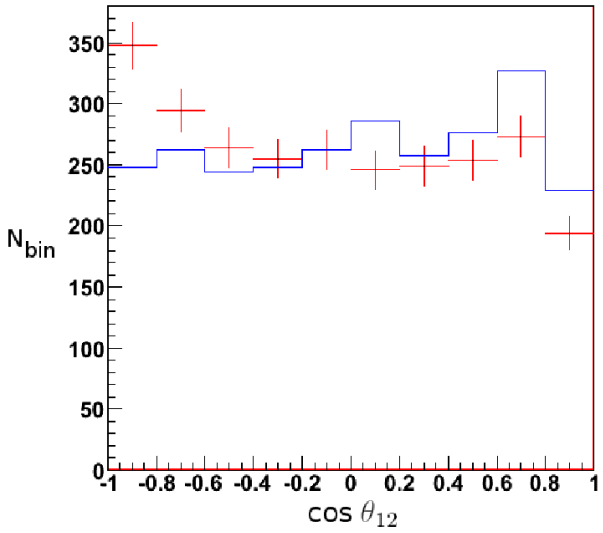

Figure 4.5: Distribution of the cosine of the angle θ_{12} between the two hardest jets in the SUSY sample ("data" points), as well as the prediction from the LHT model (histogram) with parameters $m_Q = 500$ GeV, $m_B = 100$ GeV.

clusion level of the best fit point is lowered significantly, and so the LHT model can no longer be rejected at the 3-sigma level.

4.4 Angular distribution of jets

As an example, we show the relative angular distribution of the two hardest jets in the SUSY "data" sample and for the Little Higgs model with ($m_Q = 500$ GeV, $m_B = 100$ GeV). The directional asymmetry is -0.079 $\pm$ 0.019 for the SUSY "data" and 0.008 $\pm$ 0.017 for the LHT + BG sample. Using just this observable, the χ^2 between the two models is 26.19, so that it would be excluded at the 5-sigma level.

4.5 Results

The main results of the analysis are presented in Fig. 4.2, which shows the level at which the LHT model is excluded depending on the assumed values of the parameters. For illustration purposes, we label the exclusion contours by the number of standard deviations in a single-variable Gaussian distribution corresponding to the same probability. With 200 pb^{-1} of accumulated data, the combined fit to the 10 observables excludes only about half of the LHT parameter space at better than 3-sigma level, or better than 99.7% confidence level. In the rest of the parameter space the LHT model is still consistent with data at this level, with the best-fit point at $M_Q = 650$ GeV, $M_B = 250$ GeV showing a less than 1-sigma deviation from the data. With more integrated luminosity and correspondingly smaller statistical errors, however, the LHT model can no longer fit the data. For 2 fb^{-1}, we find that the complete LHT parameter space in our study is excluded at a more than 3-sigma level, and most of the parameter space is already excluded at a 5-sigma level. Thus, it appears that in our test-case scenario, experiment can exclude the LHT interpretation of the data with a modest integrated luminosity of only a few fb^{-1}.

While we include the estimates of the systematic uncertainties for all observables in our study, some of the observables may suffer from additional uncertainties. One example is the total production cross section. We assumed a 30% systematic error on the value of the cross section computed in the LHT model, to account for the scale uncertainty of the leading-order calculation, as well as pdf and luminosity uncertainties. However, other effects, for example the possibility that the number of degenerate TOQ flavors is different from the assumed value (four), the possible presence of additional TOQ decay channels,

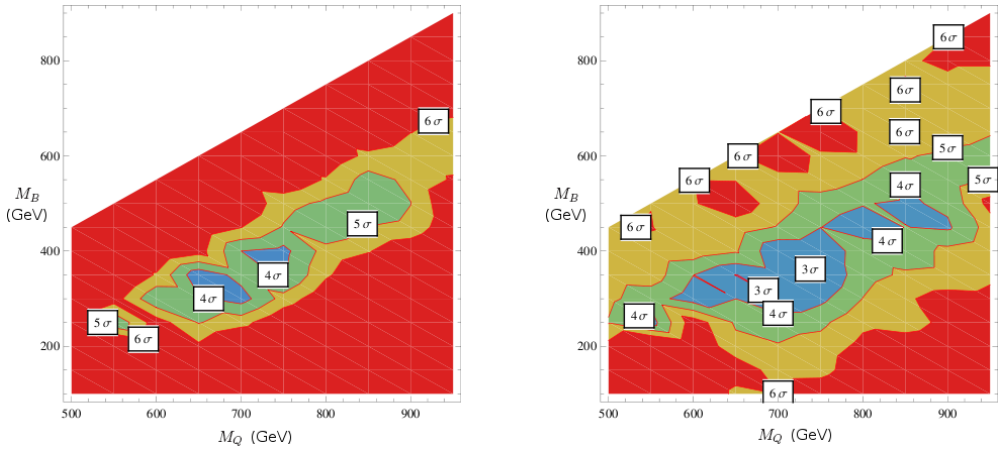

Figure 4.6: Exclusion level of the LHT hypothesis, based on the combined fit to nine/eight of the ten observables discussed in the text, with integrated luminosity of 2 fb^{-1} at the LHC. Omitted are the total production cross section (left panel) and missing transverse momentum and H_T (right panel).

etc., could significantly change this observable, keeping all others intact. Thus, it is interesting to fit the data with the LHT model without using the cross section information at all. Interestingly, this fit leads to exclusion of the LHT model at levels not much weaker than the original fit, see Fig. 4.6. In other words, the cross section information does *not* seem to play a crucial role in model discrimination: a combination of transverse-momentum and angular distributions of the two jets is sufficient. This is certainly reassuring. We have also performed a fit without using the average missing transverse momentum and H_T observables, which may suffer from unexpected instrumental systematics. The results are shown in the right panel of Fig. 4.6. The impact of removing these observables is more significant; some parameter values in the LHT model are now no longer excluded at the 3-sigma level. If those two observables are not included, it would therefore be necessary to increase the integrated luminosity to arrive at the same confidence level for the rejection of the Little Higgs hypothesis.

4.6 Conclusions

Using Monte Carlo samples, we determined χ^2 values for fitting a SUSY + BG "data" sample with Little Higgs model predictions, using the heavy TOQ and "heavy photon" masses as fit parameters and including dominant standard model backgrounds.

With 2 fb^{-1} of signal and background events, we were able to show that a combination of ten observables encoding angular and transverse momentum distributions of the observed jets contains enough information to exclude the LHT model at a 3-sigma confidence level, provided that these distributions for both models and the dominant Standard Model backgrounds can be reliably predicted by Monte Carlo simulations. We found that neither the effective cross section, which depends on potentially unknown decay branching ratios, nor information about the missing energy is crucial for this method of model discrimination.

In reality, it is likely that the LHC phenomenology is much richer than the simple scenario described here, involving, for example, competing SUSY production processes and complicated decay chains. In this case, the model-discrimination analysis would involve multiple channels, and more new particles (and hence parameters) would be required to fit. However, while the details are highly model-dependent, it should be conceptually straightforward to extend our analysis to such situations.

BIBLIOGRAPHY

[1] J. Pumplin *et al.*, "New generation of parton distributions with uncertainties from global qcd analysis," *JHEP* **0207** (2002) 012.

[2] H. E. Haber and G. L. Kane, "The search for supersymmetry: Probing physics beyond the standard model," *Phys. Rept.* **117** (1985) 75.

[3] S. P. Martin, "A supersymmetry primer," `arXiv:hep-ph/9709356`.

[4] R. Barbieri and A. Strumia, "The lep paradox," `arXiv:hep-ph/0007265`.

[5] P. Batra, A. Delgado, D. E. Kaplan, and T. M. P. Tait, "The higgs mass bound in gauge extensions of the minimal supersymmetric standard model," *JHEP* **0402** (2004) 043.

[6] R. Harnik, G. D. Kribs, D. T. Larson, and H. Murayama, "The minimal supersymmetric fat higgs model," *Phys. Rev. D* **70** (2004) 015002.

[7] R. Dermisek and J. F. Gunion, "Escaping the large fine tuning and little hierarchy problems in the next to minimal supersymmetric model and h $\rightarrow$ a a decays," *Phys. Rev. Lett.* **95** (2005) 041801.

[8] T. Roy and M. Schmaltz, "Naturally heavy superpartners and a little higgs," *JHEP* **0601** (2006) 149.

[9] C. Csaki, G. Marandella, Y. Shirman, and A. Strumia, "The super-little higgs," *Phys. Rev. D* **73** (2006) 035006.

[10] G. Burdman, Z. Chacko, H. S. Goh, and R. Harnik, "Folded supersymmetry and the lep paradox," *JHEP* **0702** (2007) 009.

[11] G. F. Giudice and R. Rattazzi, "Living dangerously with low-energy supersymmetry," *Nucl. Phys. B* **757** (2006) 19.

[12] K. Choi, K. S. Jeong, T. Kobayashi, and K. I. Okumura, "Little susy hierarchy in mixed modulus-anomaly mediation," *Phys. Lett. B* **633** (2006) 355.

[13] R. Kitano and Y. Nomura, "A solution to the supersymmetric fine-tuning problem within the mssm," *Phys. Lett. B* **631** (2005) 58.

[14] K. Choi, K. S. Jeong, and K. I. Okumura, "Phenomenology of mixed modulus-anomaly mediation in fluxed string compactifications and brane models," *JHEP* **0509** (2005) 039.

[15] A. Pierce and J. Thaler, "Prospects for mirage mediation," *JHEP* **0609** (2006) 017.

[16] K. Choi, K. S. Jeong, T. Kobayashi, and K. I. Okumura, "Tev scale mirage mediation and natural little susy hierarchy," *Phys. Rev. D* **75** (2007) 095012.

[17] R. Dermisek and H. D. Kim, "Radiatively generated maximal mixing scenario for the higgs mass and the least fine tuned minimal supersymmetric standard model," *Phys. Rev. Lett.* **96** (2006) 211803.

[18] R. Dermisek, H. D. Kim, and I. W. Kim, "Mediation of supersymmetry breaking in gauge messenger models," *JHEP* **0610** (2006) 001.

[19] R. Kitano and Y. Nomura, "Supersymmetry, naturalness, and signatures at the lhc," *Phys. Rev. D* **73** (2006) 095004.

[20] H. Baer, X. Tata, and J. Woodside, "Z0 + jets + (missing) p(t) events as a signal for supersymmetry at the tevatron collider," *Phys. Rev. D* **42** (1990) 1450.

[21] H. Baer, C. Balazs, A. Belyaev, T. Krupovnickas, and X. Tata, "Updated reach of the cern lhc and constraints from relic density, b $\rightarrow$ s γ and a(mu) in the msugra model," *JHEP* **0306** (2003) 054.

[22] R. Barbieri and G. F. Giudice, "Upper bounds on supersymmetric particle masses," *Nucl. Phys. B* **306** (1988) 63.

[23] **ALEPH** Collaboration, S. Schael *et al.*, "Search for neutral mssm higgs bosons at lep," *Eur. Phys. J. C* **47** (2006) 547.

[24] **Particle Data Group** Collaboration, W. M. Yao *et al.*, "Review of particle physics," *J. Phys. G* **33** (2006) 1.

[25] G. Degrassi, S. Heinemeyer, W. Hollik, P. Slavich, and G. Weiglein, "Towards high-precision predictions for the mssm higgs sector," *Eur. Phys. J. C* **28** (2003) 133.

[26] M. Frank, T. Hahn, S. Heinemeyer, W. Hollik, H. Rzehak, and G. Weiglein, "The higgs boson masses and mixings of the complex mssm in the feynman-diagrammatic approach," *JHEP* **0702** (2007) 047.

[27] S. Heinemeyer, W. Hollik, and G. Weiglein, "The masses of the neutral cp-even higgs bosons in the mssm: Accurate analysis at the two-loop level," *Eur. Phys. J. C* **9** (1999) 343.

[28] S. Heinemeyer, W. Hollik, and G. Weiglein, "Feynhiggs: A program for the calculation of the masses of the neutral cp-even higgs bosons in the mssm," *Comput. Phys. Commun.* **124** (2000) 76.

[29] A. Djouadi, J. L. Kneur, and G. Moultaka, "Suspect: A fortran code for the supersymmetric and higgs particle spectrum in the mssm," *Comput.Phys.Commun.* **176** (2007) 426.

[30] M. Carena, J. R. Espinosa, M. Quiros, and C. E. M. Wagner, "Analytical expressions for radiatively corrected higgs masses and couplings in the mssm," *Phys. Lett. B* **355** (1995) 209.

[31] **Tevatron Electroweak Working Group** Collaboration, E. Brubaker *et al.*, "Combination of cdf and d0 results on the mass of the top quark," arXiv:hep-ex/0608032.

[32] A. Djouadi, P. Gambino, S. Heinemeyer, W. Hollik, C. Junger, and G. Weiglein, "Leading QCD corrections to scalar quark contributions to electroweak precision observables," *Phys. Rev. D* **57** (1998) 4179.

[33] **CLEO** Collaboration, S. Chen *et al.*, "Branching fraction and photon energy spectrum for $b \to s\,\gamma$," *Phys. Rev. Lett.* **87** (2001) 251807.

[34] **BaBar** Collaboration, B. Aubert *et al.*, "Results from the babar fully inclusive measurement of $b \to x/s\,\gamma$," arXiv:hep-ex/0507001.

[35] **Belle** Collaboration, P. Koppenburg *et al.*, "An inclusive measurement of the photon energy spectrum in $b \to s\,\gamma$ decays," *Phys. Rev. Lett.* **93** (2004) 061803.

[36] **Heavy Flavor Averaging Group (HFAG)** Collaboration, E. Barberio *et al.*, "Averages of b-hadron properties at the end of 2005," arXiv:hep-ex/0603003.

[37] **Muon g-2** Collaboration, G. W. Bennett *et al.*, "Measurement of the negative muon anomalous magnetic moment to 0.7-ppm," *Phys. Rev. Lett.* **92** (2004) 161802.

[38] R. Barbieri and G. F. Giudice, "b $\to$ s γ decay and supersymmetry," *Phys. Lett. B* **309** (1993) 86.

[39] M. Muhlleitner, A. Djouadi, and Y. Mambrini, "Sdecay: A fortran code for the decays of the supersymmetric particles in the mssm," *Comput. Phys. Commun.* **168** (2005) 46.

[40] F. Maltoni and T. Stelzer, "Madevent: Automatic event generation with madgraph," *JHEP* **0302** (2003) 027.

[41] E. Boos *et al.*, "Generic user process interface for event generators," `arXiv:hep-ph/0109068`.

[42] P. Skands *et al.*, "Susy les houches accord: Interfacing susy spectrum calculators, decay packages, and event generators," *JHEP* **0407** (2004) 036.

[43] T. Sjostrand *et al.*, "High-energy-physics event generation with pythia 6.1," *Comput. Phys. Commun.* **135** (2001) 238.

[44] T. Sjostrand, S. Mrenna, and P. Skands, "Pythia 6.4 physics and manual," *JHEP* **0605** (2006) 026.

[45] J. Conway. `http://www.physics.ucdavis.edu/~conway/research/software/pgs/pgs4-general.htm`.

[46] A. J. Barr, "Using lepton charge asymmetry to investigate the spin of supersymmetric particles at the lhc," *Phys. Lett. B* **596** (2004) 205.

[47] J. M. Smillie and B. R. Webber, "Distinguishing spins in supersymmetric and universal extra dimension models at the large hadron collider," *JHEP* **0510** (2005) 069.

[48] L. T. Wang and I. Yavin, "Spin measurements in cascade decays at the lhc," *JHEP* **0704** (2007) 032.

[49] I. Low, "T parity and the littlest higgs," *JHEP* **0410** (2004) 067.

[50] J. Hubisz and P. Meade, "Phenomenology of the littlest higgs with t-parity," *Phys. Rev. D* **71** (2005) 035016.

[51] J. Hubisz, P. Meade, A. Noble, and M. Perelstein, "Electroweak precision constraints on the littlest higgs model with t parity," *JHEP* **0601** (2006) 135.

[52] M. Perelstein, "Little higgs models and their phenomenology," *Prog. Part. Nucl. Phys.* **58** (2007) 247.

[53] T. Appelquist, H. C. Cheng, and B. A. Dobrescu, "Bounds on universal extra dimensions," *Phys. Rev. D* (2001) 035002.

[54] H. C. Cheng, K. T. Matchev, and M. Schmaltz, "Bosonic supersymmetry? getting fooled at the lhc," *Phys. Rev. D* **66** (2002) 056006.

[55] R. Dermisek and I. Low, "Probing the stop sector and the sanity of the mssm with the higgs boson at the lhc," *Phys. Rev. D* **77** (2008) 035012.

[56] N. Arkani-Hamed, A. G. Cohen, and H. Georgi, "Electroweak symmetry breaking from dimensional deconstruction," *Phys. Lett. B* **513** (2001) 232.

[57] N. Arkani-Hamed, A. G. Cohen, E. Katz, and A. E. Nelson, "The littlest higgs," *JHEP* **0207** (2002) 034.

[58] M. Schmaltz and D. Tucker-Smith, "Little higgs review," *Ann. Rev. Nucl. Part. Sci.* **55** (2005) 229.

[59] H. C. Cheng and I. Low, "Tev symmetry and the little hierarchy problem," *JHEP* **0309** (2003) 051.

[60] H. C. Cheng and I. Low, "Little hierarchy, little higgses, and a little symmetry," *JHEP* **0408** (2004) 061.

[61] M. Asano, S. Matsumoto, N. Okada, and Y. Okada, "Cosmic positron signature from dark matter in the littlest higgs model with t-parity," *Phys. Rev. D* **75** (2007) 063506.

[62] M. S. Carena, J. Hubisz, M. Perelstein, and P. Verdier, "Collider signature of t-quarks," *Phys. Rev. D* **75** (2007) 091701.

[63] A. Belyaev, C. R. Chen, K. Tobe, and C. P. Yuan, "Phenomenology of littlest higgs model with t-parity: Including effects of t-odd fermions," *Phys. Rev. D* **74** (2006) 115020.

[64] A. Birkedal, A. Noble, M. Perelstein, and A. Spray, "Little higgs dark matter," *Phys. Rev. D* **74** (2006) 035002.

[65] M. Perelstein and A. Spray, "Indirect detection of little higgs dark matter," *Phys. Rev. D* **75** (2007) 083519.

[66] C. T. Hill and R. J. Hill, "t^- parity violation by anomalies," *Phys. Rev. D* **76** (2007) 115014.

[67] R. J. Hill, "Topological physics in the standard model and beyond," arXiv:0710.5791 [hep-ph].

[68] D. Krohn and I. Yavin, "Anomalies in fermionic uv completions of little higgs models," *JHEP* **0806** (2008) 092.

[69] E. Katz, J. y. Lee, A. E. Nelson, and D. G. E. Walker, "A composite little higgs model," *JHEP* **0510** (2005) 088.

[70] J. Thaler and I. Yavin, "The littlest higgs in anti-de sitter space," *JHEP* **0508** (2005) 022.

[71] K. Agashe, A. Falkowski, I. Low, and G. Servant, "Kk parity in warped extra dimension," *JHEP* **0804** (2008) 027.

[72] A. Birkedal, Z. Chacko, and M. K. Gaillard, "Little supersymmetry and the supersymmetric little hierarchy problem," *JHEP* **0410** (2004) 036.

[73] Z. Berezhiani, P. H. Chankowski, A. Falkowski, and S. Pokorski, "Double protection of the higgs potential," *Phys. Rev. Lett.* **96** (2006) 031801.

[74] K. Agashe, R. Contino, and A. Pomarol, "The minimal composite higgs model," *Nucl. Phys. B* **719** (2005) 165.

[75] L. Randall and R. Sundrum, "A large mass hierarchy from a small extra dimension," *Phys. Rev. Lett.* **83** (1999) 3370.

[76] S. R. Coleman, J. Wess, and B. Zumino, "Structure of phenomenological lagrangians. 1," *Phys. Rev.* **177** (1969) 2239.

[77] C. G. Callan, S. R. Coleman, J. Wess, and B. Zumino, "Structure of phenomenological lagrangians. 2," *Phys. Rev.* **177** (1969) 2247.

[78] Z. G. Berezhiani and G. R. Dvali, "Possible solution of the hierarchy problem in supersymmetrical grand unification theories," *Bull. Lebedev Phys. Inst.* **5** (1989) 55.

[79] R. Barbieri, G. R. Dvali, A. Strumia, Z. Berezhiani, and L. J. Hall, "Flavor in supersymmetric grand unification: A democratic approach," *Nucl. Phys. B* **432** (1994) 49.

[80] Z. Berezhiani, C. Csaki, and L. Randall, "Could the supersymmetric higgs particles naturally be pseudogoldstone bosons?," *Nucl. Phys. B* **444** (1995) 61.

[81] D. E. Kaplan and M. Schmaltz, "The little higgs from a simple group,".

[82] M. Schmaltz, "The simplest little higgs," *JHEP* **0408** (2004) 056.

[83] N. Seiberg, "Electric - magnetic duality in supersymmetric nonabelian gauge theories," *Nucl. Phys. B* **435** (1995) 129.

[84] I. R. Klebanov and M. J. Strassler, "Supergravity and a confining gauge theory: Duality cascades and chisb-resolution of naked singularities," *JHEP* **0008** (2000) 052.

[85] J. Wess and B. Zumino, "Consequences of anomalous ward identities," *Phys. Lett. B* **37** (1971) 95.

[86] E. Witten, "Global aspects of current algebra," *Nucl. Phys. B* **223** (1983) 422.

[87] Y. Kawamura, H. Murayama, and M. Yamaguchi, "Low-energy effective lagrangian in unified theories with nonuniversal supersymmetry breaking terms," *Phys. Rev. D* **51** (1995) 1337.

[88] A. Falkowski, "Note on little susy,". unpublished.

[89] C. Csaki, C. Grojean, H. Murayama, L. Pilo, and J. Terning, "Gauge theories on an interval: Unitarity without a higgs," *Phys. Rev. D* **69** (2004) 055006.

[90] C. Csaki, C. Grojean, L. Pilo, and J. Terning, "Towards a realistic model of higgsless electroweak symmetry breaking," *Phys. Rev. Lett.* **92** (2004) 101802.

[91] N. Arkani-Hamed, A. G. Cohen, and H. Georgi, "Anomalies on orbifolds," *Phys. Lett. B* **516** (2001) 395.

[92] C. Csaki, J. Hubisz, G. D. Kribs, P. Meade, and J. Terning, "Big corrections from a little higgs," *Phys. Rev. D* **67** (2003) 115002.

[93] G. Burdman, M. Perelstein, and A. Pierce, "Collider tests of the little higgs model," *Phys. Rev. Lett.* **90** (2003) 241802. Erratum-ibid. **92**, 049903 (2004).

[94] M. Perelstein, M. E. Peskin, and A. Pierce, "Top quarks and electroweak symmetry breaking in little higgs models," *Phys. Rev. D* **69** (2004) 075002.

[95] J. Hubisz, S. J. Lee, and G. Paz, "The flavor of a little higgs with t-parity," *JHEP* **0606** (2006) 041.

[96] M. Blanke, A. J. Buras, A. Poschenrieder, C. Tarantino, S. Uhlig, and A. Weiler, "Particle antiparticle mixing, epsilon(k), delta(gamma(q)), a(sl)(q), a(cp)(b/d –¿ psi k(s)), a(cp)(b/s –¿ psi phi) and b –¿ x/s,d gamma in littlest higgs model with t-parity," *JHEP* **0612** (2006) 003.

[97] M. Blanke, A. J. Buras, A. Poschenrieder, S. Recksiegel, C. Tarantino, S. Uhlig, and A. Weiler, "Rare and cp-violating k and b decays in the littlest higgs model with t-parity," *JHEP* **0701** (2007) 066.

[98] M. Blanke, A. J. Buras, B. Duling, A. Poschenrieder, and C. Tarantino, "Charged lepton flavour violation and $(g\text{-}2)_\mu$ in the littlest higgs model with t-parity: a clear distinction from supersymmetry," *JHEP* **0705** (2007) 013.

[99] A. Datta, K. Kong, and K. T. Matchev, "Discrimination of supersymmetry and universal extra dimensions at hadron colliders," *Phys. Rev. D* **72** (2005) 096006. Erratum-ibid. D **72**, 119901 (2005).

[100] C. Athanasiou, C. G. Lester, J. M. Smillie, and B. R. Webber, "Distinguishing spins in decay chains at the large hadron collider," *JHEP* **0608** (2006) 055.

[101] C. Kilic, L. T. Wang, and I. Yavin, "On the existence of angular correlations in decays with heavy matter partners," *JHEP* **0705** (2007) 052.

[102] A. Alves, O. Eboli, and T. Plehn, "It's a gluino," *Phys. Rev. D* **74** (2006) 095010.

[103] M. Burns, K. Kong, K. T. Matchev, and M. Park, "A general method for model-independent measurements of particle spins, couplings and mixing angles in cascade decays with missing energy at hadron colliders," *JHEP* **0810** (2008) 081.

[104] L. T. Wang and I. Yavin, "A review of spin determination at the lhc," *Int.J.Mod.Phys.A* **23** (2008) 4647.

[105] A. J. Barr, "Measuring slepton spin at the lhc," *JHEP* **0602** (2006) 042.

[106] J. Hubisz, J. Lykken, M. Pierini, and M. Spiropulu, "Missing energy look-alikes with 100 pb^{-1} at the lhc," *Phys. Rev. D* **78** (2008) 075008.

[107] C. Csaki, J. Heinonen, and M. Perelstein, "Testing gluino spin with three-body decays," *JHEP* **0710** (2007) 107.

[108] T. Han, H. E. Logan, B. McElrath, and L. T. Wang, "Phenomenology of the little higgs model," *Phys. Rev. D* **67** (2003) 095004.

[109] J. Alwall, P. Artoisenet, S. de Visscher, C. Duhr, R. Frederix, M. Herquet, and O. Mattelaer, "New developments in madgraph/madevent," *AIP Conf.Proc.* **1078** (2009) 84.

[110] A. Heister *et al.*, "Measurement of jets with the cms detector at the lhc," `CMS Note 2006/036`.

[111] **CMS** Collaboration, P. Sphicas, "Cms: The tridas project. technical design report, vol. 2: Data acquisition abd high-level trigger," `CERN-LHCC-2002-026`.

[112] "Cms physics technical design report volume i,".

[113] P. Meade and M. Reece, "Top partners at the lhc: Spin and mass measurement," *Phys. Rev. D* **74** (2006) 015010.